Bridging seismology and geomorphology: investigations of the 2006 and 2007 Kuril Island tsunamis

Breanyn Tiel MacInnes

A dissertation
submitted in partial fulfillment of the
requirements for the degree of

Doctor of Philosophy

University of Washington

2010

Program Authorized to Offer Degree:
Earth and Space Sciences

University of Washington
Graduate School

This is to certify that I have examined this copy of a doctoral dissertation by

Breanyn Tiel MacInnes

and have found that it is complete and satisfactory in all respects,
and that any and all revisions required by the final
examining committee have been made.

Chair of the Supervisory Committee:

_____
Joanne Bourgeois

Reading Committee:

_____
Joanne Bourgeois

_____
Robert Weiss

_____
Heidi B Houston

Date:_____

In presenting this dissertation in partial fulfillment of the requirements for the doctoral degree at the University of Washington, I agree that the Library shall make its copies freely available for inspection. I further agree that extensive copying of the dissertation is allowable only for scholarly purposes, consistent with "fair use" as prescribed in the U.S. Copyright Law. Requests for copying or reproduction of this dissertation may be referred to ProQuest Information and Learning, 300 North Zeeb Road, Ann Arbor, MI 48106-1346, 1-800-521-0600, to whom the author has granted "the right to reproduce and sell (a) copies of the manuscript in microform and/or (b) printed copies of the manuscript made from microform."

Signature _____

Date _____

University of Washington

Abstract

Bridging seismology and geomorphology: investigations into the 2006 and 2007 Kuril Islands earthquakes and tsunamis

Breanyn Tiel MacInnes

Chair of the Supervisory Committee:
Professor Joanne Bourgeois
Earth and Space Sciences

Numerous geophysical and geological observations of the 15 November 2006 and 13 January 2007 Kuril Island earthquake doublet and associated tsunamis help link earthquakes' seismological characteristics with tsunamis' coastal effects. Expression of the tsunamis in the central Kurils remained unknown until post-tsunami surveys in summers of 2007 and 2008. Surveyed runup in 192 locations over a distance of 600 km averaged ~10 m, maximum ~20 m. Higher runup generally occurred along steep, protruding headlands, and longer inundation distances on lower, flatter coastal plains.

As often observed but rarely measured in other cases, the Kuril tsunamis were dominantly erosional, while also leaving deposits. Pre- and post-tsunami surveys, including reoccupied topographic profiles, provide confidence to attribute changes to tsunami processes, in some cases to quantify these changes. Areas with low runup (<8 m) experienced limited geomorphic change, near the shore; regions with high runup (>15 m) experienced

massive erosion. Where sandy beaches existed, sheetlike tsunami deposits reached ~90% of tsunami runup and inundation. The volume of eroded sediment far outweighed the amount deposited on land in all cases studied. The tsunamis eroded the beach landward, stripped vegetation, created scours and trim lines, cut through ridges, and plucked rocks from the soil. The effects were dominantly erosive because high-relief topography accelerated tsunami outflow.

Post-tsunami surveys primarily found and measured only one tsunami wrackline, indicative of the largest onshore wave, with few clues as to which tsunami formed it. Simulations of tsunamis based on published slip distributions of both earthquakes using the numerical MOST model (Method of Splitting Tsunamis) help untangle the events. These simulations suggest that the larger tsunami in most places was 2006, but that 2007 was larger on Matua and parts of Rasshua islands.

The effect of slip distribution on nearfield tsunami runup was investigated using a diversity of slip-distribution inversions. The slip distribution in outer-rise earthquakes like 2007 causes less variation in runup patterns than is the case in subduction-zone earthquakes like 2006. Differences in length and width of inversions' subfaults also affect runup patterns when these differences affect up-dip or down-dip distribution of slip.

TABLE OF CONTENTS

LIST OF FIGURES

LIST OF TABLES

ACKNOWLEDGEMENTS

I am very grateful for funding provided by the Kuril Biocomplexity Project (National Science Foundation grant 0508109, Principal Investigator Ben Fitzhugh). Additional fieldwork support was provided by the Institute of Marine Geology and Geophysics, Far East Division, Russian Academy of Sciences, Yuzhno-Sahkalinsk, Russia (Director, Boris Levin). The following people contributed or assisted with field observations used in this dissertation: Jody Bourgeois, Tatiana Pinegina, Ekaterina Kravchunovskaya, Nadezhda Razhigaeva, Kirill Ganzey, Andrew Ritchie, Sergei Chirkov, Andrei Kharlamov, Douglas Querl, Victor Kaistrenko, Misty Nikula, Natalia Slobodina, Michael Etnier, Dimitri Frolov, Nikolai Vasilenko, Ben Fitzhugh, Boris Levin, Mikhail Nosov, Molly Odell, Erik Gjesfeld, Jesse Einhorn, and Elena Sassorova. Ben Fitzhugh made it possible for all of us to get to the Kuril Islands, the most beautiful place on earth.

Alexander Rabinovich, Alexei Ivashchenko and Kenji Satake gave helpful reviews of Chapter 2. Brian McAdoo, Martitia Tuttle, and two anonymous reviewers gave thorough reviews of Chapter 3. Jody Bourgeois, Heidi Houston and Robert Weiss helped review Chapter 4. Cecilia Bitz's help was instrumental in recovering weather data for the central Kurils used in Chapter 3. Harvey Greenburg, Andrew Ritchie, David Sullivan helped me create the bathymetry and topography files in ArcGIS used in Chapter 4.

Much gratitude goes to my advisor Jody Bourgeois, whose enthusiasm and endless capacity for draft revisions gave just enough push to see this dissertation to completion. My academic siblings, Beth Martin, Andy Ritchie, and Bretwood Higman, and my academic

"grandmother" Charlotte Schreiber, have truly made graduate school a wonderful community. I am also grateful for the many helpful discussions, Friday group meetings, and countless tea breaks I had with other faculty members and my fellow graduate students. Finally, this work would not have been possible without the support of my parents Dave and Barbara, who inspired me from a young age, my brothers Colin and Gavin, who pushed me to do better, and my boyfriend Kyle, whose support is unwavering.

CHAPTER 1

Introduction

A scientifically fortuitous pair of great earthquakes occurred in the central Kuril Islands between field seasons of the Kuril Biocomplexity Project (KBP)[1]. The 15 November 2006 Kuril Island earthquake generated the largest trans-Pacific tsunami since 1964 Alaska. The tsunami was considered "small" by the press at the time, even though tide gauges measured waves with almost one meter amplitude, 16,000 km away (Talcahuano, Chile; NGDC database); Crescent City, California, 13,000 km away, suffered at least $9.2 million dollars worth of damage to its harbor, when boats smashed into piers and docks were pulled off their moorings (Dengler et al., 2009). Only 60 days following the 2006 earthquake, a second earthquake occurred on 13 January 2007, sending yet another trans-Pacific tsunami. This second tsunami was one third as large on the far side of the Pacific and did less damage, although it possibly was larger than the 2006 tsunami in the Kuril Islands (Rabinovich et al., 2008). This dissertation focuses on these two earthquakes and the tsunamis they unleashed.

Although global seismometers registered teleseismic waves from both earthquakes (cf. Ji, 2006; 2007; Ammon et al., 2008), there are no settlements within 400 km of the earthquake epicenters; all eyewitness accounts are farther from the source. Nevertheless, thanks to on-going research of KBP and IMGG[2] that began in 2006, the aftermath of the 2006 and 2007 tsunamis has been studied in detail. One or a combination of the tsunamis left

[1] The Kuril Biocomplexity Project (KBP) is a five-year, multi-disciplinary joint Russian-American-Japanese project studying the effects of environment on human migration in the Kurils over the last 5,000 years. My role in the project includes the developing of a paleo-tsunami history and determining the effects of tsunami inundation on maritime settlements.

[2] Institute for Marine Geology and Geophysics in Yuzhno-Sakhalinsk, Russia

devastation, dramatic erosion and a continuous wrackline of debris across the coastal plains of the central Kurils, in many places more than 10 times higher than any circum-Pacific tide-gauge measurement. The findings from July and August of 2007 and 2008 of the post-tsunami expeditions funded by KBP and IMGG, summarized in Chapter 2, indicate an average of 10-m high-runup in the central Kuril Islands.

The variety of data now available for the 15 November 2006 and 13 January 2007 earthquakes and resultant tsunamis has generated countless opportunities for scientists to investigate earthquake and tsunami behavior. For example, for the first time, a group of tsunami geologists surveyed a coastal area both before and after a large tsunami. The field data provide an extensive network of observations to compare against numerical model simulations. In particular, these field data allow me to address two compelling questions regarding tsunami behavior: (1) How do tsunamis affect coastal geomorphology? and (2) Can we evaluate earthquake slip distributions using nearfield observations?

How do tsunamis affect coastal geomorphology?

Over long time scales of coastal development in tsunami-prone regions, tsunamis may be important agents of geomorphic change. To study the full impact of tsunamis on coastal geomorphology, it is essential to understand their role in both the addition and removal of coastal sediment. The effects of tsunamis are of broad interest to coastal geomorphologists (Dawson, 1994; Kench et al., 2008), and the concept of inherent differences between coastlines that do and do not experience tsunami is an unexplored topic. The first step in determining the long-term effects of tsunami interaction with coastlines is to measure and to describe geomorphic changes from modern events (Chapter 2 and 3).

The dataset from the Kuril Islands provides a remarkable opportunity to quantify the constructive and destructive effects of tsunamis on a coastline because teams observed coastal geomorphology before and after tsunami inundation. While tsunami-generated geomorphic change to inundated coastlines has been a common observation of post-tsunami surveys, many studies of the effects of tsunamis are limited by unknown specific prior conditions (cf. Dawson, 1994; Gelfenbaum and Jaffe, 2003; Choowong et al., 2007; Umitsu et al., 2007). Qualitative observations suggest that most tsunami-induced changes in coastal geomorphology are driven by erosion, during either inflow or outflow. Erosional changes to a landscape can be temporary (Kurian et al., 2006), permanent (Andrade, 1992), or continue an ongoing trend (Kench et al., 2006, 2008). Tsunamis remove vegetation and damage man-made structures (Dawson, 1994; Maramai and Tinti, 1997). Tsunami erosion causes beach retreat either as large-scale scour features or as smaller scallops, and tsunamis can breach beach berms and other ridges (Andrade, 1992; Dawson, 1994; Maramai and Tinti, 1997; Gelfenbaum and Jaffe, 2003; Kench et al., 2006; Kurian et al., 2006; Choowong et al., 2007; Umitsu et al., 2007). Tsunamis also alter drainage patterns by widening river mouths and creating new drainage networks, especially in topographic lows (Andrade, 1992; Maramai and Tinti, 1997; Umitsu et al., 2007).

Similar to tsunami erosion, tsunami deposition can occur during inflow or outflow. Tsunamis add, or rearrange, material in terrestrial coastal settings in the form of a tsunami deposit— a sand sheet that typically thins and fines landward, following topography (Dawson and Shi, 2000). Deposits are more extensive where tsunamis overtop erodible beach ridges and coastal dunes (Bourgeois et al., 1999). Many factors, from sediment availability to coastal topography to the velocity profile of the incoming and outgoing waves, play a role in

sedimentation. Modern and paleo-deposit surveys suggest that the form and lateral extent of a tsunami deposit depend on many of these factors, but there is fidelity between deposit extent and actual tsunami extent.

The Kuril Island dataset extends the field of tsunami geomorphology into new settings with the "before and after" findings presented in Chapter 3; only with pre-tsunami observations can we quantify coastal geomorphic change from measurements of the addition, removal, and shaping of coastal sediment. The few published studies that incorporate pre-tsunami measurements are in locations dramatically different than the Kuril Islands. To date, other quantified before-and-after studies focus on areas with low-relief topography (elevation changes < 2-3 m); in all these cases the beach berm is the highest topographic feature of the coastal plain. These studies in particular are from beach profiles or atoll-island surveys from the 2004 Indian Ocean tsunami in southwestern India and the Maldives (Kurian et al., 2006; Kench et al., 2006; 2008) and low coastal plains inundated by the 1998 Papua New Guinea tsunami (Gelfenbaum and Jaffe, 2003). The central Kuril Island coasts contain steep topographic gradients, and range in type from beach-ridge plains, to steep slopes, to rocky headlands— all forms that are common on tectonically active, tsunami-prone coastlines. Thus the Kurils dataset adds an important new perspective on tsunami geomorphology.

Can we evaluate earthquake slip distributions using nearfield observations (or vice versa)?

Of utmost interest to the tsunami-modeling and tsunami-hazard-assessment communities is the degree to which earthquake characteristics need to be considered in producing reliable runup and inundation models. However, a standard method of predicting

tsunami runup on a coastline uses generic uniform earthquake ruptures (e.g. Titov and Gonzales, 1997; Titov et al., 2001; Titov et al., 2005) and therefore could be unrealistic in predicting tsunami runup in the nearfield. Geist and Dmowska (1999) and Geist (2002) theorized that earthquake characteristics, such as slip distribution along a rupture, strongly affect nearfield tsunamis. Even in the farfield, heterogeneous rupture patterns for larger events appear to be noticeable on tide-gauge records (Johnson and Satake, 1999; Baba et al., 2006; Fujii and Satake, 2008).

Studying earthquake slip distributions using nearfield tsunami observations is a relatively untested method, although some work has been done. In hypothetical M_W 8.1 earthquakes, Geist (2002) ascribes a factor-of-three variation in peak tsunami wave heights in the nearfield to differences in earthquake slip distributions, but his hypothesis was not tested against observations. In MacInnes et al. (2010), we modeled tsunami runup from possible uniform slip distributions for the 1952 Kamchatka M_W 9.0 earthquake, from a variety of heterogeneous slip distributions and from a published slip distribution. We then compared these resultant tsunamis to nearfield observations and tsunami-deposit elevations to show that concentrations of slip are necessary to match deposit records.

The Kuril Islands case is a data-rich opportunity for testing whether nearfield tsunami runup can resolve internal variations in earthquake slip from standard, homogeneous slip distributions. Because of the plethora of data available for the 2006 and 2007 Kuril earthquakes and the availability of several different inversion techniques, published studies have determined many different potential slip distributions for each earthquake. Slip-distribution inversion techniques are based on seismic, tsunami tide-gauge, or GPS data (Chapter 4). The 192 measurements of tsunami runup in the central Kuril Islands presented in

Chapter 2— the nearfield for both the 2006 and 2007 events—provide a dataset against which models can be compared.

Simulating the relative difference in tsunami runup and inundation between 2006 and 2007 is an important contribution to untangling the records of both events (Chapter 4) and is a necessary consideration in my study of the relative geomorphic effects of the two events (Chapter 5). Recently, Rabinovich et al. (2008) modeled the 2006 and 2007 tsunamis in the central Kurils and concluded that the 2007 tsunami was larger than the 2006 tsunami. While field observers inferred that they were looking at the effects of the 2006 tsunami, Rabinovich et al. (2008)'s work raised the possibility that some observed geomorphological changes in the Kurils may have been from the 2007 tsunami or a combined effect of both tsunamis. Because both the 2006 and 2007 tsunamis occurred between field seasons, tsunami models are likely the best method currently available for estimating the extent of coastline inundated by both events.

Overview of dissertation

Each of the three main chapters in this dissertation is written to be a stand-alone paper; the first two chapters have already been published and the third is being prepared for submission. Chapter 2, entitled "Field survey and geological effects of the 15 November 2006 Kuril tsunami in the central Kuril Islands," offers an overview of the observations of the post-tsunami survey research from 2007 and 2008. This chapter helps set the scene for the subsequent, more in-depth chapter on tsunami geomorphology, and presents the observations of the KBP and IMGG teams used in the chapter on tsunami modeling. Descriptions of post-tsunami survey observations include topographic profiles to determine

distances and elevations of tsunami runup and inundation. I also describe and record the location of erosion, thicknesses of tsunami deposits, and the landward extent of erosional and depositional features on many profiles. This chapter was published in a special edition of *Pure and Applied Geophysics* entitled "Tsunami Science Four Years After the 2004 Indian Ocean Tsunami; Part II Observation and Data Analysis" edited by Cummins, Kong, and Satake (MacInnes et al., 2009a).

Chapter 3, entitled "Tsunami geomorphology: erosion and deposition from the 15 November 2006 Kuril Island tsunami" focuses on the details of the effect of the tsunamis on the geomorphology of the central Kuril coastline. I present in-depth analysis of four cases of tsunami erosion in locations where topography was measured by transit in 2006 and was re-surveyed by transit in 2007 using GPS and landmarks to relocate. I also compare the scale of erosional and depositional effects in 11 locations with in-depth sediment-thickness measurements. Analysis of field data illustrates that the 2006 and 2007 Kuril tsunamis were dominantly erosive. The total volume of tsunami erosion relates to distance from shore, topography, and tsunami runup. The tsunamis induced dominant offshore transport in the central Kurils, in contrast with other cases (Gelfenbaum and Jaffe, 2003; Kurian et al., 2006) where tsunamis flowing over low-relief coastlines generated net onshore transport, even if erosion was present locally. Thus the Kurils study appears to confirm the hypothesis proposed by Umitsu et al., (2007) that high elevation gradients, such on the Kuril Island beach-ridge plains, result in higher velocity outflow (and therefore net offshore transport). This chapter was published in *Geology* (MacInnes et al., 2009b).

The final main chapter, entitled "Using tsunami modeling and earthquake slip distributions to interpret enigmatic runup measurements of the 2006 and 2007 Kuril Island

tsunamis" uses the runup measurements presented in Chapter 2 to explore 2006 and 2007 earthquake characteristics and the differences between the two associated tsunamis. I numerically simulate many versions of the 2006 and 2007 Kuril tsunamis using NOAA's Method of Splitting Tsunami (MOST) computer model (Titov and Synolakis, 1995, 1998; Titov and Gonzolas, 1997) for tsunami propagation. The MOST model is a standard forecasting model that propagates an impulse-generated wave across a set bathymetry (Titov and Synalokis, 1998) and has the capability to calculate runup and inundation. The number and diversity of available inversions of earthquake slip distribution provides the opportunity to investigate effects of slip distribution on nearfield tsunami runup. Differences in slip resolution (length and width of subfaults used in inversion techniques) can have a significant impact on tsunami runup when it affects the up-dip or down-dip distribution of slip. Resolving average slip over a larger area can increase or decrease width and maximum amplitude of seafloor deformation, causing changes in the tsunami waveform and leading to measurable differences in nearfield runup. The distribution of slip in an outer-rise earthquake similar to the 2007 Kuril Islands event causes less variation in nearfield runup than is the case for a subduction-zone earthquake similar to the 2006 Kuril Island event.

Through the entire dissertation, I investigate the 2006 and 2007 tsunamis from both ends of their existence— the earthquakes that initially formed them, and their on-land manifestations as destructive, erosional waves. This work bridges seismology and geomorphology to investigate the ultimate question of what happened, unobserved by human eyes, in the central Kuril Islands in the winter of 2006-2007. Field data in Chapter 2 and 3 suggest the 2006 tsunami was the dominant agent of geomorphic change in the central Kurils, as opposed to the 2007 tsunami or storm waves. The largest 2006 wave was followed

by a smaller, later wave that appears to be from the 2007 tsunami in some locations. Chapter 2 discusses evidence for compaction between two layers of tsunami deposit that suggests the passage of time between deposition of the two units. However, simulations of tsunamis from many different slip distributions of both earthquakes— inverted from teleseismic waves, tsunami waveforms and/or GPS-measured ground motion— in Chapter 4 suggest that a combination of the two tsunamis may be more likely responsible for the highest tsunami runup observed in the field. Chapter 2 and 3 do not discuss the possibility of a 2007 tsunami larger than 2006 in some locations because my tsunami modeling initiated after these chapters were published. Simulated tsunamis show that both 2006-style or 2007-style simulated tsunamis can produce runup comparable to surveyed elevations in the central Kurils, depending on specific earthquake scenarios, although none matched observations entirely. The tsunami responsible for many of the observed phenomena was likely generated by the 2006 earthquake, but 2007 was more likely responsible for the largest wave on Matua Island and on parts of Rasshua Island.

Significance of dissertation contributions

By approaching the study of tsunamis from many angles, I show how several disciplines can combine to give a more complete understanding of tsunami behavior. My field research focuses on sedimentological and geomorphological features created by modern tsunamis that can be correlated to and give insights into paleo-tsunami studies. My use of the numerical MOST code focuses on relating simulated tsunamis to earthquake slip distributions to determine the extent to which earthquake characteristics need to be considered for predicting nearfield tsunami behavior.

I chose to investigate an earthquake doublet that bridges at least one boundary between studies of modern events and paleo-events in that there were no local eyewitness accounts; my results provide both reassurances and cautions for paleo-tsunami studies. The analysis in Chapter 3 regarding extent of tsunami deposits can be directly applied to paleo-tsunami deposits in coastal settings similar to the Kuril Islands. Geologists interpreting these paleo-tsunamis should be reassured that deposits can be a reliable proxy for tsunami runup and inundation, though the necessary paleo-geographic reconstructions remain challenging, especially in light of tsunami erosion. My study of two tsunamis leaving almost indistinguishable records is a cautionary example to paleo-tsunami research that one presumed event may in fact be two or more. Given the well-known tendency of earthquakes to cluster, it could be misleading to interpret one apparently correlatable paleo-tsunami deposit as generated by one earthquake. Furthermore, my data and analyses provide important information about tsunami hazard on high-relief coastlines around the world and are significant for geologists interested in understanding tsunami flow properties, in defining tsunami erosion and deposition patterns (tsunami geomorphology), and in determining coastal geologic histories in tsunami-affected regions.

Understanding the effects of earthquake characteristics on tsunami generation is important and useful for hazard planners, tsunami inundation modelers and vulnerable coastal communities. Earthquake slip characteristics cannot be ignored when determining probabilistic tsunami hazards of low-lying coastal areas. In Chapter 4, I show how even for an M_w 8.4 subduction zone earthquake, differences in slip can cause variations of 5-20 m of runup in the nearfield. On the other hand, I also show how an M_w 8.3 outer-rise earthquake may produce a tsunami with only 2-3 m runup difference, and thus slip distribution may not

be as important in hazard planning for an outer-rise event. Nevertheless, communities that plan only for subduction-zone earthquakes may be unprepared for locally higher runup from a possible, large outer-rise aftershock.

The combination of a dense network of geophysical and geological observations of the 15 November 2006 and 13 January 2007 Kuril Island earthquake doublet and associated tsunamis allows us to take a first step in bridging the gap between seismological characteristics of an earthquake and coastal effects of a tsunami. Chapter 2 and 3 provide a solid basis for future tsunami-geomorphology and paleo-tsunami studies. The tsunami simulations presented in Chapter 4 are a first-order attempt to understand the utility of slip-distribution inversions for tsunami modeling in the nearfield. The studies presented in this dissertation provide a future foundation for determining whether a specific tsunami behavior with its associated onshore geomorphic response can be directly related to an earthquake's heterogeneous slip distribution.

CHAPTER 2

Field survey and geological effects of the 15 November 2006 Kuril tsunami in the central Kuril Islands

Disclaimer

This chapter was first published in the journal *Pure and Applied Geophysics* with the following citation:

MacInnes, B.T., Pinegina, T.K., Bourgeois, J., Razhegaeva, N.G., Kaistrenko, V.M., and Kravchunovskaya, E.A., 2009a, Field survey and geological effects of the 15 November 2006 Kuril tsunami in the middle Kuril Islands: Pure and Applied Geophysics, v. 166, doi 10.1007/s00024-008-0428-3.

 Minor modifications to the original article include the addition of observations from the 2008 field season and the removal of the abstract, acknowledgements, and any sections not contributed by the first author. Figure 2.2 was originally drafted by Joanne Bourgeois; Figure 2.5 and the upper left section of Figure 2.4 was originally drafted by Tatiana Pinegina. The assumption presented here that the 2006 tsunami was universally larger than 2007 does not incorporate conclusions from the tsunami modeling presented in Chapter 4, as that work had not begun when this chapter was published.

Introduction

A pair of tsunamigenic great earthquakes occurred seaward of the central Kuril Islands in November 2006 and January 2007—one of the largest earthquake doublets on

record (Ammon et al., 2008). The 2006 earthquake occurred along the plate boundary, whereas the 2007 earthquake was produced by normal faulting on the outer rise.

Everywhere the 2006 and 2007 Kuril tsunamis were measured, the 2006 tsunami was larger (NGDC database[3] and HTDBWLD database[4]). Moreover, the 1994 Shikotan tsunami was an average of 1.5 times larger than the 2007 tsunami on trans-Pacific tide gauges (NGDC database). The records in the database, as well as arguments we make herein, lead us to interpret our surveyed tsunami effects in the central Kurils as the product of the 2006 tsunami.

The 15 November 2006 central Kuril Island tsunami was widely reported in the media to be small, a report based principally on its early expression in northern Japan, where later tsunami waves had tide-gauge water heights[5] of up to 0.6 m. Tide-gauge heights in Hawaii ranged up to 0.76 m, and on the far side of the Pacific, in Crescent City, California, a 0.88-m-high wave (1.76 m peak to trough) generated $9.2 million worth of damage (Dengler et al., 2009) in the harbor. Tide-gauge records from the southern Kurils include maximum water heights of about 80 cm (Rabinovich et al., 2008), but there are no stations in the central Kurils. Local runup for this tsunami remained unknown until our surveys in summer of 2007 (preliminary results reported in Levin et al., (2008)). No one lives in this remote area and logistics for visiting the islands are complex and expensive.

Two expeditions sponsored by the Institute of Marine Geology and Geophysics, Yuzhno-Sakhalinsk, Russia (IMGG) and the NSF-funded Kuril Biocomplexity Project (KBP)

---

[3] NGDC database—National Geophysical Data Center Tsunami Database, http://www.ngdc.noaa.gov/hazard/tsu_db.shtml (last accessed December 2010).

[4] HTDBWLD— Historical Tsunami Database for the World Ocean, http://tsun.sscc ru/nh/tsunami.php (last accessed December 2010).

[5] "Water height" is the term used in the NGDC database for vertical deviation from zero, which is approximately equal to amplitude, which in turn is half the trough-to-peak wave height.

worked together in the central Kurils in July and August of 2007 and 2008 to survey inundation, runup and geomorphic effects of the 2006 tsunami. Inundation and runup are standard descriptions of tsunami size and report the tsunami's maximum inland distance and the elevation of that position, respectively, for any given stretch of coastline (Farreras, 2000). Surveys of geomorphic impacts of tsunamis are less standardized and can include field descriptions or measurements of erosion, deposits, and other tsunami effects. Post-tsunami surveys included a total of four working groups who documented tsunami effects at 192 locations in 25 sites, over a distance of about 600 km, along the rupture zone of the 15 November 2006 and 13 January 2007 earthquakes. Several members of the expeditions had surveyed parts of these islands in the summer of 2006, under the aegis of the KBP. Our prior surveying provided a remarkable opportunity to make direct measurements and comparisons, at the same time of year, of shorelines before and after the tsunamis.

15 November 2006 and 13 January 2007 earthquakes and tsunamis

The two central Kuril great earthquakes of 2006 and 2007 filled a seismic gap (Figure 2.1). Previously, a large earthquake had not occurred in the central Kurils Islands in at least 150 years—an earthquake and tsunami were believed to have occurred off Simushir Island in the central Kurils in 1780 (Laverov et al., 2006). The central Kuril region had been interpreted as a seismic gap by Fedotov as early as 1965. However, there had been recent speculation as to whether this segment was slipping quietly (e.g. Kuzin et al., 2001; Song and Simons, 2003). Our paleo-tsunami field studies in the summers of 2006 and 2007 agree with the seismic-gap hypothesis (MacInnes et al., 2009a), as also confirmed by the recent earthquake doublet.

The 2006 earthquake released more total energy and lasted longer, whereas the 2007 earthquake had a higher peak energy release (Ammon et al., 2008). The 15 November 2006 earthquake commenced at 11:14 UTC, according to the U.S. Geological Survey, at a depth of ~30 km on the subduction zone. The epicenter for 2006 was off Simushir Island, and propagation proceeded northward (Ji, 2006; Vallée, 2006; Yagi, 2006). The 13 January 2007 earthquake, which commenced at 04:23 UTC at a crustal depth of ~10 km, was a normal-faulting, outer-rise event on the Pacific Plate, directly east of the Kuril-Kamchatka trench (Ji, 2007; Vallée, 2007, Yagi, 2007). According to the U.S. Geological Survey, the epicenter was approximately 100 km ESE of the 2006 event. Global CMT solutions record the 2006 event as a M_W 8.3 and the 2007 event as a M_W 8.1, although analysis of tsunami waveform inversions by Fujii and Satake (2008) suggest that M_W 8.1 and M_W 7.9 for 2006 and 2007, respectively, are more appropriate. Ammon et al. (2008) calculate M_W 8.4 for 2006 and M_W 8.1 for 2007 based on source radiation characteristics.

Both the 2006 and 2007 earthquakes produced measurable tsunamis around the Pacific Rim, although 2007 was smaller at every reported location. Observations from 113 locations for the 2006 event, and 35 locations for 2007, are archived in the NGDC Global Tsunami Database, and a few non-overlapping points in the Historical Tsunami Database for the World Ocean (HTDBWLD)[6]. Reported 2006 tide-gauge water heights range from <0.1 m at several locations to values of 0.4 to 0.9 m at some stations in the southern Kurils, Japan, New Zealand, Chile, the Marquesas, Hawaii, the west coast of the U.S., and the Aleutian Islands. Of the records of the 2007 tsunami, the maximum reported tide-gauge water heights are about 0.4 m at Malokurilsk (Rabinovich et al., 2008) and Chichijima Island, ~0.3 m at

[6] Note that the NGDC database reports water heights above zero, whereas the HTDBWLD database reports peak-to-trough wave heights. We are only using tide-gauge records for this comparison.

Shemya in the Aleutians, ~0.25 m at Port Orford and Crescent City, USA. The closest measurements of the 2007 Kuril tsunami on a directed path of the earthquake, in Hawaii, are an average of 3.5 times less than those of the 2006 Kuril tsunami.

Neo-tectonic and geomorphic setting

The Kuril Islands are a volcanic arc associated with subduction of the Pacific Plate under the Okhotsk Plate (Cook et al., 1986) along the Kuril-Kamchatka trench. Subducting crust is ~100 million years old, and the convergence rate is ~80 mm/yr (DeMets et al., 1990), excluding Okhotsk Plate rotation (Apel et al., 2006). The Kuril Island chain includes more than 25 islands with around 30 active volcanoes and many prominent volcanic edifices (Gorshkov, 1970; Melekestsev, 1980).

The islands surveyed in the central Kurils— Simushir to Matua islands (Figure 2.2)— are morphologically different than islands to the north and south. The central Kurils span a ~20º bend in the arc and are smaller and more widely spaced than northern and southern islands. Primarily, the central islands are single or multiple volcanic edifices, with the most common coastline being steep sea cliffs. Study sites fall into two broad geomorphologic categories—bouldery pocket beaches or broad embayments with gravelly to sandy shorelines (Figures 2.2 and 2.3). The coastal plain in almost all field locations is backed by a cliff or steep slope. The largest embayments have up to 500 m of sandy coastal plain before this cliff, but more than half of profiles measured were along rocky beaches with coastal plain widths averaging around 50 m (Figure 2.3).

Tsunami survey methods

Up to four teams operated simultaneously to measure topographic profiles, to record maximum runup and inundation, to collect tsunami-deposit samples and descriptions, and to make observations about erosion. Many sites visited in 2007 and 2008 had been observed by team members previously, which helped us distinguish tsunami erosion and deposition from other processes.

Except where noted in Table 2.1, we made all measurements with a tripod, level and rod, with individual measurement error of 0.3 cm vertically and 30 cm horizontally. This error does not accumulate in a measured segment (until the level is moved), so that cumulative vertical error is less than 30 cm and horizontal error generally less than a few meters; each measurement was checked for error in the field. In a few cases, we used a hand level and tape, with error of 2 cm vertically per measurement and about 5% error horizontally, the latter due to irregularities on the ground. Also, where slopes were steep, we converted taped measurements trigonometrically from on-the-ground to horizontal. Whenever possible, we also checked horizontal measurements with distances calculated from GPS points (Table 2.1).

We measured profiles to or from local sea level and in most cases corrected for tide at the time of measurement from local tide tables. Measurements were not corrected for tide at the time of the earthquake, which began about mid-tide on the flood phase, in a low-amplitude tidal cycle (less than 0.5 m), based on tide tables and nearby tide gauges; storm waves were active at the same time. Tidal range is typically 0.5 – 1.5 meters, so even without corrections, error in the elevation of mean sea level is small relative to runup.

At nearly every location surveyed, we could find evidence for an inland limit of tsunami penetration. Our primary criteria for defining runup were lines of floatable debris—typically driftwood, cut wood, plastic bottles and floats, glass floats, and styrofoam. In regions with short grasses and flowers, debris lines were obvious, and often one measurement accurately reflected runup. Where floated debris was obscured by that year's growing vegetation so that a debris line was not clear, we bushwacked, traced debris through the vegetation, and measured multiple points along 10-50 lateral meters. Both individual measurements and averages are reported in Table 2.1 and summarized in Table 2.2 and Figure 2.4. Single pieces of debris, such as one plastic bottle, were not considered adequate, as small or lightweight debris can blow in the wind. We observed some movement of debris material by animals, such as foxes, but it was rare. With the exception of southern Urup (briefly surveyed) and a small abandoned camp on Matua, we have no evidence that people had visited these islands since our visit in summer 2006. In a few cases, we measured heights of draped grass and seaweed on shrubs, but we saw few such flow-depth indicators. Corroborative evidence of runup, not used independently, included the limit of consistently seaward-oriented stems of tall grasses and flowers, the limit of sand and gravel deposits on top of turf and dead vegetation, and the elevation of fresh erosion of turf.

2006 or 2007?

We assumed our maximum runup and inundation limits were due to the 2006, not 2007, tsunami partly based on survey and database records. First, the 2007 tsunami was measured to be smaller at *every* catalogued location around the Pacific. At the closest locations with records, the 2007 tsunami was five times smaller than 2006 at Yuzhno-Kurilsk

(~550 km to the south of our field area), and less than half as high at Malokurilsk (~500 km to the south of our field area)—refer to Rabinovich et al, 2008 for tide gauge records. Furthermore, the M_w 8.1-8.3 1994 Shikotan tsunami— potentially comparable to 2007 because it was an intra-Pacific earthquake (Harada and Ishibashi, 2007)— had a larger tsunami than 2007 at most trans-Pacific sites (NGDC database). The local expression of 1994 was relatively small; runup was typically 3-8 m (max. 10 m) in the Habomai island group close to the Kuril-Kamchatka trench, and 1-4 m (max 6 m) in the southern Kurils themselves (Yeh et al., 1995; Kaistrenko, 1997; NGDC database). Average runup at sites in the nearfield of the 1994 source is less than 5 m, whereas the average runup we surveyed parallel to the 2006 and 2007 ruptures (see below) is about 10 m.

In addition to arguments based on measured tsunami height and runup, we argue that the effects we surveyed were primarily from 2006 because local conditions on the islands were different for the two tsunamis. A Landsat image of Dushnaya Bay from 22 November 2006 shows extensive regions without snow at lower elevations. However, weather records from December 2006 and early January 2007 in the coastal cities of Severo-Kurilsk and Yuzhno-Kurilsk (to the north and south of the field area) indicate that there would have been snow accumulation at low elevations before the 2007 tsunami. Thus a frozen, snow-covered coast in January would be less susceptible to erosion and subsequent deposition, including movement of the beach debris we used to indicate runup. Tsunamis do not necessarily erode snow (particularly if ice-covered snow) during inundation (Minoura et al., 1996).

In Dushnaya Bay on Simushir Island, there was evidence along many profiles for a smaller wave postdating the largest wave to come ashore—we cannot confidently attribute this evidence to a later wave of 2006 or to 2007. For example, we observed a thin wrack line

from a smaller wave (~3-5 m elevation). Also, we observed complex tsunami deposits on several profiles, where a patchy sand deposit (average maximum elevation 5 m) lay above a layer of flattened vegetation, which, in turn, covered a continuous, coherent deposit. Such a depositional sandwich is what we expect from a second tsunami wave inundating over snow (Figure 2.5), in which case these deposits would be from a smaller, 2007 tsunami.

Runup observations and inundation

Measured runup in the central Kuril Islands (Simushir to Matua, about 200 km along strike) from the 2006 tsunami was typically 5-15 m, with a range of 2-22 m (Table 2.1 and 2.2, Figure 2.4), and a raw average of 10.4 m (9.6 m for the entire field area). Measured inundation varied from 20 to 500 m, with a raw average of 96 m. Average runup in the central Kurils gives the tsunami a 3.87 (or 3.76 for the whole field area) on the S. Soloviev Tsunami Intensity scale (Soloviev, 1972), the standard intensity scale used in the NGDC and NTL global tsunami databases:

$$I = ½ + \log_2 H_{av}$$

where H_{av} is the average height of the tsunami on the nearest coast. This scale does not take into account the distance along shoreline of the surveyed region.

On some profiles (e.g. Dushnaya Bay profile in Figure 2.3), seaward of maximum inundation, the tsunami over-topped beach ridges or sand dunes that were higher elevation than runup, which is by definition, elevation at maximum inundation. For these cases, Table 2.1 provides both runup and also maximum elevation along the profile, seaward of (maximum) inundation. Elevations along the profile do not take into account tsunami water depth, so the water height would have been even higher. We include the intra-profile data, in

addition to runup and inundation, because they help represent the magnitude and behavior of the tsunami wave.

Variability in runup and inundation of the 2006 central Kurils tsunami was in large part due to coastal geomorphology. Naturally, our longer inundation values are from lower, flatter coastal plains, and higher runup values generally from steep, protruding headlands (Table 2.2). In many of the cases we studied, the steep slope or cliff backing the coastal plain limited tsunami penetration. When a tsunami hits a reflector, such as a sea cliff, the energy not reflected back to sea will be converted into vertical runup, increasing its height (Briggs et al., 1996; Pelinovsky et al., 1999). Tsunami modeling will enable us to determine the degree to which coastal geomorphology, as well as bathymetry, affected tsunami runup.

Tsunami sediment transport and deposition

All affected shorelines showed evidence of erosion and deposition, and we made systematic measurements on many profiles (Table 2.3). Where loose sediment was available on the beach or in the nearshore, we observed deposits of sand, gravel, and cobbles on the coastal plain surface, burying turf and dead vegetation (Figure 2.6B and D). Most deposits resemble sediment of the beach; more detailed analyses are forthcoming. In addition to beach sand and gravel, sediment also was derived from eroded scarps, from plucked turf and cobbles, and from artificial structures. Where the beach was composed of sediment larger than small cobbles, no coherent, continuous deposit was present, although scattered boulders moved by the tsunami were common (see Bourgeois and MacInnes, 2010). Where solid rock outcrop existed on the shore (observed on Ketoi and Matua), this rock was not noticeably affected by the tsunami.

We observed continuous tsunami sand sheets (e.g. Figure 2.6D) in areas with sandy beaches, which also coincide with most low-relief profiles. As has been repeatedly seen elsewhere (cf. Shi et al., 1995; Gelfenbaum and Jaffe, 2003; Bourgeois, 2009), the 2006 Kurils tsunami deposits in these cases were typically thin (<5 cm), thinning and fining landward. Over the 13 profiles where we made detailed observations, deposits were typically a few centimeters or less in thickness. Local variability in deposit thickness reflected previous topography; for example, a 0.5-cm-thick deposit locally thickened to 2-5 cm in a rodent burrow. In general, only close to the shore or in these locally low pockets did deposits exceed 5 cm in thickness.

Total volumes (average sediment thicknesses summed over distance) of sediment deposited ranged from 0.4 to 6.3 m^3/unit width (Table 2.3). The deposits used in these calculations were all on vegetated surfaces, with no evidence for subsequent erosion. Sediment volume is influenced by the amount of available sediment and by topographic variations controlling the velocity of the flow (Gelfenbaum and Jaffe, 2003). Profiles with less volume of sediment deposited had narrower and rockier beaches and lower runup. Largest volumes of sediment deposition came from profiles with severe beach erosion and higher runup.

Sediment transport was not limited to sand- to cobble-sized material—across the central Kurils, we found evidence of tsunami transport of boulders, ranging from 10s of cm up to 3 m in diameter (Table 2.3). Moved boulders, known as *tsunami ishi* (Kato and Kimura, 1983), were sourced from the nearshore, beach, coastal plain, and artificial structures (Figure 2.6C). We easily identified tsunami *ishi* from the nearshore by recently deceased sea life on the boulders, such as attached seaweed, encrusted bryozoan communities, and kelp holdfasts

(Bourgeois and MacInnes, 2010). *Ishi* derived from artificial structures could generally be traced back to the dam or pier or other military structure from which they were derived. We commonly identified the source location of boulders from within the vegetated beach plain by the holes left behind (see tsunami erosion section below for further discussion). Other than typically being clean and rounded, tsunami *ishi* that originated on the beach are associated with no identifiable characteristics so we only assume that if other equivalent-sized boulders moved, the ones on the beach could have been moved. We recorded some tsunami *ishi* to have been transported at least >85 m (Table 2.3), but we did not have time to conduct an exhaustive survey of all boulders transported.

Tsunami erosion

Geomorphic effects of the 2006 tsunami on the landscape varied from almost unnoticeable to devastating; two of our short-term camps from the summer field season of 2006 would have been obliterated. In general, erosion is produced by local temporal or spatial increases in boundary shear stress and clearly can also be affected by bed characteristics such as grain size and cohesion. Konno et al. (1961) identified three types of tsunami flow over land where erosion may occur: sheet flow, linear (or concentrated, channelized) flow, and eddy flow. Holding other factors constant (such as soil cohesion, vegetation type, etc.), sheet flow results in uniform erosion, concentrated flow in spatially variable erosion, and eddies in small-scale features. The different forms of tsunami flow are generated by topography (as in Umitsu et al., 2007). Evidence is widespread for erosion from all three types of flow in the 2006 tsunami case in the central Kuril Islands.

Far and away the two most common cases of erosion in our survey are what we call scouring and soil stripping. Documentation of scours and stripped areas are also common in tsunami literature (e.g. Gelfenbaum and Jaffe, 2003; Goff et al, 2006; Kurian et al., 2006; Okal et al., 2006), and such erosional features are typically associated with sudden changes in topography or in soil characteristics. The literature most often addresses scour associated with man-made features, such as roads, buildings, bridge pylons, etc. (e.g. Goff et al., 2006; Maheshwari et al., 2006; Malik et al., 2006). Individual scour depressions generally form from either linear or eddy flow, but the largest scours (e.g. Figure 2.7C) suggest erosional sheet flow (Konno et al., 1961). The upstream steep wall in a scour (and downstream sediment berm) form from eddies within the scour on the upstream side of the direction of flow (as in Konno et al., 1961; Alonso et al., 2002).

Visually, we identified scours in our survey by localized pits or eroded strips of coastline with a steeper wall at one end (Figures 2.6E and 2.7C). We define a "scour" as a localized depression generated by erosion, where vegetation and topsoil are removed entirely. Scours varied in size from less than a meter in diameter, to 100's of meters long by 10's of meters wide, and had scour depths of centimeters to meters. Scours occurred in both natural and artificial landforms; those in natural settings often had sediment accumulated in the downstream end of the depression (Figure 2.6E).

We identified soil stripping by removed vegetation and generally called an area stripped rather than scoured if there was not a distinct depression. In these cases, soil or sediment removal is uniform in depth and does not significantly extend below the turf zone, or in some cases, below a cinder layer near the surface (Figure 2.6F). Due to its uniformity, soil stripping suggests sheet flow (cf. Konno et al., 1961) without the development of strong

eddies. Commonly in our field area, the tsunami exploited shallow networks of rodent burrows or WWII military trenches to initiate erosion and strip the surface. In some locations, one edge of eroded turf was still attached and the upper soil layers were flipped over in the direction of flow as if the area has been scalped (Figure 2.6F).

The prevalent styles of erosion on central Kurils coastlines with a narrow beach plain, where the tsunami ran up a steep slope, were trim lines and slope-base erosion. A trim line is where (all) soil and vegetation are removed up to an approximately uniform elevation on a slope. In contrast, we define slope-base erosion as more isolated patches than trim lines and only extending a meter or two above the change in slope. Trim lines (Figure 2.7A) are visually striking and observable from a distance, and the uniformity of a trim line suggests sheet flow (cf. Konno et al., 1961). In our survey, maximum runup and inundation were in close proximity to the location of the trim line (Table 2.3); the tsunami typically continued only a meter or two above and a few meters beyond the trim line. Slope-base erosion (Figure 2.6G) is not as closely tied to maximum runup as trim lines are. This kind of erosion was clearly associated with sharp slope change and may have occurred during both inflow and outflow. Because slope-base erosion is selective, it suggests linear (channelized) flow, or eddy flow associated with the sharp change in slope.

Other styles of erosion we observed—plucking of rocks embedded in soil, cliff retreat of sandy back-beach edges or stream channel walls (Figure 2.7E), and breaches in beach ridges (Figure 2.7D)—were strongly dependent on location variables. Rocks as large as 30 cm in diameter were pulled out of soil leaving distinct, coherent holes in the surface. We traced some rocks a few meters to their source hole in both the seaward and landward direction, but the tsunami also removed some boulders and cobbles entirely from land,

presumably transporting them offshore. We only observed plucking in locations where the tsunami had no other source of sediment and was likely sediment starved.

Cliff retreat occurred in two forms—either *en masse*, or as scallops or gullies. *En masse*, or uniform, tsunami erosion has been previously reported along the beach edge (e.g. Kurian et al., 2006; Maramai and Tinti, 2007) and along a few stream channels (Maramai and Tinti, 2007). It is more likely to occur during inflow, when topographic effects are less important (e.g. Umitsu et al., 2007). In our surveys, we identified *en masse* cliff retreat by evidence that an extended stretch of coastline eroded landward in a fairly uniform way. For example, compared to our 2006 observations, in 2007 most back-beach scarps or stream channel walls (e.g. Figure 2.7E) exposed to the ocean appeared more straight and regular. We observed or measured up to >50 m of *en masse* erosion, the largest amount occurring in Ainu Bay, Matua (see Chapter 3).

Irregular scallops and gullies generally represent zones of concentrated outflow as they are produced primarily in locations where troughs intersect stream channels, or where a section of beach plain is lower then its immediate neighbors (e.g. Umitsu et al., 2007). Gelfenbaum and Jaffe (2003) and Umitsu et al. (2007) found that incoming tsunamis flowed nearly perpendicular to the shore, but backwash returned obliquely to the shore in local topographic lows. In our survey of 2006 tsunami effects in the central Kurils, gullies and scallops were common, especially where there was a preexisting backbeach scarp. The tsunami dug some gullies as deep as 3 m down into the preexisting beach scarp; these gullies in 2007 resembled dry waterfalls (Figure 2.7B). Some of these dramatic gullies were produced or enhanced where inflow over a steep beach face was then concentrated

(channelized) between two beach ridges, and then outflow was focused into what we presume were preexisting lows in the seaward-most beach ridge.

Although we are confident that almost all of the features we documented in our survey were due to erosion from the 15 November 2006 tsunami, the unvegetated beach is a location of constant change, and it can be difficult to say what changes are directly related to a tsunami (or in our case, two tsunamis), especially over the course of a full year (Shepard et al., 1950). For this reason, we did not pay much attention to changes on the unvegetated portion of our profiles. Besides the back-beach cliff retreat mentioned previously, the only other kind of beach change we could attribute to the tsunami with any amount of confidence was localized breaching through the back-beach cliff and seaward-most beach ridge. In three locations in Dushnaya Bay, we found breaches (width on the scale of meters) through the first beach ridge, at least one of which is known to have formed between 2006 and 2007 (Figure 2.7D). A few older beach ridges in our field area are also breached; we tentatively suggest these breaches are preserved geomorphic change from paleo-tsunamis.

Where the 2006 tsunami was large, erosion extended farther inland, and commonly the inland limit of erosion exceeded that of deposition (Table 2.3). A direct comparison of before and after using three topographic profiles from 2006, reoccupied in 2007, shows that the tsunami removed many times more sediment than it deposited on land. Even where erosion was at a minimum, and deposits extended almost to the limit of inundation, more sediment was eroded than can be accounted for by the tsunami deposit (see Chapter 3), and we presume this sediment was transported offshore.

Others have also documented beach-profile changes due to tsunami erosion. Kurian et al. (2006) measured before and after (unvegetated) beach profiles in India and found some

areas that experienced erosion and others that experienced deposition, but were uncertain as to what was directly from the tsunami and what was from previous or subsequent beach processes. Umitsu et al. (2007) also noted that beaches retreated or vanished following the 2004 Indian Ocean tsunami in Indonesia and Thailand, but were not able to quantify the change. Breaches by tsunami have been previously documented in Japan from the 1960 Chile event (Konno et al., 1961) and the Maldives from the 2004 Indian Ocean event (Fritz et al., 2006).

Summary

The nearfield runup of the 15 November 2006 central Kurils tsunami is more than 10 times higher than water heights recorded on any Pacific Ocean tide gauges (NGDC database). Average runup in the central Kurils was about 10 m, with some field sites recording >20 m. In many locations the tsunami inundated the entire coastal plain area and reflected off cliffs backing the plain. Maximum inundation reached as far as 400 m and was almost always limited by topography.

Wherever fine-grained (primarily sand-sized) sediment was available on the beach or nearshore, we found continuous tsunami deposits. Areas deficient in sand still showed evidence of sediment transport, with tsunami *ishi* up to 3 m in diameter pulled up from offshore, transported within the coastal plain, or washed out to sea. The presence of paleo-tsunami deposits in the central Kurils confirms that large ruptures in this section of the subduction zone are not uncommon, although the source characteristics of these paleoevents may vary. Many of the paleo-tsunami deposits are more extensive than deposits of the 15 November 2006 tsunami (MacInnes et al., 2009a).

Erosion from the 2006 tsunami was greatest where runup was more than 10 m. We predict some scours and gullies will likely be permanent alterations of the geomorphology of the coastline. At sites with high runup, erosion extended almost as far as inundation. However, erosion was minimal where runup was less than 10 m, such as in central Dushnaya Bay, Simushir; in these localities the geomorphic effect of the tsunami will be indistinguishable in the near future.

Table 2.1: Summary of Kuril Island post-tsunami surveys of runup and inundation ordered by latitude (additional parameters can befound in MacInnes et al., 2009b)

Date	Team*	Location				Method§	Runup			Inundation	
		Island	Locality name	Latitude of profile†	Longitude of profile†		Number of runup readings	Runup on profile (m)[%]	Runup average near profile (m)[%]	Measured inundation (m)	GPS calculated inundation (m)
07/05/07	VMK	Urup	Os'ma Bay-2	45.58223	149.45068	TL	1	*4.4*	-	170	-
07/05/07	VMK	Urup	Os'ma Bay-1	45.58285	149.45138	TL	1	*5.0*	-	48	-
07/05/07	JB	Urup	Os'ma Bay-1-2006	*45.58300*	*149.45350*	TL	1	*4.8*	-	50	-
08/21/08	BTM	Urup	Kostrikum Cape-225	46.21145	150.54547	TL	4	7.9	8.0	80	79
08/21/08	BTM	Urup	Kostrikum Cape-232	46.21520	150.54867	TL	3	5.2	5.2	61	51
08/19/08	JB	Chirpoi	Peschanaya South-V153	*46.53294*	*150.89059*	HLT	1	5.4	-	70	-
08/19/08	JB	Chirpoi	Peschanaya South-V150	46.53397	150.89264	HLT	2	10.5	10.4	91	81
08/19/08	BTM	Chirpoi	Peschanaya-221	46.53865	150.89644	TL	1	5.5	-	43	42
08/19/08	BTM	Chirpoi	Peschanaya-217	46.54120	150.90598	TL	3	5.9	5.6	31	30
08/19/08	BTM	Chirpoi	Peschanaya-219	46.54148	150.90152	TL	4	7.5	8.5	40	43
07/13/07	NGR	Simushir	Spaseniya Bay-37	46.83173	151.87659	HL	1	3.9	-	180	141
07/13/07	NGR	Simushir	Spaseniya Bay-39	46.83411	151.87962	HL	1	2.3	-	146	127
07/12/07	VMK	Simushir	Spaseniya Bay-82	46.83668	151.88249	HL	1	*7.2*	-	75	51
07/12/07	VMK	Simushir	Spaseniya Bay-77b	46.84178	151.89000	HL	1	*5.7*	-	109	54
08/09/08	JB	Simushir	Spaseniya Bay-2	46.84244	151.89121	HLT	4	7.5	7.5	127	118
07/13/07	NGR	Simushir	Spaseniya Bay-36	46.84520	151.89542	HL	1	1.3	-	212	172
08/09/08	JB	Simushir	Spaseniya Bay-1	46.84772	151.89931	HLT	5	7.0	7.0	111	116
07/19/07	NGR	Simushir	Spaseniya Bay-79	46.85087	151.90409	HL	1	6.2	-	80	59
07/19/07	NGR	Simushir	Spaseniya Bay-78	46.85281	151.90750	HL	1	4.4	-	140	115
08/18/08	BTM	Simushir	Opasnaya Bay-215	46.94008	152.05510	TL	2	6.9	6.7	79	79
08/18/08	BTM	Simushir	Opasnaya Bay-213	46.94306	152.05847	TL	3	8.5	8.5	98	99
08/18/08	BTM	Simushir	Opasnaya Bay-212	46.94655	152.06214	TL	1	6.3	-	136	131
07/11/07	TKP	Simushir	Dushnaya Bay-1	47.04313	152.15841	TL	1	20.0	-	83	79
07/11/07	TKP	Simushir	Dushnaya Bay-2	47.04530	152.15915	TL	1	12.4	-	75	92
07/10/07	VMK	Simushir	Dushnaya Bay-57	*47.04684*	*152.15963*	HL	1	*9.3*	-	136	115
07/10/07	VMK	Simushir	Dushnaya Bay-54	*47.04769*	*152.16070*	HL	1	*11.7*	-	44	-
07/11/07	TKP	Simushir	Dushnaya Bay-3	47.04942	152.16235	TL	1	7.9	-	123	135
07/12/07	TKP	Simushir	Dushnaya Bay-5	47.05409	152.16471	TL	1	11.3	-	132	128
07/12/07	TKP	Simushir	Dushnaya Bay-6	47.05628	152.16650	TL	1	4.4	-	106	98
07/12/07	TKP	Simushir	Dushnaya Bay-7	47.05807	152.16878	TL	1	6.3	-	139	139
07/13/07	TKP	Simushir	Dushnaya Bay-8	47.05979	152.17162	TL	1	8.6	-	118	120
07/13/07	TKP	Simushir	Dushnaya Bay-9	47.06094	152.17313	TL	1	7.3	-	151	154
07/10/07	JB	Simushir	Dushnaya Bay-2-2006 (central)	47.06201	152.17549	TL	1	6.7	-	122	125
07/14/07	TKP	Simushir	Dushnaya Bay-12	47.06393	152.17726	TL	1	6.9	-	120	115
07/14/07	TKP	Simushir	Dushnaya Bay-11	47.06582	152.17981	TL	1	8.2	-	115	109
07/14/07	TKP	Simushir	Dushnaya Bay-10	47.06772	152.18230	TL	1	9.9	-	133	121
07/13/07	JB	Simushir	Dushnaya Bay-110	47.06960	152.18429	TL	11	10.0	8.8	114	107
07/14/07	JB	Simushir	Dushnaya Bay-1-2006	47.06971	152.18614	TL	8	10.4	10.6	100	102
07/13/07	JB	Simushir	Dushnaya Bay-109	47.07039	152.18792	TL	10	8.9	9.1	59	56
07/09/07	VMK	Simushir	Dushnaya Bay-24	*47.07085*	*152.18777*	HL	1	*8.7*	-	77	-
07/13/07	JB	Simushir	Dushnaya Bay-108	47.07124	152.19088	TL	9	12.0	11.9	61	57
07/13/07	JB	Simushir	Dushnaya Bay-107	47.07312	152.19315	TL	12	18.4	15.3	85	74
07/12/07	JB	Simushir	Dushnaya Bay-106	47.07537	152.19476	TL	10	11.4	13.0	70	66
07/12/07	JB	Simushir	Dushnaya Bay-105	47.07754	152.19528	TL	10	15.3	15.5	93	102
07/11/07	JB	Simushir	Dushnaya Bay-104	47.07809	152.19888	TL	7	13.1	13.0	52	52
07/11/07	JB	Simushir	Dushnaya Bay-103	47.07818	152.20214	TL	10	10.3	10.8	49	46
07/11/07	JB	Simushir	Dushnaya Bay-102	47.07835	152.20566	TL	8	7.5	7.7	51	50
07/11/07	JB	Simushir	Dushnaya Bay-101	47.07880	152.20884	TL	5	8.8	8.8	44	39
07/11/07	JB	Simushir	Dushnaya Bay-100	47.07971	152.21016	TL,HLT	1	13.3	-	68	-
07/08/07	JB	Ketoi	Yuzhni Bay-3	47.29640	152.49141	HLT	9	6.8	6.5	44	27
07/08/07	VMK	Ketoi	Yuzhni Bay-10c	47.29659	152.49009	HL	1	6.7	-	79	38
07/08/07	VMK	Ketoi	Yuzhni Bay-13	*47.29774*	*152.48760*	HL	1	9.2	-	67	43
08/10/08	JB	Ketoi	SE coast-V111	47.29801	152.50985	HL	1	11.2	-	44	46
07/08/07	JB	Ketoi	Yuzhni Bay-2	47.29807	152.48616	HLT	9	7.3	7.4	58	54
08/10/08	JB	Ketoi	SE coast-V109	47.29816	152.50784	HL	1	10.2	-	80	49
07/08/07	JB	Ketoi	Yuzhni Bay-1c	47.29834	152.48416	HLT	16	7.5	6.7	55	51
08/10/08	JB	Ketoi	SE coast-V114	47.29867	152.51329	HL	1	10.1	-	47	42
07/08/07	JB	Ketoi	Yuzhni Bay-1b	47.29868	152.48257	HL	9	7.1	6.9	-	75
08/10/08	JB	Ketoi	SE coast-V116	47.29893	152.51373	HL	1	10.5	-	30	28
07/08/07	JB	Ketoi	Yuzhni Bay-1a	47.29924	152.48283	HLT	7	6.6	6.5	52	39

Date	Team*	Location				Method§	Runup			Inundation	
		Island	Locality name	Latitude of profile†	Longitude of profile†		Number of runup readings	Runup on profile (m)[%]	Runup average near profile (m)[%]	Measured inundation (m)	GPS calculated inundation (m)
07/11/07	VMK	Ketoi	Yuzhni Bay-73	47.29960	152.47238	HL	1	6.8	-	37	23
07/11/07	VMK	Ketoi	Yuzhni Bay-10b	47.29966	152.47368	HL	1	6.2	-	37	-
07/11/07	VMK	Ketoi	Yuzhni Bay-71	*47.29966*	*152.47368*	HL	1	6.2	-	37	-
07/11/07	VMK	Ketoi	Yuzhni Bay-69	47.29968	152.47460	HL	1	7.9	-	54	35
08/11/08	JB	Ketoi	SE coast-V121	47.29972	152.51536	HL	1	8.6	-	26	27
07/08/07	VMK	Ketoi	Yuzhni Bay-3b	47.29979	152.48218	HL	1	10.6	-	63	47
07/11/07	VMK	Ketoi	Yuzhni Bay-62	47.30022	152.47934	HL	1	6.0	-	37	18
07/11/07	VMK	Ketoi	Yuzhni Bay-67	47.30025	152.47754	HL	1	9.7	-	34	-
07/11/07	VMK	Ketoi	Yuzhni Bay-64	47.30033	152.47762	HL	1	10.4	-	42	22
07/11/07	VMK	Ketoi	Yuzhni Bay-61	*47.30043*	*152.48006*	HL	1	6.3	-	52	-
07/11/07	VMK	Ketoi	Yuzhni Bay-59	47.30047	152.48114	HL	1	6.8	-	67	37
08/11/08	JB	Ketoi	SE coast-V122	47.30130	152.51790	HL	1	11.9	-	41	45
08/11/08	JB	Ketoi	SE coast-V124	47.30271	152.52079	HL	1	11.1	-	55	63
08/11/08	JB	Ketoi	SE coast-V126	47.30438	152.52267	HL	1	11.5	-	72	60
08/11/08	JB	Ketoi	SE coast-V128	47.30534	152.52402	HLT	1	10.6	-	80	72
08/10/07	TKP	Ushishir	Yankicha-257	47.52596	152.82620	TL	2	13.6	13.5	57	70
08/09/07	TKP	Ushishir	Ryponkicha-238	47.53181	152.82719	TL	4	10.1	11.7	52	50
08/12/08	JB	Ushishir	Ryponkicha-V135	47.53207	152.82801	HLT	1	9.2	-	47	-
08/09/07	TKP	Ushishir	Ryponkicha-245	47.53244	152.82906	TL	5	11.4	11.2	56	55
08/09/07	NGR	Ushishir	Ryponkicha-185	47.53287	152.82868	HL	1	10.1	-	60	48
08/09/07	TKP	Ushishir	Ryponkicha-249	47.53324	152.83098	TL	3	11.6	11.2	46	42
08/09/07	TKP	Ushishir	Ryponkicha-251	47.53508	152.83231	TL	1	12.0	-	45	55
08/09/07	TKP	Ushishir	Ryponkicha-253	47.53632	152.83617	TL	5	12.1	11.0	50	47
08/09/07	TKP	Ushishir	Ryponkicha-255	47.53742	152.84057	TL	3	7.1	7.4	25	30
08/09/07	NGR	Ushishir	Ryponkicha-180	47.54934	152.85081	HL	1	5.7	-	54	47
08/09/08	BTM	Rasshua	SE coast-187	47.68511	152.97311	TL	3	10.3	10.5	46	48
08/08/08	BTM	Rasshua	SW coast-177	47.68617	152.96642	TL	1	6.9	-	38	57
08/08/08	BTM	Rasshua	SW coast-179	47.69037	152.96786	TL	1	7.6	-	42	41
08/09/08	BTM	Rasshua	SE coast-189	47.69040	152.97519	TL	3	9.6	10.0	99	93
08/09/08	BTM	Rasshua	SE coast-191	47.69449	152.97826	TL	5	11.2	11.2	84	75
08/08/08	BTM	Rasshua	SW coast-181	47.69501	152.96827	TL	4	7.1	7.4	50	52
08/09/08	BTM	Rasshua	SE coast-193	47.69648	152.98709	TL	1	10.9	-	57	53
08/11/07	NGR	Rasshua	SW coast-198	47.69893	152.96575	HL	1	5.0	-	66	-
08/11/07	NGR	Rasshua	SW coast-196	47.69963	152.96543	HL	1	4.2	-	64	-
08/08/08	BTM	Rasshua	SW coast-183	47.70066	152.96200	TL	1	5.0	-	73	74
08/11/07	JB	Rasshua	Landing cove-507	47.70630	152.96405	HL	1	9.4	-	56	53
08/10/08	BTM	Rasshua	Nepristupnaya Bay-195	47.70983	153.02418	TL	3	10.7	11.5	43	36
08/10/08	BTM	Rasshua	Nepristupnaya Bay-central	*47.71077*	*153.02597*	A	1	22	-	-	-
08/10/08	BTM	Rasshua	Nepristupnaya Bay-north	47.71166	153.02907	A	3	-	11	-	50
08/15/08	ACR	Rasshua	IMGG cove-V144	47.71964	152.97135	HLT	1	8.2	-	63	64
08/15/08	ACR	Rasshua	IMGG cove-V142	47.72330	152.97303	HLT	1	8.5	-	33	40
08/14/08	BTM	Rasshua	Severniy Cape-205	47.79095	153.04941	TL	4	10.5	10.6	51	34
08/11/08	BTM	Rasshua	Severniy Cape-201	47.79513	153.05030	TL	2	11.3	11.4	111	107
08/14/08	BTM	Rasshua	Severniy Cape-209	47.80009	153.04924	TL	3	12.2	12.4	75	78
08/11/08	BTM	Rasshua	Severniy Cape-203	47.80408	153.04496	TL	3	20.1	20.2	71	57
08/06/07	NGR	Matua	South Bay-153	48.03749	153.27090	HL	1	7.8	-	254	129
08/07/07	TKP	Matua	South Bay-222	48.03976	153.23971	TL	2	6.8	7.3	174	170
08/04/07	NGR	Matua	Ainu Bay-142	48.03980	153.22876	HL	1	12.9	-	164	128
08/07/07	TKP	Matua	South Bay-224	48.04023	153.24302	TL	1	5.7	-	215	219
08/06/07	NGR	Matua	South Bay-152	48.04034	153.26773	HL	1	7.8	-	147	126
08/07/07	NGR	Matua	Dvoynaya Bay-160	48.04124	153.27865	HL	1	7.3	-	56	55
08/07/07	TKP	Matua	South Bay-228	48.04127	153.24595	TL	1	7.1	-	233	205
08/02/07	NGR	Matua	Ainu Bay-126	48.04154	153.22731	HL	1	20.8	-	436	315
08/07/07	NGR	Matua	Dvoynaya Bay-161	48.04193	153.27764	HL	1	6.1	-	108	92
08/06/07	TKP	Matua	South Bay-216 (central)	48.04199	153.24922	TL	1	5.7	-	223	221
08/06/07	NGR	Matua	South Bay-151	48.04202	153.26372	HL	1	7.9	-	95	60
08/06/07	NGR	Matua	South Bay-148	48.04234	153.25296	HL	1	4.9	-	174	139
08/06/07	NGR	Matua	South Bay-149	48.04244	153.25585	HL	1	6.4	-	134	101
08/03/07	NGR	Matua	Ainu Bay-133	48.04266	153.22644	HL	1	20.2	-	503	417
08/06/07	NGR	Matua	South Bay-150	48.04267	153.25930	HL	1	5.7	-	176	146
08/06/07	BTM	Matua	Ainu Bay-2-2006 (south)	48.04269	153.22650	TL	6	18.2	18.1	432	411

Date	Team*	Location				Method§	Runup			Inundation	
		Island	Locality name	Latitude of profile†	Longitude of profile†		Number of runup readings	Runup on profile (m)[%]	Runup average near profile (m)[%]	Measured inundation (m)	GPS calculated inundation (m)
08/03/07	NGR	Matua	Ainu Bay-132	48.04284	153.22588	HL	1	18.3	-	398	376
08/07/07	NGR	Matua	Dvoynaya Bay-162	48.04349	153.27506	HL	1	8.1	-	109	116
08/04/07	BTM	Matua	Ainu Bay-1-2006 (north)	48.04412	153.22497	TL	1	17.1	-	327	313
08/03/07	NGR	Matua	Ainu Bay-130	48.04444	153.22463	HL	1	17.1	-	356	315
08/07/07	NGR	Matua	Dvoynaya Bay-164	48.04504	153.27429	HL	1	8.6	-	124	110
08/04/07	NGR	Matua	Ainu Bay-139	48.04537	153.22430	HL	1	18.1	-	315	288
08/05/07	NGR	Matua	Ainu Bay-143	48.04599	153.22315	HL	1	17.1	-	244	200
08/07/07	NGR	Matua	Dvoynaya Bay-165	48.04660	153.27397	HL	1	8.6	-	122	101
08/04/07	NGR	Matua	Ainu Bay-144	48.04707	153.22058	HL	1	14.0	-	120	119
08/07/07	NGR	Matua	Dvoynaya Bay-166	48.04751	153.27489	HL	1	9.6	-	56	56
08/04/07	NGR	Matua	Ainu Bay-145	48.04786	153.21894	HL	1	13.6	-	121	68
08/07/07	NGR	Matua	Dvoynaya Bay-167	48.04854	153.27534	HL	1	10.4	-	71	67
08/07/07	NGR	Matua	Dvoynaya Bay-170	48.04985	153.27407	HL	1	9.9	-	55	48
08/03/07	TKP	Matua	Dvoynaya Bay-142	48.05172	153.27181	TL	3	14.1	14.3	51	54
08/03/07	TKP	Matua	Dvoynaya Bay-145	48.05310	153.26861	TL	3	11.6	12.2	62	55
08/03/07	TKP	Matua	Dvoynaya Bay-147	48.05498	153.26675	TL	1	17.0	-	49	48
08/03/07	TKP	Matua	Dvoynaya Bay-149	48.05728	153.26618	TL	1	15.3	-	60	56
08/04/07	TKP	Matua	Dvoynaya Bay-152	48.05941	153.26706	TL	1	21.9	-	48	41
08/04/07	TKP	Matua	Dvoynaya Bay-154	48.06177	153.26918	TL	1	16.7	-	46	26
08/04/07	TKP	Matua	Dvoynaya Bay-157	48.06401	153.26918	TL	3	11.8	12.1	69	79
08/03/07	BTM	Matua	Dvoynaya Bay-86	48.06642	153.26921	TL,HLT	3	15.7	15.7	56	52
08/03/07	BTM	Matua	Dvoynaya Bay-83	48.06911	153.26872	TL	4	17.0	16.8	38	35
08/03/07	BTM	Matua	Dvoynaya Bay-79	48.07098	153.26668	TL	4	19.8	19.0	50	45
08/08/07	JB	Matua	Toporkov-231	48.07213	153.28239	HLT	2	9.3	9.3	40	40
08/08/07	JB	Matua	Toporkov-234	48.07238	153.28224	HLT	1	>8.0	-	37	42
08/03/07	BTM	Matua	Dvoynaya Bay-73	48.07340	153.26681	TL	1	18.1	-	93	106
08/08/07	JB	Matua	Toporkov-230	48.07375	153.28205	HLT	2	10.1	9.9	42	27
08/03/07	BTM	Matua	Dvoynaya Bay-69	48.07510	153.26518	TL	1	12.6	-	59	94
08/08/07	JB	Matua	Toporkov-235	48.07510	153.28164	HLT	1	11.3	-	28	26
08/08/07	JB	Matua	Toporkov-237	48.07637	153.28168	HLT	4	10.3	10.0	41	-
08/02/07	BTM	Matua	Dvoynaya Bay-136	48.07707	153.26329	TL	4	10.6	10.7	36	34
08/02/07	BTM	Matua	Dvoynaya Bay-133	48.07906	153.26357	TL	1	12.5	-	38	44
08/02/07	BTM	Matua	Dvoynaya Bay-129	48.08123	153.26444	TL	3	10.5	10.6	54	42
08/02/07	BTM	Matua	Dvoynaya Bay-125	48.08323	153.26612	TL	4	11.8	11.8	118	103
08/02/07	BTM	Matua	Dvoynaya Bay-120	48.08416	153.26740	TL	6	13.1	12.0	70	68
08/05/08	BTM	Matua	NE Bay-5	48.09483	153.24565	A	1	18	-	-	56
08/05/08	BTM	Matua	NE Bay-4	48.09620	153.24276	A	2	-	16	-	43
08/05/08	BTM	Matua	NE Bay-3	48.09751	153.24232	HL	3	-	14	-	36
08/05/08	BTM	Matua	NE Bay-2	48.09776	153.24250	A	3	-	13	-	47
08/05/08	BTM	Matua	NE Bay-1	48.09836	153.24240	A	1	10	-	-	43
07/22/08	BTM	Shiashkotan	Voskhodnaya Bay	*48.78556*	*154.08406*	A	20	-	5.5	-	60
07/22/08	JB	Shiashkotan	Voskhodnaya Bay-1	*48.78817*	*154.08586*	TL	1	7.1	-	56	-
07/23/08	BTM	Kharimkotan	1933 Landslide	*49.12374*	*154.60002*	A	7	-	3	-	400
07/31/08	BTM	Kharimkotan	Severgina Bay-south	49.16001	154.49450	A	3	-	5	-	30
07/31/08	BTM	Kharimkotan	Severgina Bay-north	49.16329	154.48074	A	2	-	6	-	66
07/27/08	BTM	Onekotan	Mussel Bay-south	49.38688	154.82825	A	4	-	5	-	36
07/27/08	BTM	Onekotan	Mussel Bay-central-A	49.38814	154.82450	A	3	-	4	-	127
07/27/08	BTM	Onekotan	Mussel Bay-central-B	49.38814	154.82450	A	1	8	-	-	41
07/27/08	BTM	Onekotan	Mussel Bay-north-A	49.38891	154.82392	A	1	4	-	-	180
07/27/08	BTM	Onekotan	Mussel Bay-north-B	49.38891	154.82392	A	3	-	6	-	123
07/26/08	BTM	Onekotan	Cape Lissii Bay-south	49.39499	154.82517	A	2	-	7	-	38
07/26/08	BTM	Onekotan	Cape Lissii Bay-central-A	49.39749	154.82366	A	1	5	-	-	125
07/26/08	BTM	Onekotan	Cape Lissii Bay-central-B	49.39749	154.82366	A	3	6	-	-	63
07/28/08	BTM	Onekotan	Cape Lissii Bay-north	49.40006	154.82539	A	1	8	-	-	27
07/30/08	BTM	Onekotan	Cape Lisii-lighthouse	49.40051	154.82888	A	3	-	7	-	38
07/28/08	BTM	Onekotan	Blakiston Bay-8	49.40144	154.81968	A	1	10	-	-	39
07/29/08	BTM	Onekotan	Blakiston Bay-9-A	49.40588	154.81512	A	1	5	-	-	158
07/29/08	BTM	Onekotan	Blakiston Bay-9-B	49.40588	154.81512	A	2	-	10	-	89
07/29/08	BTM	Onekotan	Blakiston Bay-9-C	49.40588	154.81512	HLT	1	8.5	-	83	89
07/28/08	BTM	Onekotan	Blakiston Bay-7-A	49.41474	154.81187	A	2	-	5	-	223
07/28/08	BTM	Onekotan	Blakiston Bay-7-B	49.41474	154.81187	A	2	-	11	-	114

Date	Team*	Location				Method§	Runup			Inundation	
		Island	Locality name	Latitude of profile†	Longitude of profile†		Number of runup readings	Runup on profile (m)%	Runup average near profile (m)%	Measured inundation (m)	GPS calculated inundation (m)
07/28/08	BTM	Onekotan	Blakiston Bay-6-A	49.42438	154.81009	A	1	5	-	-	200
07/28/08	BTM	Onekotan	Blakiston Bay-6-B	49.42438	154.81009	A	2	-	10	-	99
07/28/08	BTM	Onekotan	Blakiston Bay-5-A	49.43465	154.80873	A	4	-	8	-	159
07/28/08	BTM	Onekotan	Blakiston Bay-5-B	49.43465	154.80873	A	1	11	-	-	57
07/28/08	BTM	Onekotan	Blakiston Bay-4-A	49.44043	154.80874	A	4	-	5	-	430
07/28/08	BTM	Onekotan	Blakiston Bay-4-B	49.44043	154.80874	A	1	10	-	-	105
07/25/08	BTM	Onekotan	Blakiston Bay-3	49.45092	154.80956	A	4	-	4	-	311
07/25/08	BTM	Onekotan	Blakiston Bay-2-A	49.46020	154.81065	A	1	4	-	-	162
07/25/08	BTM	Onekotan	Blakiston Bay-2-B	49.46020	154.81065	A	1	6	-	-	77
07/25/08	BTM	Onekotan	Blakiston Bay-1	49.47269	154.81434	A	1	7	-	-	103

* Initials of team leaders: NGR (Nadezhda Razhigaeva), VMK (Viktor Kaistrenko), JB (Joanne Bourgeois), TKP (Tatiana Pinegina), BTM (Breanyn MacInnes), ACR (Andrew Ritchie)

† Lat/Long at sea level unless italic

§ Method: TL (transit level and rod), HLT (hand level, rod and tape), HL (hand level, rod for elevation and distance), A (altimeter (+/- 1 m error) and GPS)

% Runup values in italics are not correct for tide at time of measurement

- = unknown, not measured, or not applicable

Table 2.2: Average runup and inundation for each bay surveyed, differentiated by coastal geomorphology

Island	Locality name	Coastline type	Average runup (m)	Average inundation (m)
Urup	Cape Kastrikum	coastal plain	6.5	71
Chirpoi	Peschanaya Bay	short, steep	7.1	53
Simushir	Spaseniya Bay	coastal plain	5.2	106
Simushir	Opasnaya Bay	coastal plain	7.3	103
Simushir	Dushnaya Bay	coastal plain	8.1	121
Simushir	Dushnaya Bay	short, steep	12.6	65
Ketoi	Yuzhni Bay	short, steep	7.5	39
Ketoi	SE coast	short, steep	10.4	48
Ushishir	Yankicha, Ryponkicha	short, steep	10.4	49
Rasshua	SW coast	short, steep	7.0	59
Rasshua	SE coast	short, steep	10.4	67
Rasshua	IMGG camp	short, steep	8.9	52
Rasshua	Nepristurnaya Bay	short, steep	15.0	43
Rasshua	Severniy Cape	short, steep	13.6	69
Matua	Ainu Bay	coastal plain	17.0	268
Matua	South Bay	coastal plain	6.6	152
Matua	Toporkov Island	short, steep	9.8	35
Matua	Dvoynaya Bay	coastal plain	9.2	108
Matua	Dvoynaya Bay	short, steep	13.4	57
Matua	NE coast	short, steep	12.4	45
Shiashkotan	Voskhodnaya Bay	coastal plain	6.6	58
Kharimkotan	Severgina	short, steep	6.0	48
Kharimkotan	1933 landslide	other[$]	4	400
Onekotan	Mussel Bay	short, steep	6.7	67
Onekotan	Mussel Bay	other[#]	4.3	154
Onekotan	Cape Lisiy Bay	short, steep	8.8	58
Onekotan	Blakiston Bay	short, steep	9.1	86
Onekotan	Blakiston Bay	other[#]	5.3	215

[$] hummocky landslide topography

[#] narrow river valley

Table 2.3: Characteristics of onland effects of the 2006 Kuril tsunami for selected localities.

Island	Locality name	Types of erosion*	Distance between erosion and max inundation (m)	Sandy deposit noted?	Deposit volume (m^3/unit width)	Distance between deposition and max inundation (m)	Tsunami *ishi*, min. distance moved (m)	Evidence of smaller tsunami wave
Simushir	Dushnaya Bay-100	SB, SS	~0	yes	-	30	no	no
Simushir	Dushnaya Bay-101	SS, SC	10	yes	-	-	no	no
Simushir	Dushnaya Bay-102	SS, SC	13	yes	1.4	4	no	yes
Simushir	Dushnaya Bay-103	SS, SC	34	no	-	-	no	yes
Simushir	Dushnaya Bay-104	SB, SS, SC	10	yes	-	21	no	yes
Simushir	Dushnaya Bay-105	SB, SS, SC	14	yes	-	20	yes, 30	no
Simushir	Dushnaya Bay-106	SB, SS, SC, B	6.5	yes	-	-	yes	yes
Simushir	Dushnaya Bay-107	SB, SS, SC, P	13	no	-	-	yes	no
Simushir	Dushnaya Bay-108	SC, B, P	18	yes		10	yes	no
Simushir	Dushnaya Bay-109	SS, B, P	18	yes	0.4	13	yes, 10	no
Simushir	Dushnaya Bay-1-2006	SS, SC, B	1	yes	-	3	yes, 85	yes
Simushir	Dushnaya Bay-110	SS, SC, B	40	yes	-	-	no	yes
Simushir	Dushnaya Bay-12	SS, B	57	yes	0.9	3	no	yes
Simushir	Dushnaya Bay-2-2006	B	70	yes	1.2	2	no	yes
Simushir	Dushnaya Bay-9	SS, B	-	yes	3	0	no	no
Simushir	Dushnaya Bay-7	SS, B	-	yes	1.7	0	no	yes
Simushir	Dushnaya Bay-6	-	-	yes	1.2	0	no	yes
Simushir	Dushnaya Bay-2	SS, B	15	yes	0.9	3	no	no
Ketoi	Yuzhni Bay-1a	-	-	no	-	-	no	yes
Ketoi	Yuzhni Bay-1b	SB, SS	7.5	no	-	-	no	no
Ketoi	Yuzhni Bay-1c	SB, SS, SC	3.6	no	-	-	yes	no
Ketoi	Yuzhni Bay-2	SS	8	no	-	-	no	no
Ketoi	Yuzhni Bay-3	SC	0	no	-	-	no	no
Ushishir	Yankicha-257	SC	15	yes	-	9	no	no
Ushishir	Ryponkicha-238	SC, B	12	no	-	-	no	no
Ushishir	Ryponkicha-245	B	29	no	-	-	yes	no
Ushishir	Ryponkicha-253	SB	8	no	-	-	no	no
Ushishir	Ryponkicha-255	SS SC, SB	6	no	-	-	no	no
Ushishir	Ryponkicha-249	B	10	no	-	-	no	no
Ushishir	Ryponkicha-251	SC	13	no	-	-	no	no
Rasshua	Landing Cove-507	SC	8	no	-	-	no	no
Matua	Dvoynaya Bay-120	SS, SC, B	11	yes	-	14	no	no
Matua	Dvoynaya Bay-125	SS, SC, B, P	9	yes	1.3	9	no	no
Matua	Dvoynaya Bay-129	T, SS, SC, B	2.5	no	-	-	yes	no
Matua	Dvoynaya Bay-133	T, SS, SC	3	yes	-	-	yes, 10	no
Matua	Dvoynaya Bay-136	T, SS	2	no	-	-	no	no

Island	Locality name	Types of erosion*	Distance between erosion and max inundation (m)	Sandy deposit noted?	Deposit volume (m^3/unit width)	Distance between deposition and max inundation (m)	Tsunami *ishi*, min. distance moved (m)	Evidence of smaller tsunami wave
Matua	Dvoynaya Bay-69	T, SS, SC, B	5	yes	-	6	yes, 5	no
Matua	Dvoynaya Bay-73	T, SC, B	13	yes	-	34	yes, 40	no
Matua	Dvoynaya Bay-79	T, SC	5	no	-	-	yes, 20	no
Matua	Dvoynaya Bay-83	T, SS, SC	4	no	-	-	no	no
Matua	Dvoynaya Bay-86	SS, SC	4	yes	-	12	yes, 15	yes
Matua	South Bay-216	SS, B	60	yes	3.4	4	no	no
Matua	Ainu Bay-1-2006	SS, SC, B	10	yes	4.8	15	yes	yes
Matua	Ainu Bay-2-2006	SS, SC, B	6	yes	6.3	10	yes, 50	yes
Matua	Toporkov-237	T, SC	11	no	-	-	no	no
Matua	Toporkov-235	T, SC, B	2	no	-	-	no	no
Matua	Toporkov-230	T, SC	-	no	-	-	no	no
Matua	Toporkov-231	T, SC	3	no	-	-	no	no
Matua	Toporkov-234	T, SS, SC	1.5	no	-	-	no	no

*types of erosion:

T	trim line
SB	slope-base erosion
SS	soil stripping
SC	scours
B	beach erosion
P	rock plucking

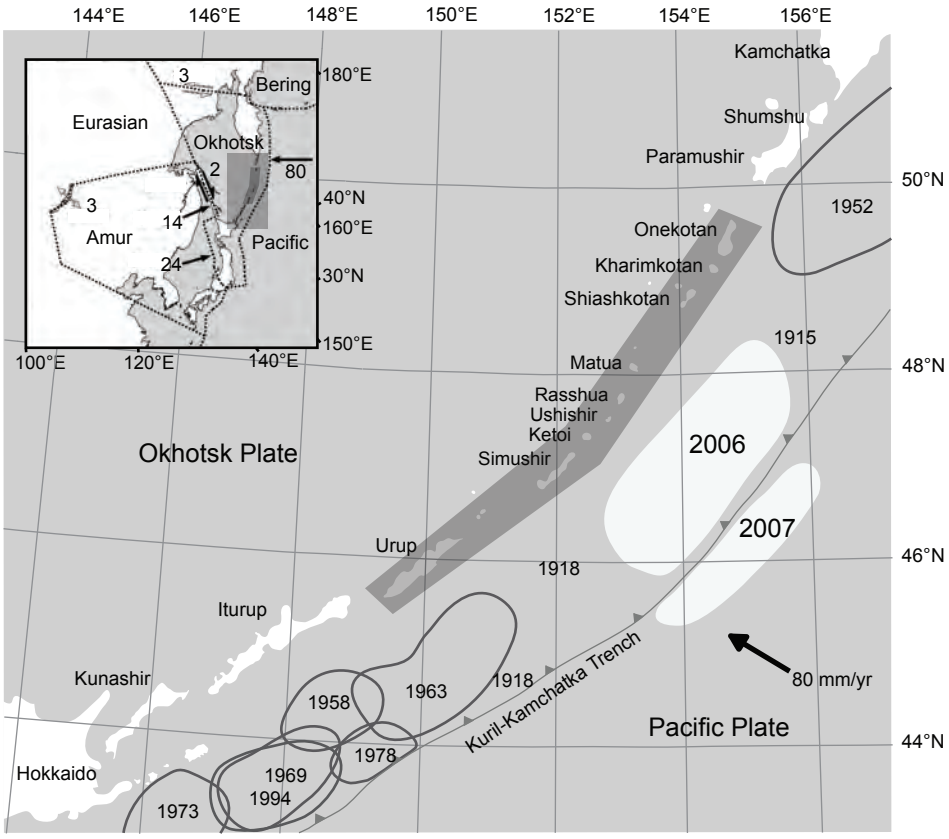

Figure 2.1: Tectonic setting of the Kuril Islands. Includes all historical tsunamigenic earthquakes with known source regions (after Fedotov et al., 1982). Inset in the upper left: Plate tectonic map of the region including plate motions, after Apel et al. (2006). Measured plate motions are in mm/yr.

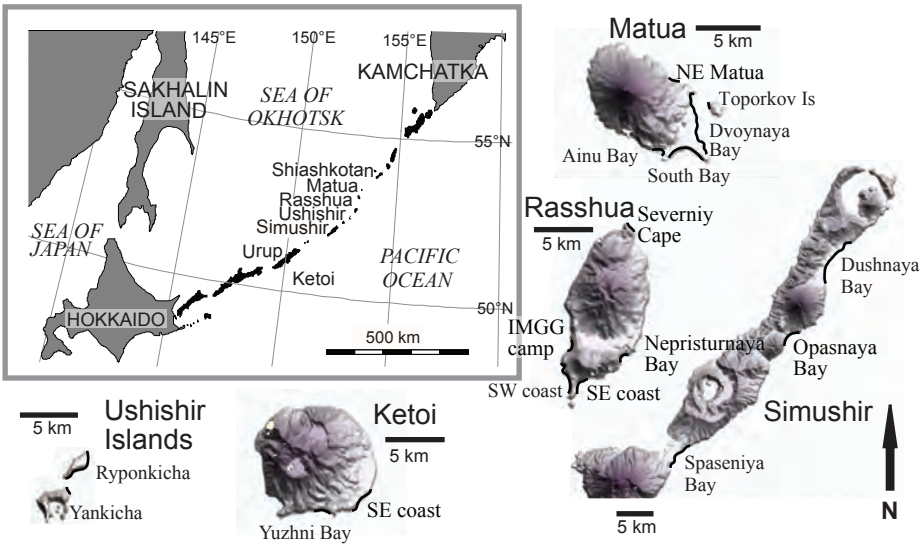

Figure 2.2: Overview of the basic morphology of central Kuril Islands surveyed in 2007 and 2008, including site names from Table 2.1. The scale bar for each island is 5 km.

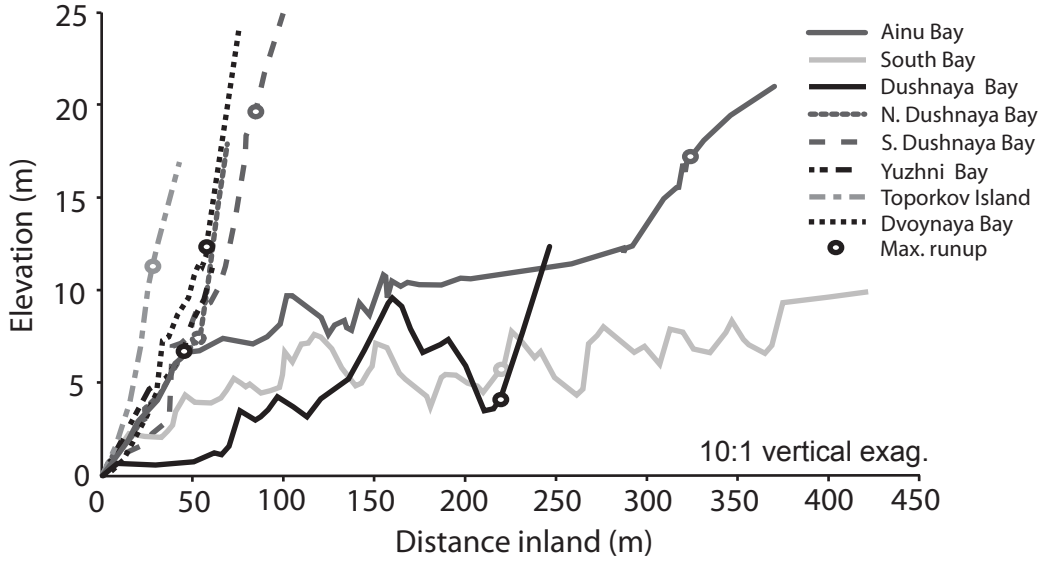

Figure 2.3: Example profiles that illustrate differences among short, steep coastlines (dashed lines) and broad coastal plains (solid lines). The Dushnaya Bay profile is an example where maximum runup elevation is less than maximum elevation seaward on the profile.

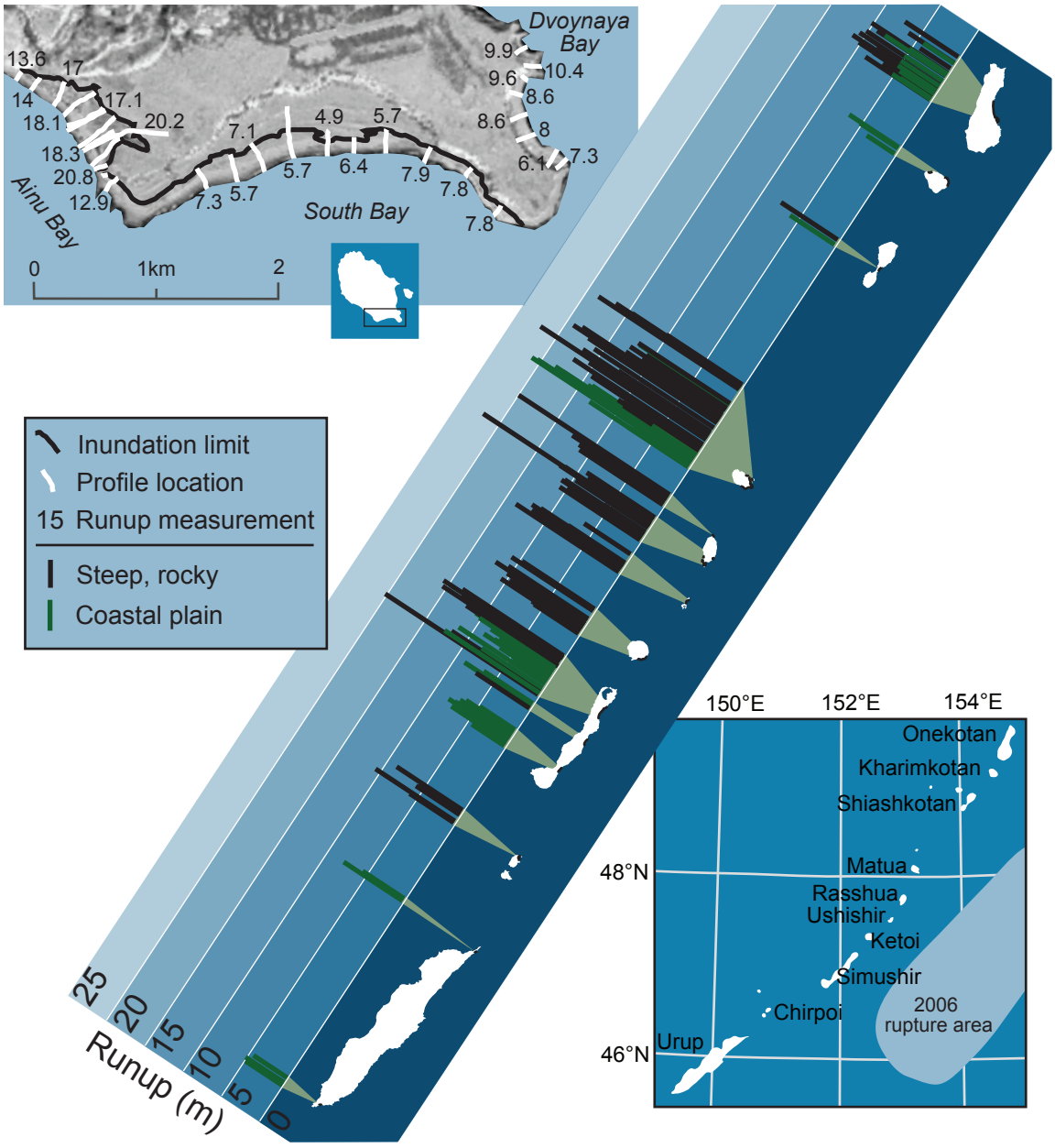

Figure 2.4: Summary of maximum runup of the 15 November 2006 tsunami, by location, for 192 field measurements. Values are categorized by the regional coastal geomorphology (refer to Figure 2.3). Inset upper left: Detailed map of inundation and runup for southern Matua Island. Inset lower right: Location of the survey area.

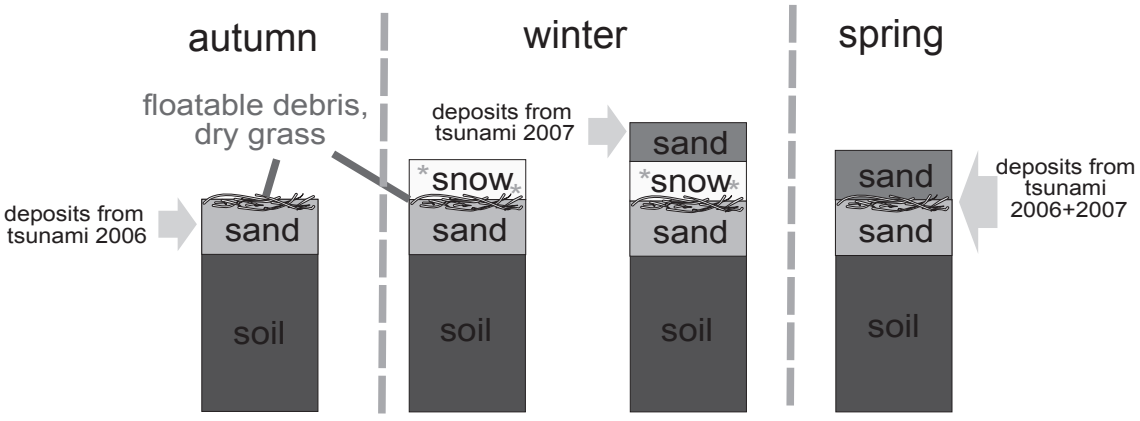

Figure 2.5: Schematic diagram of how the stratigraphic relationship of the 15 November 2006 and 13 January 2007 tsunami deposits appeared in the field. Snow that fell after the first tsunami would bury the 2006 deposit, floatable debris, and any vegetation still standing. The snow is not necessarily eroded in all locations by the second tsunami, and the resulting complex deposit has a thin layer of debris and vegetation in the middle.

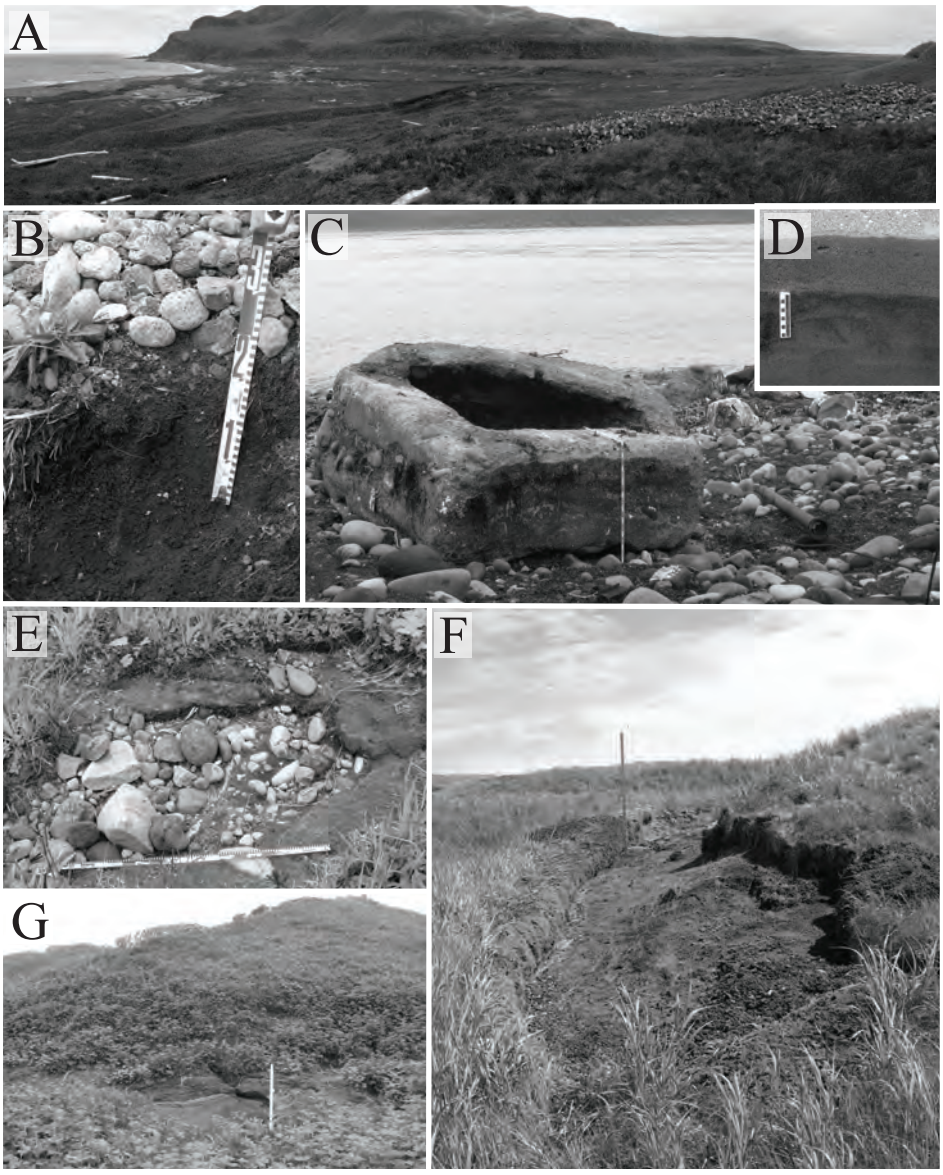

Figure 2.6: Deposition and erosion from the 15 November 2006 tsunami as observed in the central Kurils. A: Ainu Bay, Matua, which experienced the maximum amount of inundation we observed (400-500 m). White flecks in the distance are large logs moved by the tsunami. B: A deposit of pebbles on top of soil and turf in Dushnaya Bay, Simushir (near profile 105). New vegetation is beginning to grow through. Measuring tape is 30 cm. C: A tsunami ishi, which was once an artificial structure offshore, with kelp holdfasts and bryozoan communities still attached. Measuring tape is 1 m. Dvoynaya Bay, Matua, profile 83. D: Continuous sand sheet from Ainu Bay, Matua, Profile 2. Here, the deposit is the thickest observed anywhere (at 20 cm thick) and is filling a drained lake bed. E: A scour pit in Dushnaya Bay, Simushir, Profile 106. Direction of flow was from right to left. Measuring tape is 1 m. F: Soil stripping in Ainu Bay, Matua, Profile 2. Turf and soil are still attached, but flipped over on the left (landward). The rod is 2 m high. G: Slope-base erosion in Dushnaya Bay, Simushir, Profile 107. The rod is 2 m high.

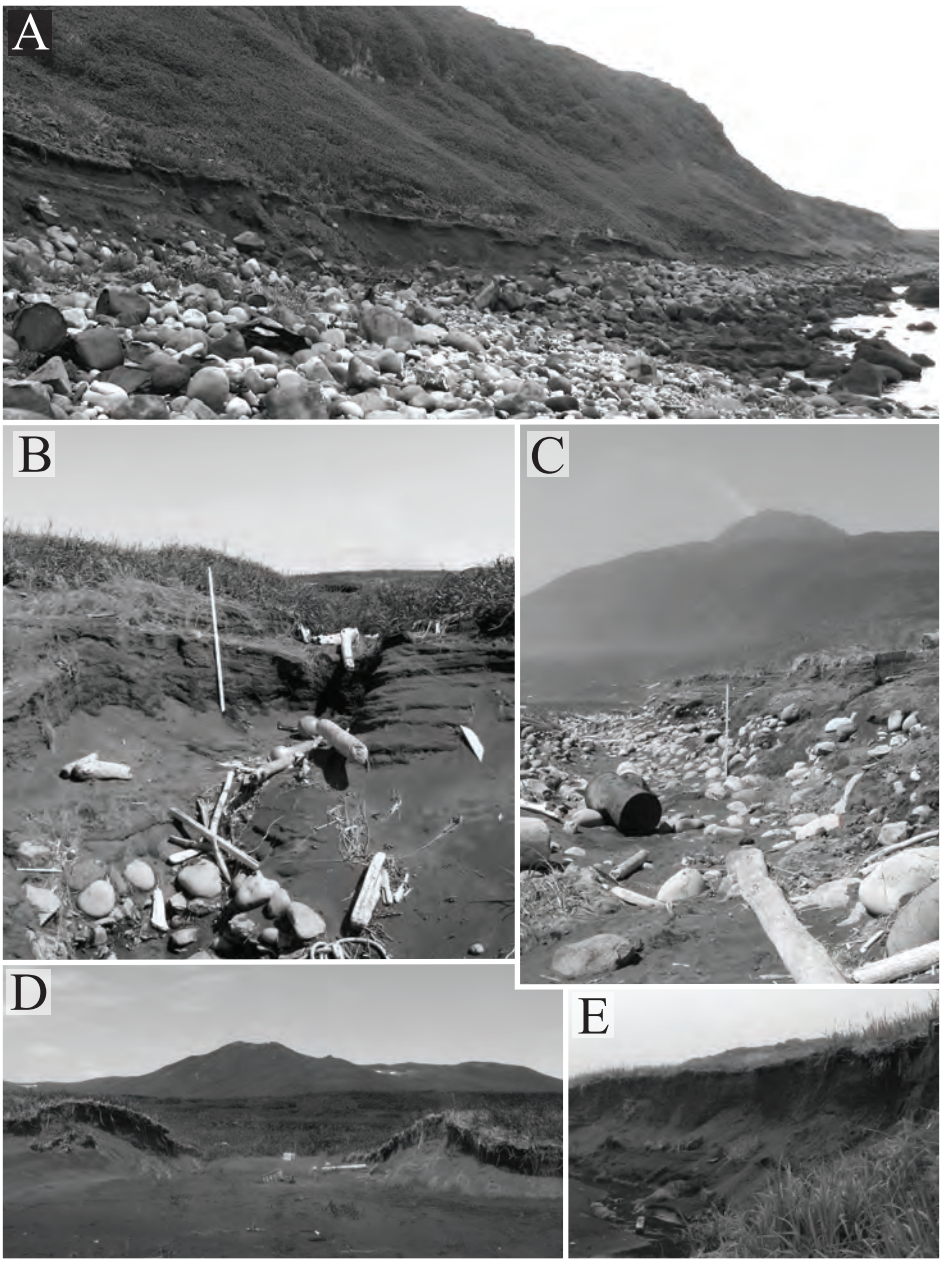

Figure 2.7: Examples of kinds of erosion from the 15 November 2006 tsunami as observed in the central Kurils. A: Trim line in Dvoynaya Bay, Matua. B: Gullying from outflow, Ainu Bay, Matua, Profile 2. Rod is 2 m high. C: Large-scale scour that extends >100 m laterally, in Ainu Bay, Matua, Profile 1. Rod is 2 m high. D: Breach through the first beach ridge in central Dushnaya Bay, Simushir, near Profile 10. Shovel in center of photo is ~1.5 m high. E: *En masse* erosion of a stream channel wall in Dushnaya Bay, Simushir, near Profile 12. Bank height is ~4 m, and the cliff was eroded back ~ 3 m between 2006 and 2007.

CHAPTER 3

Tsunami geomorphology: erosion and deposition from the 15 November 2006 Kuril Island tsunami

Disclaimer

This chapter was first published in the journal *Geology* with the following citation:

MacInnes, B.T., Bourgeois, J., Pinegina, T.K., and Kravchunovskaya, E., 2009b, Tsunami geomorphology: erosion and deposition from the 15 November 2006 Kuril Island tsunami: Geology, *v. 37, p. 995-998.*

Copyright permission has been obtained for the contents of the article to appear in this dissertation. The only modifications to the original article are the removal of the abstract and acknowledgements, and the insertion of all electronic supplementary material into the text. Figures 3.10 and 3.12 were originally drafted by Joanne Bourgeois; Figures 3.4B and 3.13 were originally drafted by Tatiana Pinegina. The assumption presented here that the 2006 tsunami was universally larger than 2007 does not incorporate conclusions from the tsunami modeling presented in Chapter 4, as that work had not begun when this chapter was published.

Introduction

To study the full impact of tsunamis on coastal geomorphology, it is essential to understand their role in both addition and removal of coastal sediment. However, most studies of tsunami geology have focused on tsunami deposition rather than erosion (Bourgeois, 2009). Yet on certain coastlines, tsunamis may be important geomorphic agents,

causing long-term changes in coastal systems. Pre- and post-tsunami measurements of coastal geomorphology are necessary in order to calculate coastal change and sediment movement during a tsunami— topics of utmost interest to the tsunami community (cf. Gelfenbaum and Jaffe, 2003; Jaffe and Gelfenbaum, 2007; Huntington et al., 2007) and of broad interest to coastal geomorphologists (Dawson, 1994; Kench et al., 2008).

Tsunami-induced erosional changes of coastlines have been difficult to quantify because pre-event controls are lacking (cf. Dawson, 1994; Choowong et al., 2007; Umitsu et al., 2007). To date, the only quantified before-and-after studies are beach profiles and atoll-island surveys from the 2004 Indian Ocean tsunami in southwestern India and the Maldives (Kurian et al., 2006; Kench et al., 2006; 2008). Also, Gelfenbaum and Jaffe (2003) estimated depth of erosion by the 1998 Papua New Guinea tsunami from exposed tree roots.

Despite the few quantified studies, many qualitative observations suggest that most tsunami-induced changes in coastal geomorphology are driven by erosion, during either inflow or outflow. Erosional changes to a landscape can be temporary (Kurian et al., 2006), permanent (Andrade, 1992), or continue an ongoing trend (Kench et al., 2006, 2008). Tsunamis remove vegetation and damage man-made structures (Dawson, 1994; Maramai and Tinti, 1997). Tsunami erosion causes beach retreat either as large-scale scour features or as smaller scallops (Dawson, 1994; Gelfenbaum and Jaffe, 2003; Kench et al., 2006; Kurian et al., 2006; Umitsu et al., 2007; Choowong et al., 2007). Tsunamis breach beach berms and other ridges, or erode the surface uniformly (Andrade, 1992; Dawson, 1994; Maramai and Tinti, 1997; Gelfenbaum and Jaffe, 2003; Choowong et al., 2007; Umitsu et al., 2007). They also alter drainage patterns by widening river mouths and creating new drainage networks,

especially from topographic lows (Andrade, 1992; Maramai and Tinti, 1997; Umitsu et al., 2007).

From a geologically fortuitous series of field seasons bracketing the 15 November 2006 Kuril Island tsunami, we have been able to quantify tsunami erosion as well as deposition. In four examples of detailed topographic profiles from before and after the tsunami, as well as in numerous post-tsunami study sites, erosion was the primary response of the coastline to the 2006 tsunami in the Kuril Islands. Dominant motion of sediment was offshore, resulting in significant alteration of coastal geomorphology in some areas.

Background

We surveyed coastlines on the Kuril Islands in summers of 2006-2008, focusing on paleo-tsunami records and coastal geomorphology as a part of the multi-disciplinary Kuril Biocomplexity Project (KBP). The Kurils are a volcanically active arc with many small islands in the central region (Figure 3.1). Accordingly, dominant coastal geomorphologies are rocky cliffs or boulder to gravel beaches, with some sandy embayments.

Between our first and second field seasons, the 15 November 2006 earthquake (M_w 8.1 – 8.4) in the Kuril-Kamchatka subduction zone (Figure 3.1) produced a large tsunami (Fujii and Satake, 2008; Ammon et al., 2008). Following the November events, an outer-rise earthquake occurred on 13 January 2007 (M_w 7.9–8.1), adjacent to the 2006 rupture zone (Ammon et al., 2008; Fujii and Satake, 2008), also generating a tsunami. These tsunamis partially refocused our field efforts in 2007 and 2008 to include post-tsunami surveys and detailed examination of tsunami-caused change.

Until our post-tsunami surveys, there were no runup data from the uninhabited central Kuril Islands. However, around the Pacific Rim, tide gauges recorded tsunami amplitudes from the November 2006 event (archived for 113 locations by the National Geophysical Data Center (NGDC) Global Tsunami Database), ranging from <0.1 m (Solomon Islands) to 1.76 m (Crescent City, CA). The ensuing (January 2007) tsunami was on average three times smaller than the 2006 tsunami on tide gauges in the NGDC database.

Methods

Our 2006 (pre-tsunami) survey focused on open embayments where paleo-tsunami records could be preserved, limiting quantified pre- and post-tsunami comparisons to three sandy beach-ridge plains open to the Pacific—Dushnaya Bay on northern Simushir Island, and South Bay and Ainu Bay on Matua Island (Figures 3.1 and 3.2). All contain beach ridges greater than 5 m above mean sea level. These sites are vegetated primarily with beach rye (*Elymus arenarius*) and coastal-meadow grasses and flowers. All three sites were trenched by military in WWII, which locally allowed enhancement of tsunami erosion and deposition; for the purpose of this study, we avoided these anthropogenic effects where possible.

Post-tsunami survey teams in summers of 2007 and 2008 documented tsunami inundation (local maximum penetration distance), runup (elevation above mean sea level at inundation), erosion, and deposition. We surveyed 9 sites visited in 2006 or earlier, and 18 new sites, measuring in total 192 runup transects along a distance of ~600 km (Figure 3.1; Table 2.1) We identified tsunami inundation and runup by the farthest inland wrackline of floatable debris. Nearfield measurements of tsunami runup average 10 m and range up to 22 m (Table 2.1).

We quantified erosional change on four 2006 topographic profiles (Figures 3.3 and 3.4) by re-measuring the profiles using a transit and rod; to relocate we used a combination of landmarks such as trenches and ridge crests, and GPS. On many other profiles, we described and recorded the position of erosional features, measured thicknesses of tsunami deposits, and documented the deposit's landward-most extent (Table 3.1).

Volume of erosion and deposition

In cases where we could quantify the volume of erosion or deposition along a profile (reported as m^3 per unit width), we plotted those estimates relative to runup and to runup times inundation, the latter an approximation of onland tsunami volume (Figure 3.5). We calculated the volume of tsunami erosion along a profile by measuring the area missing in 2007/2008 below profile lines measured in or reconstructed from 2006 (e.g. Figure 3.3). We calculated deposit volume along a profile by taking measured thickness of fresh tsunami deposits at survey points (as in Figure 3.3) and integrating between them to generate the cross-sectional area covered by tsunami deposit along a given profile. We assigned ±10% error to the calculations. There is not a robust correlation of runup to volume of erosion and deposition for runup of less than 13 m (Figure 3.5A); the higher runup in Ainu Bay clearly produced greater geomorphic change. There is a better trend shown by comparing erosion and deposition volumes to runup times inundation (Figure 3.5B), which is a better overall scale of tsunami size. In Figure 3.5B, however, there is an even larger gap between the high numbers of Ainu Bay and the rest of the data.

Were all observed changes from the 2006 tsunami?

Because 10 months (September-June) passed between field observations, we must address the question of whether the 2006 tsunami was the primary cause of observed changes. Other possible agents acting during these unobserved periods include the 2007 Kuril tsunami, erosion and deposition due to storms, and seasonal beach-profile variations. We reason that 2006 did cause most observed changes, based on the smaller size of the 2007 tsunami, on the fact that the 2007 tsunami occurred when the shoreline was frozen, and on the lack of large regional storms between field seasons.

We reason that the 2007 Kuril tsunami had little impact on the coastline because of its relative size and because of the time of year (Chapter 2). Field observations suggest that the 2007 Kuril tsunami had runup of less than 5 m (Chapter 2), making its influence on much of the vegetated coastline negligible. Moreover, the average temperature in the central Kurils between the 2006 and 2007 tsunamis was -3 to -6 ºC[7], potentially resulting in a frozen upper beach and coastal plain at the time of the 2007 tsunami, inhibiting marked erosion.

We also reason that all measured change above and most measured change below storm high tide (defined by the presence of dense vegetation and seaweed wracklines) resulted from the 2006 tsunami and not from storms. Storms affecting the coasts of Kurils in 2006, 2007, and 2008 were not abnormally large and therefore likely did not cause measurable changes above storm wracklines observed in 2006 or on the vegetated coastal plain. Wind-speed reanalysis records suggest no unusual storms occurred in the field area between the pre- and post- tsunami surveys (Figure 3.6). Also, in 2007 and 2008 surveys we

[7] Based on four-times daily temperature records; NCEP Reanalysis data provided by the NOAA/OAR/ESRL PSD, Boulder, Colorado, USA, from their website at http://www.cdc noaa.gov/

observed no fresh storm effects beyond the beach on coastlines where the tsunamis also did not surpass the beach.

Below storm high tide, beaches may actively change (cf. Shepard et al., 1950), and in our study, we did not measure winter-beach profiles, but we argue that the 2006 tsunami is also responsible for most beach-profile changes because the beaches did not recover between 2007 and 2008 (Figure 3.7).

Observations

The 2006 Kuril Island tsunami altered the coastline of the central Kurils in sandy embayments and on boulder beaches. The three sandy embayments focused on in this study—Dushnaya, South and Ainu bays—experienced a range of tsunami size, from low runup (<8 m) to high (>15 m) and exhibited a range of erosional and depositional features.

We observed a greater volume of erosion and deposition where runup was higher (Table 3.1; Figure 3.5) and fewer erosional features where runup was lower. In Dushnaya Bay, the tsunami was smaller in the center (Figure 3.1), with runup of 5–20 m and inundation of 40–150 m (Table 2.1). Central Dushnaya Bay, the location of a before-and-after profile (Figure 3.6A), recorded ~6-9 m runup and ~100-150 m inundation; erosion was limited and a sand sheet preserved (Table 3.1). Runup in South Bay was low (5–8 m), with inundation of ~100–200 m (Table 2.1). We found tsunami deposits almost as far as water carried debris, with patches of erosion on vegetated beach ridges (Figure 3.3B; Table 3.1). In Ainu Bay, runup was typically 14–20 m, with inundation up to ~500 m (Table 2.1), generating massive erosion, with erosional patches extending farther inland than we found tsunami deposits (Table 3.1).

Illustrations of tsunami effects

While the Dushnaya Central profile (Figure 3.3) on Simushir Island was virtually unchanged across its vegetated surface (Figure 3.8), the tsunami rearranged the beach and locally eroded the beach scarp (Figure 3.9). In northern Dushnaya Bay, runup was higher, with common stripping of turf and soil (Figure 3.10) and deposition of gravel (Figure 3.11). In southern Dushnaya Bay, a very steep, sandy profile exhibited dramatic local erosional scours and enlarged drainage (Figure 3.12). The effects on the shoreline along South Bay, Matua Island (Figure 3.13), were similar to Central Dushnaya Bay, with a greater volume of beach erosion (Figure 3.3; Table 3.1). The most dramatic tsunami effects were in Ainu Bay on Matua Island, where stratigraphic analysis suggests tsunamis may have repeatedly produced coastal erosion (Figure 3.14). In the north, young landforms from the beach to 160 m inland were removed or denuded (Figure 3.15) and a long scour developed at the boundary between older and younger landforms (Figure 3.16). In the south, erosion was also severe, especially close to the shoreline (Figure 3.17).

Sediment removal and erosional features

Low runup

Erosion in central Dushnaya Bay (Figures 3.3, 3.4, 3.8) can be generalized as small-scale retreat of the back-beach scarp (Figure 3.9), surficial sediment removal in areas lacking cohesive soils, and local scour associated with focused water withdrawal, especially into stream channels. At one point, the tsunami breached the seaward beach ridge. Comparison of before and after profiles (Figure 3.3A) could not resolve landward retreat of the beach scarp, although nearby we measured up to 3 m of retreat. The only quantifiable change on the

profiles was on the unvegetated beach (Figure 3.3A), where ~5 m^3 (per unit width) of sediment had been removed between 2006 and 2007 (Table 3.1).

In South Bay, before and after profiles (Figures 3.3B, 3.13) show a significant difference in the active beach, with ~50 m^3 (per unit width) of sediment missing in 2007. In beach-ridge troughs along the profile, our 2006 excavated turf blocks and some flagging tape remained virtually undisturbed in 2007. Small, shallow patches of erosion on high points up to 160 m inland (Table 3.1) and larger ones elsewhere in South Bay were on seaward sides of beach ridges. Along the shoreline away from the profile, the tsunami removed blocks of turf off the back-beach scarp.

High runup

Much of the erosion in Ainu Bay can be considered persistent geomorphic change (Figures 3.14–3.17). The tsunami removed ~200 m^3 (per unit width) of sediment along the Ainu Bay reoccupied profiles (Figure 3.3C,D, Table 3.1). On both profiles, continuous, deep erosion of vegetation and sediment occurred for ~160 m inland, including landward widening of the beach by up to 55 m (Figures 3.2, 3.3D) via back-beach cliff retreat. The tsunami removed seaward-most beach ridges, reduced others in size, and eroded seaward-facing slopes primarily by stripping young, sandy sediment off the surface (Figure 3.3C,D). As a particular example, a continuous scour extending over 100 m laterally formed on a seaward-facing slope of compact soil (at 160 m inland in Figure 3.3C; Figure 3.16).

Throughout Ainu Bay, smaller-scale but still dramatic erosion included patches of eroded soil and stripped vegetation up to 5 m in diameter. Eroded patches were especially associated with rodent burrow networks and volcanic cinder layers below the sod, both of

which facilitated soil stripping. These patches were common at the bases of slopes, some even landward of a recognizable tsunami deposit (Table 3.1). In areas with sandy soils, gullying and scouring were common where the tsunami was steered by low-lying topography. The tsunami also breached and drained a lake (Figure 3.3D, 3.17). Most indicators of flow direction, such as plunge pools and gullies, primarily recorded outflow; some, such as a flipped-over sod, recorded inflow.

Sediment deposition

Irrespective of tsunami runup height and inundation distance, there was evidence of deposition on all studied sites (Figure 3.3; Table 3.1). Where sand was available along the shore, the tsunami deposited a landward thinning, continuous sheet of that sand across vegetated surfaces. Sand deposits averaged 2.5 cm thick (20 cm maximum) and were generally thicker in beach-ridge troughs than on crests. Along the sandy beach ridges of Dushnaya, South and Ainu bays, the tsunami added a thin veneer of sediment, ~1-6 m^3 per unit width of profile (Table 3.1). Shorelines along boulder to gravel beaches exhibited patchy tsunami deposits of pebbly gravel, and relocated cobbles and boulders generally <1 m diameter. On most shorelines, the tsunami eroded and deposited blocks of sod, more abundant and larger (up to 3 m diameter) on coarser-grained shorelines.

Sandy tsunami deposits were nearly as extensive as the tsunami (Table 3.1). The maximum elevation of deposits was on average 90% of runup elevation, and never <71% (a case with limited sand supply). The landward terminus of the deposit averaged 95% of tsunami inundation (as marked by floated debris); the horizontal difference was <10 m in nine cases, and at most 22 m (Table 3.1).

Deposition versus erosion

Even with ubiquitous deposition, less sediment was deposited than eroded on every profile studied in detail. In the eight cases with measured volumes (per unit width) of both erosion and deposition, the amount of tsunami-transported sand preserved on the coastal plain was usually <10% of that eroded (Table 3.1); only one of those profiles exhibited focused erosion (Profile 2 in Dushnaya Bay; Figures 3.4, 3.12). Even in Dushnaya Bay, where the tsunami was the smallest, erosion the least, and deposition the most extensive, about three times more sediment was removed from the coast then deposited on land.

Discussion and conclusions

Our survey of tsunami deposits in the Kuril Islands strengthens the argument that on sandy shorelines tsunami-deposit extent can be used as proxy for tsunami runup and inundation (Table 3.1; Martin et al., 2008), provided the pre-tsunami shoreline position can be reconstructed. Recent post-tsunami studies of low-relief coastlines have shown that tsunami deposits commonly extend to 90% of water runup and inundation limits (Table 3.2). On the high-relief coastlines of the Kuril Islands, tsunami deposits are equally representative of onshore tsunami metrics.

The volume of tsunami erosion is related to tsunami runup, distance from shore, and topography; vegetation and local roughness can clearly be factors as well, but in our study they do not measurably vary. That greatest erosion from tsunamis occurs closer to the shore is a common observation of post-tsunami surveys (cf. Gelfenbaum and Jaffe, 2003; Umitsu et al., 2007). Farther from the shore (100s of m in the Ainu Bay case), patches of erosion

typically occur where the topography generates local water acceleration, enhancing the erosive capacity of tsunamis.

Some erosional features generated by tsunamis should become preserved geomorphology. In Ainu Bay, the removal of the seaward beach ridges, breaching of a lake and development of inland scours should all be visible for decades or centuries. Indeed, previous (undated) instances of deep coastal erosion and breached lakes can be seen in Ainu Bay stratigraphy (Figure 3.14). Even in cases of relatively low runup, breached beach ridges should remain discontinuous, and we have observed such breaches in older beach ridges in Dushnaya Bay and also along the Pacific coast of Kamchatka.

Our findings agree with previous studies indicating that net direction of tsunami sediment transport is dependent on capacity of the coastline to generate backwash or offshore flow (Umitsu et al., 2007). Tsunamis flowing over low-relief coastlines (Kurian et al., 2006; Gelfenbaum and Jaffe, 2003) generated net onshore transport. On high-relief coastlines such as the Kuril Islands, tsunami backwash can be accelerated to a greater velocity than on low-relief topography, thereby generating net offshore transport. The case where a tsunami completely overtops low-relief islands, as in the 2004 Indian Ocean tsunami washing over the low-relief Maldives, is more complex (Kench et al., 2008).

For the first time, a group of tsunami geologists surveyed a coast both before and after a large tsunami. Our quantitative comparison of erosional and depositional volumes in this case showed that erosion clearly dominated deposition. Nevertheless, geologists interpreting paleo-tsunamis should be reassured that deposits can be a reliable proxy for tsunami runup and inundation, though the necessary paleogeographic reconstruction remains challenging, especially in light of tsunami erosion. Our data and analyses are also significant

for geologists interested in understanding tsunami flow properties, in defining tsunami erosion and deposition patterns (tsunami geomorphology), and in determining coastal geologic histories in tsunami-affected regions. Moreover, while the central Kurils are currently uninhabited, this study may help explain why there are fewer coastal archaeological sites on the Pacific side of the Kurils. It also provides important information about tsunami hazard on high-relief coastlines around the world.

Table 3.1: Characteristics of the 15 November 2006 tsunami wave, sand deposits, and coastal erosion in the central Kurils Islands

Topographic profile*	Water limit		Approximate deposit volume (m^3)	Deposit limit		Approximate erosion volume (m^3)	Erosion limit	
	Runup† (m)	Inundation (m)		Vertical† (m)	Horizontal (m)		Vertical† (m)	Horizontal (m)
Dushnaya Bay central	6.7	122	1.2	6.6	120	5	5.1	55
South Bay	5.7 (7.6)	223	3.4	5.0 (7.6)	217	50	5.3 (7.6)	160
Ainu Bay north	17.1	327	4.8	14.8	305	200	16.3	310
Ainu Bay south	18.1	432	6.3	17.4	422	200	17.4	422
Dushnaya Bay-2	12.4	75	0.9	12.1	72	>50§	11.9	62
Dushnaya Bay-6	4.4 (10.3)	106	1.2	4.4 (10.3)	106	-	-	-
Dushnaya Bay-7	6.3	139	1.7	6.3	139	-	5.9	122
Dushnaya Bay-9	7.3 (12.6)	151	3.0	7.3 (12.6)	151	-	-	-
Dushnaya Bay-12	6.9	120	0.9	5.8	112	-	3.2	59
Dushnaya Bay-109	9.1	59	Little sand, 0.4	7.5	49	5§	5.6	41
Dushnaya Bay-106	13.0	70	Local gravel only	-	-	>5§	8.2	63
Dushnaya Bay-102	7.7	51	1.4	6.7	46	>5§	5.1	37
Sarychevo-125	11.8	118	1.3	8.4	97	-	9.5	102
NE Rasshua-201	11.4	111	1.4	10.2	109	5§	9.2	105

*See Figure 2.2 or Table 2.1 for locations

†(7.6) = Cases with higher topography seaward of runup

§Minimum estimates because beach change not measurable without pre-tsunami topography

- = not measured

Table 3.2: Data from surveys relating tsunami sediment distribution to tsunami runup and inundation

Ref.[&]	Tsunami	Name of profile or transect	Water inundation (m)	Water runup (m)	Sediment inundation (m)	Sediment runup (m)	% sed inundation (%)	% sed runup* (%)	Total relief † (m/m)	Max. relief (m/m)	Max. elevation (m)
1	1998 PNG	Waipo	320	1.25	280	1.5	88	120	0.004	0.150	3.2
1	1998 PNG	Arop	720	1.5	680	2	94	133	0.002	0.010	2.5
1	1998 PNG	Otto	160	-0.2	130	0.25	81	125	-0.001	0.150	0.75
1	1998 PNG	Sissano	575	1	575	1	100	100	0.002	0.027	3.1
2	2004 Indian Oc.	Jantang 3	665	19.7	628	4	94	20	0.030	0.432	19.7
3	1993 Hokkaido	Miyano, Taisei A	445	4.75	370	4	83	84	0.011	0.050	4.75
3	1993 Hokkaido	Miyano, Taisei B	460	5	420	4.5	91	90	0.011	0.050	5
5	1992 Nicaragua	Salina	425	2.2	425	2.2	100	100	0.005	0.110	2.75
5	1992 Nicaragua	Yellow house	380	2.5	320	2.4	84	96	0.007	0.067	3
5	1992 Nicaragua	Mangrove	300	1.8	230	1.75	77	97	0.006	0.081	3.25
5	1992 Nicaragua	Beach rock	362	2.2	300	2.15	83	98	0.006	0.107	3.5
4	2004 Indian Oc.	Thiruvidandai	330	6	300	4	91	67	0.018	0.092	6
4	2004 Indian Oc.	Vadanemmeli	220	3.75	220	3.75	100	100	0.017	0.017	3.75
4	2004 Indian Oc.	Kalpakkam	445	4	445	4	100	100	0.009	0.025	4
4	2004 Indian Oc.	§Mamallapuram	650	4.3	620	5	95	116	0.007	0.080	5
4	2004 Indian Oc.	Kadalore	70	4.2	70	4.2	100	100	0.060	0.150	4.2
6	1992 Flores Is.	#Lato	140	3.5	75	1.75	54	50	0.025	0.100	3.5
7	*2006 Kuril Island*	*Dushnaya 2006-2*	*122*	*6.7*	*120*	*6.6*	*98*	*99*	*0.055*	*1.500*	*6.7*
7	*2006 Kuril Island*	*Dushnaya Bay 2*	*75*	*12.4*	*72*	*12.1*	*96*	*98*	*0.165*	*4.840*	*12.4*
7	*2006 Kuril Island*	*South Bay-211*	*223*	*5.7*	*217*	*5*	*97*	*88*	*0.026*	*1.290*	*7.6*
7	*2006 Kuril Island*	*Ainu Bay 2006-1*	*327*	*17.1*	*305*	*14.8*	*93*	*87*	*0.052*	*1.040*	*17.1*
7	*2006 Kuril Island*	*Ainu Bay 2006-2*	*432*	*18.1*	*422*	*17.3*	*98*	*96*	*0.042*	*0.810*	*18.1*
7	*2006 Kuril Island*	*Dushnaya Bay-102*	*51*	*7.7*	*46*	*6.7*	*90*	*87*	*0.151*	*5.490*	*7.7*

Ref.[&]	Tsunami	Name of profile or transect	Water inundation (m)	Water runup (m)	Sediment inundation (m)	Sediment runup (m)	% sed inundation (%)	% sed runup* (%)	Total relief † (m/m)	Max. relief (m/m)	Max. elevation (m)
7	*2006 Kuril Island*	*Dushnaya Bay-6*	*106*	*4.4*	*106*	*4.4*	*100*	*100*	*0.042*	*0.662*	*10.3*
7	*2006 Kuril Island*	*Dushnaya Bay-109*	*59*	*9.1*	*49*	*7.5*	*83*	*82*	*0.154*	*2.480*	*9.1*
7	*2006 Kuril Island*	*Dushnaya Bay-12*	*120*	*6.9*	*112*	*5.8*	*93*	*84*	*0.058*	*0.635*	*6.9*
7	*2006 Kuril Island*	*Dushnaya Bay-7*	*139*	*6.3*	*139*	*6.3*	*100*	*100*	*0.045*	*1.870*	*6.3*
7	*2006 Kuril Island*	*Dushnaya Bay-9*	*151*	*7.3*	*151*	*7.3*	*100*	*100*	*0.048*	*1.050*	*12.6*
7	*2006 Kuril Island*	*Dvoynaya Bay-125*	*118*	*11.8*	*97*	*8.4*	*82*	*71*	*0.100*	*1.010*	*11.8*
7	*2006 Kuril Island*	*NE Rasshua-201*	*111*	*11.4*	*109*	*10.2*	*98*	*89*	*0.102*	*0.520*	*11.4*
2	2004 Indian Oc.	Jantang, L1-2	518	14.9	513	-	99	-	-	-	-
2	2004 Indian Oc.	Lhok Kruet 1	376	12.6	275	-	73	-	-	-	-
2	2004 Indian Oc.	Lhok Kruet L1-4	415	17.4	334	-	81	-	-	-	-
2	2004 Indian Oc.	Lhok Leupung	903	12.2	856	-	95	-	-	-	-
2	2004 Indian Oc.	Kuala Meurisi	1820	12.9	1803	-	99	-	-	-	-
2	2004 Indian Oc.	Langi Island	524		493	-	94	-	-	-	-
2	2004 Indian Oc.	Langi field	441	3	235	-	53	-	-	-	-
2	2004 Indian Oc.	Langi village	294	10.9	277	-	94	-	-	-	-
2	2004 Indian Oc.	Langi 102	335	7.3	331	-	99	-	-	-	-
2	2004 Indian Oc.	Busung 2	82	3.1	68	-	83	-	-	-	-
2	2004 Indian Oc.	Busung 1	130	4.1	109	-	84	-	-	-	-

*Numbers >100% are cases where slope goes down at end

† "total relief" = runup/inundation

§Disagreement between text and figure; profile plot may be in error

Fringing reef

[&] References as follows:

1. Gelfenbaum and Jaffe, 2003
2. Jaffe et al., 2006
3. Nanayama et al., 2008
4. Srinivasalu et al., 2007
5. J. Bourgeois, unpublished field notes, see also Higman and Bourgeois, 2008
6. Shi et al., 1995
7. *This study*

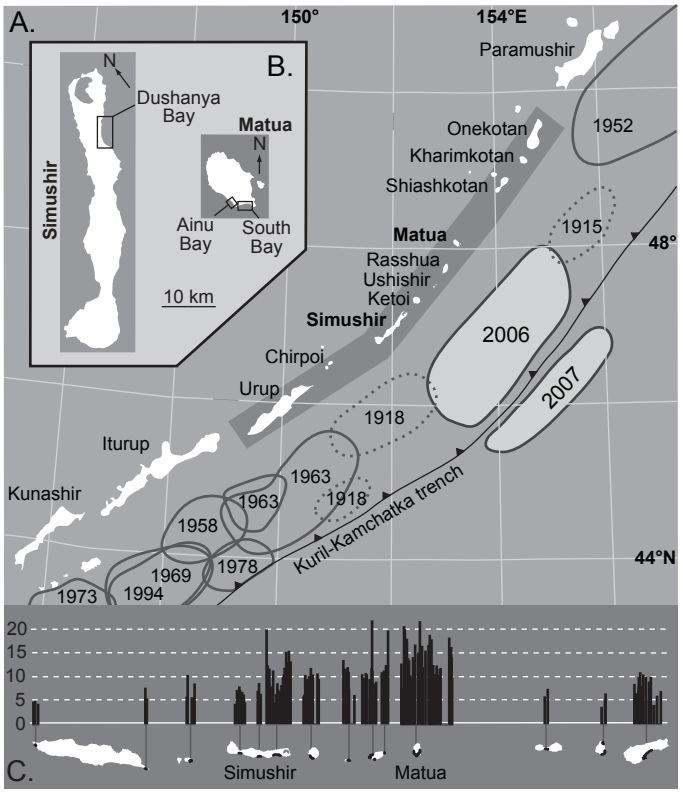

Figure 3.1: A. Historical tsunamigenic earthquakes on the Kuril-Kamchatka trench, after Fedotov et al. (1982). The 2007 earthquake was an outer-rise event in the Pacific Plate; all others occurred on the Pacific/Okhostk plate interface. B. Location of bays with pre-tsunami and post-tsunami topographic measurements. C: Runup elevation in meters from the 2007 and 2008 post-tsunami surveys (Table 2.1) for shaded area of islands in A.

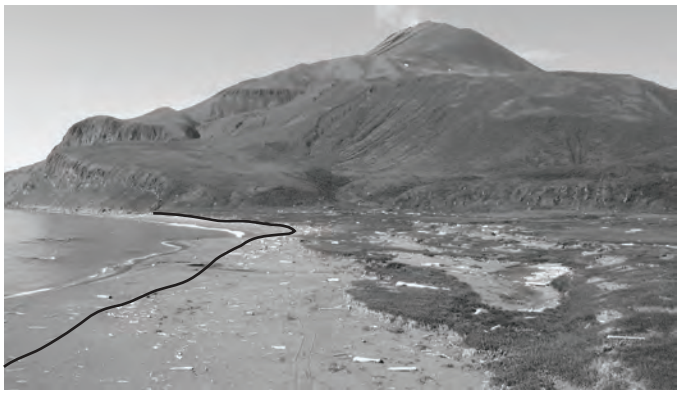

Figure 3.2: Post-tsunami (2007) view of Ainu Bay, Matua (Figure 3.1). Black line marks seaward extent of vegetation in 2006.

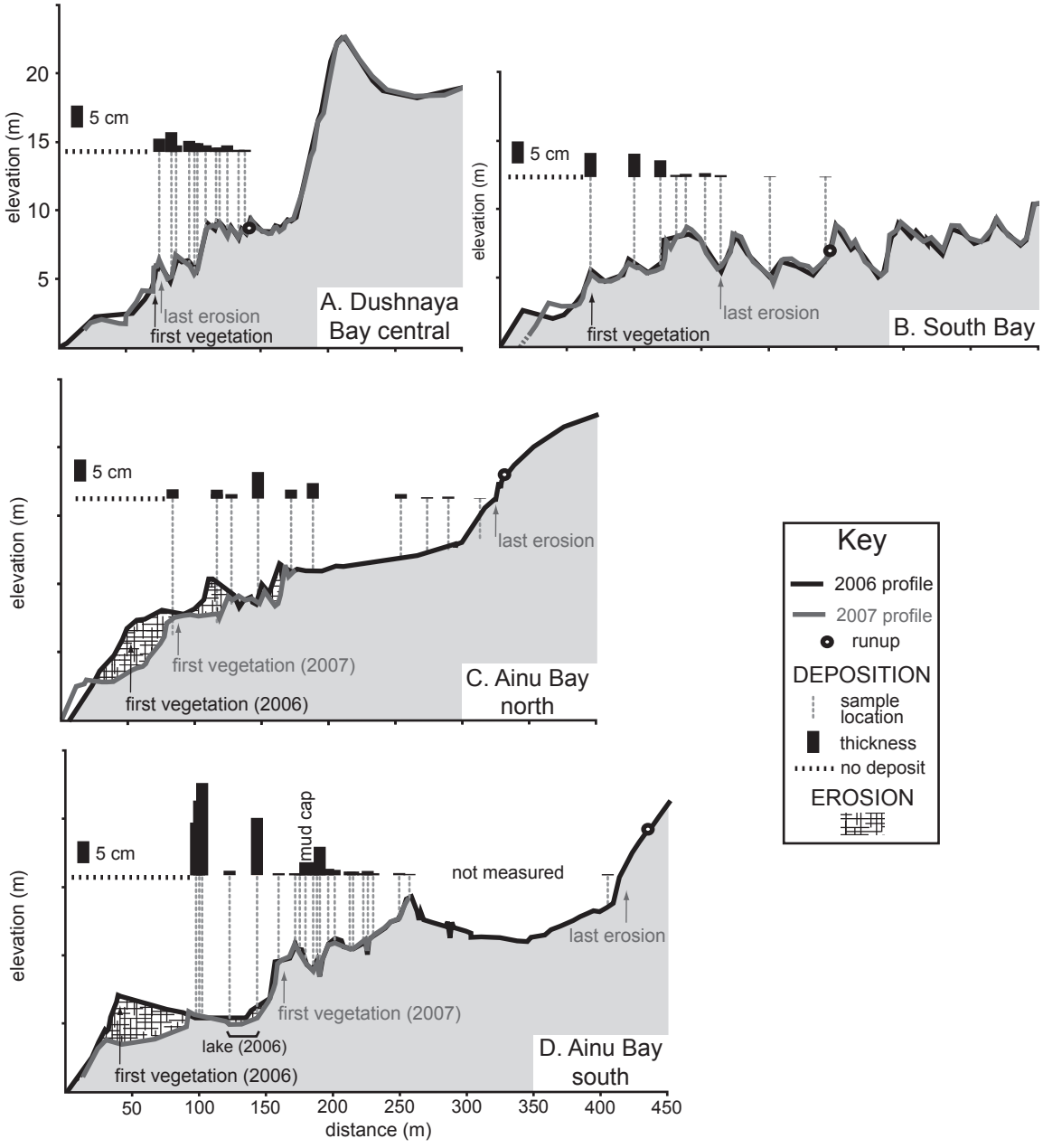

Figure 3.3: Before (2006) and after (2007) topographic profiles from Dushnaya Bay, Simushir Island (**A)** and South Matua Island (**B**, **C**, **D**) (locations on Figure 3.1). **A** and **B** are cases of low runup and **C** and **D** of high runup. "First vegetation" refers to the seaward limit of vegetation covering the surface; on **A** and **B**, the location of first vegetation did not significantly change between 2006 and 2007. On **D** the lake was present in 2006 but not in 2007; in the area marked "not measured," seaward-derived sand deposits were mixed with locally eroded cinders and gravel. Additional images: **A**: Figures 3.8–3.9. **B**: Figure 3.13. **C**: Figures 3.14–3.16. **D**: Figures 3.7, 3.17.

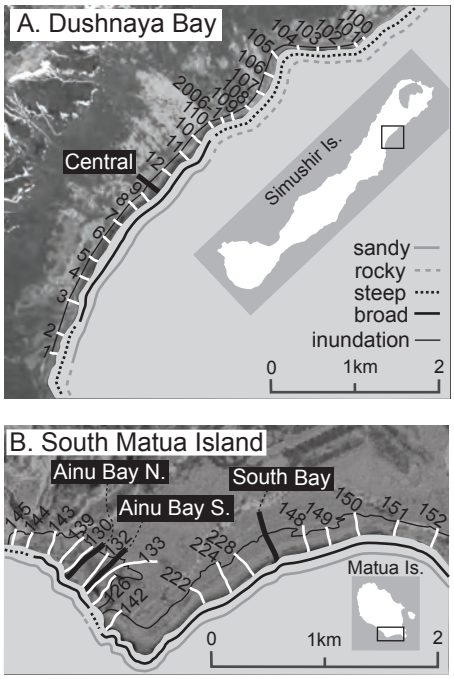

Figure 3.4. Location of topographic profiles and mapped inundation limits in Dushnaya Bay, Simushir, and Ainu and South bays, Matua Island. Profiles measured both in 2006 and 2007 are named. Coastal plain type (sandy or rocky and steep or broad) is noted. **A**. Digital Globe image. **B**. ASTER image.

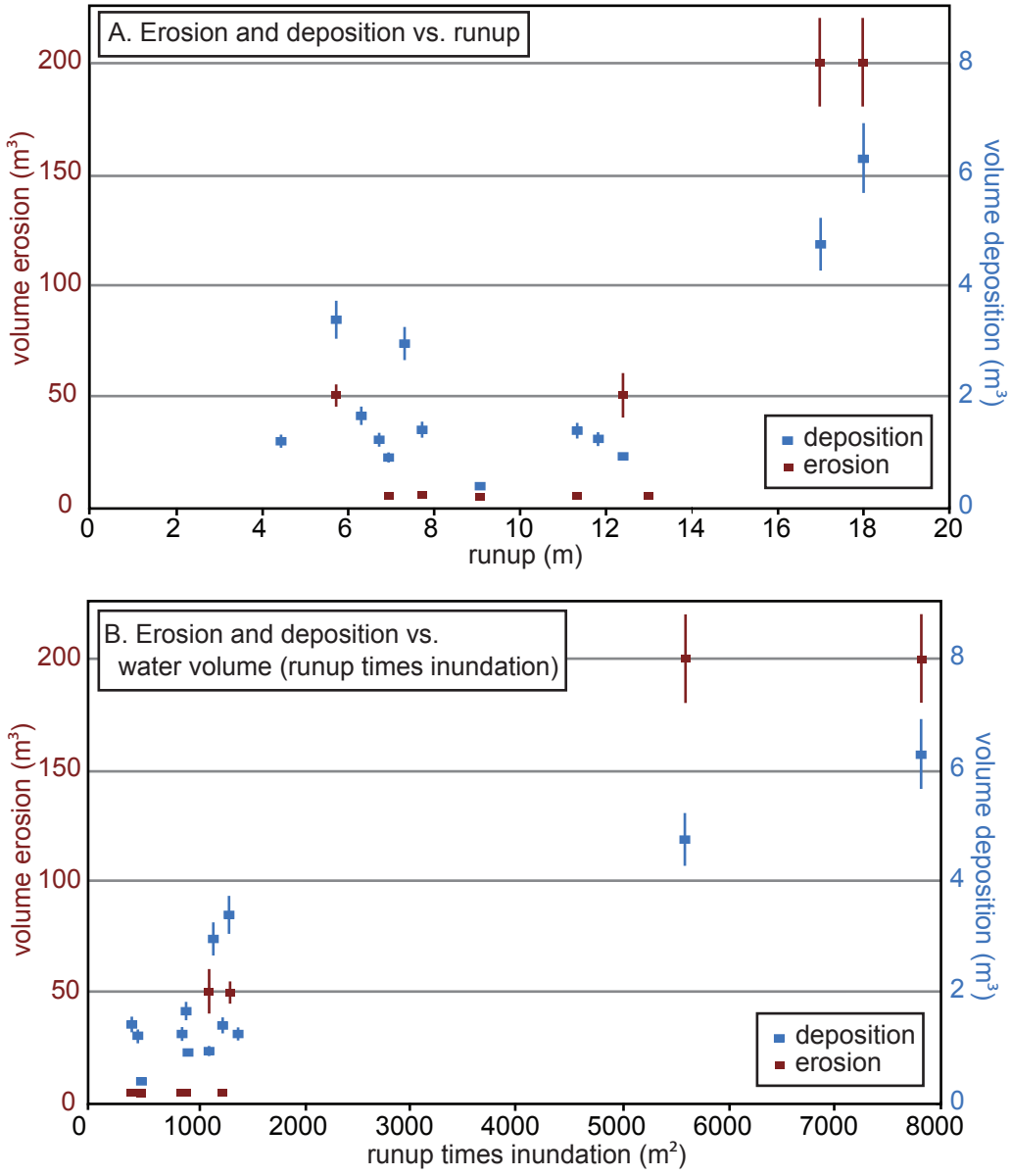

Figure 3.5: Calculated and estimated volumes of tsunami erosion and deposition plotted against **A**-runup and **B**-runup times inundation. Plotted data are given in Table 3.1.

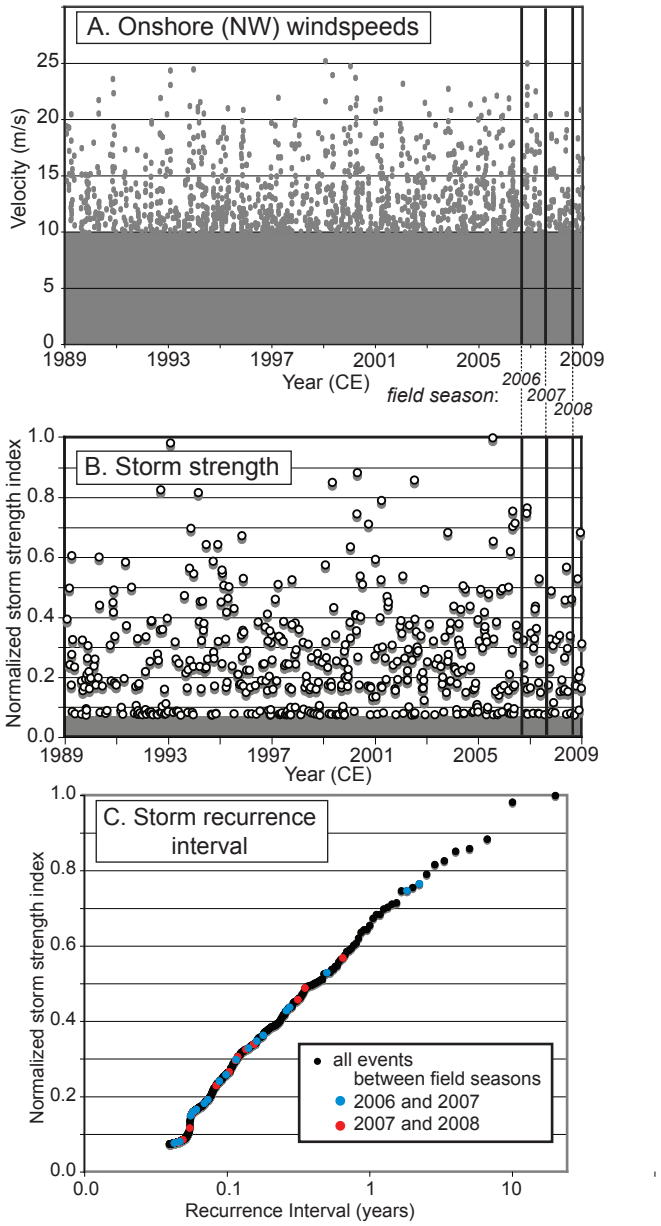

Figure 3.6. A. Calculated wind speed >10 m/s in the onshore (NW) direction in the central Kuril Islands from Jan 1989-Dec 2008. Data are averaged over 2.5° latitude and longitude centered on 45° N, 150° E and 47.5° N, 152.5° E, derived from 4-times-daily surface winds from NCEP Reanalysis data provided by NOAA/OAR/ESRL PSD, Boulder, Colorado, USA, http://www.cdc.noaa.gov/. The three vertical lines represent the three summer field seasons of KBP. B. Same data as in A normalized to a comparative index of storm strength to account for storm duration. Wind speeds (in m/s) are multiplied by the length (in days) of sustained >10 m/s wind speeds. Two large events (index = 0.75) occurred in early November 2006 (6-7 Nov and 11-12 Nov), but nothing as large since then. C. Recurrence interval for all events with >10 m/s onshore wind speeds between January 1989 and December 2008. The two largest events between field seasons have recurrences of 1.8 and 2.2 years and occurred in 2006 before the tsunami.

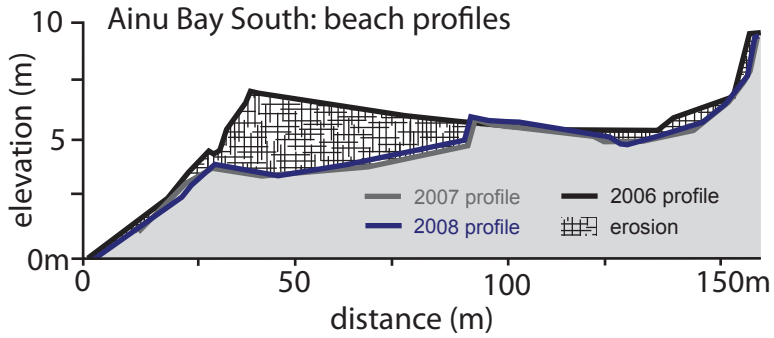

Figure 3.7: Topography of the beach on the Ainu Bay south profile from surveys in 2006, 2007, and 2008. That the 2007 and 2008 profiles remain nearly identical (within measurement error) suggests that the large difference from 2006 to 2007/8 is due to tsunami erosion removing sediment entirely from the littoral zone.

Figure 3.8: Stitched panorama centered on Dushnaya Bay Central profile (located in Figure 3.4, illustrated in Figure 3.3). Photographer Bourgeois is on high ridge at the back of the profile; the three people are landward of 2006 runup and inundation; some tsunami transported wood is visible near right edge, center. Person in center background is along the profile track. No significant erosion occurred on this profile landward of the backbeach scarp; see Figure 3.9. A thin sand layer extended almost to the limit of runup and inundation (Figure 3.3; Table 3.1).

Figure 3.9: Before (summer 2006) and after (summer 2007) photoset- Central Dushnaya Bay, near Profile 10 (see Figure 3.4). A red circle identifies approximately the same point in each photo. The 2007 photo shows evidence of some backbeach cliff retreat—hanging and fallen fresh turf. Also, between photos, the beach has been rearranged so that the backbeach valley has been filled in (as in Dushnaya Central profile, Figure 3.3). 2006 photo: Dena Berkey; 2007 photo: MacInnes.

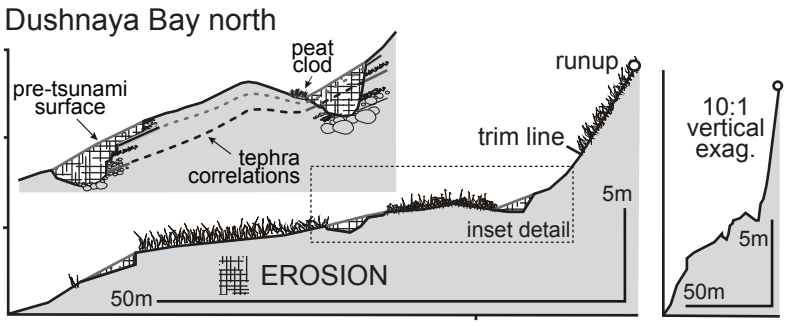

Figure 3.10: A steep, well-vegetated profile measured in 2007 from northern Dushnaya Bay, Simushir (2:1 vertical exaggeration). The former surface was inferred from the current surface and the location of soil stripping; also, in erosion zones, remaining root rhizomes often indicated original soil elevation. The soil was cohesive and eroded mainly through block removal, preferentially along certain tephra layers – cinders in particular (see inset). Tephra correlations also show that the surface is progressively younger toward the sea, indicating net progradation since about 2000 – 3000 years ago (from preliminary radiocarbon dates in peat). Photos in Figure 3.11 were taken near this profile.

Figure 3.11: Before (summer 2006) and after (summer 2007) photoset from northern Dushnaya Bay near profile 106 (between 105 and 106; see Figure 3.4 for location; see Figure 3.9 for a profile near this spot). Our team in 2006 chose a convenient but foolish spot for one overnight. 2006 photo: Beth Martin; 2007 photo: MacInnes.

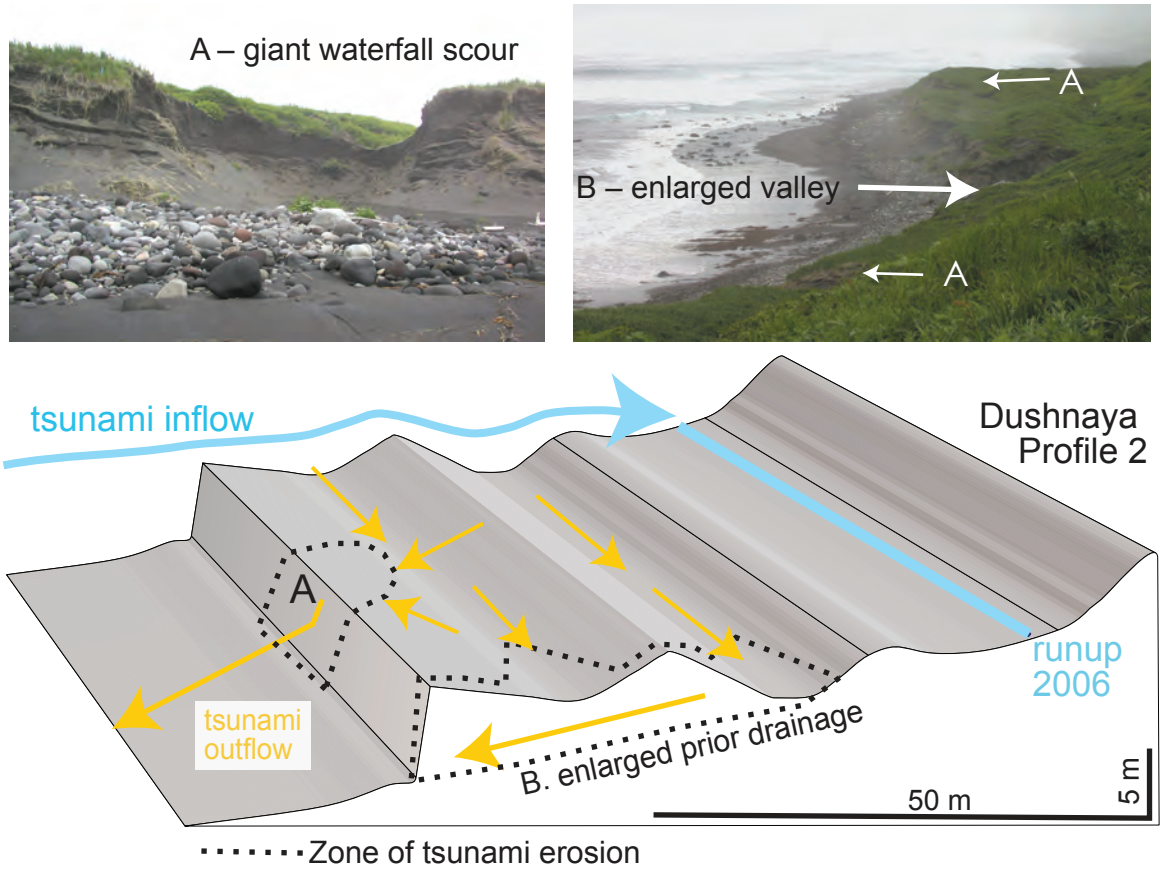

Figure 3.12. A steep, short, sandy profile from southern Dushnaya Bay measured in 2007, extruded to show schematically the 3-D tsunami effects. This profile is located on Figure 3.4, with some data given in Table 3.1 (runup 12.4 m). Recreated tsunami inflow shown in blue, outflow in orange. Near this profile, the outgoing tsunami removed sand during outflow over the back-beach scarp, creating at least two giant scour/waterfalls about 7 m high. The left picture views one of the scours from the beach, the right picture shows the location of the two scours from the ridge behind and above the scours. In the middle of the right picture is an enlarged prior drainage valley. The outgoing (and possibly also incoming) tsunami enlarged steep stream valleys already cut through the beach ridges. Both photos: T.K. Pinegina; right photo is reversed to look similar to profile perspective.

Figure 3.13. Before (summer 2006) and after (summer 2007) photoset – South Bay profile on Matua (see Figure 3.4 for location; Figure 3.3 for profile). The approximate location of the profile is shown by a red line; a red circle identifies approximately the same point in each photo. Trenches and other excavations from WWII can be seen on both photos, especially well from 2007. On the 2007 (after) photo, the tsunami inundation is visible as gray lines of driftwood, near the top of the picture. The (unseen) unvegetated beach was rearranged between 2006 and 2007 (see Figure 3.3), but other erosion was not dramatic. A thin sheet of tsunami sand was deposited almost to the limit of runup and inundation. Both photos: T.K. Pinegina.

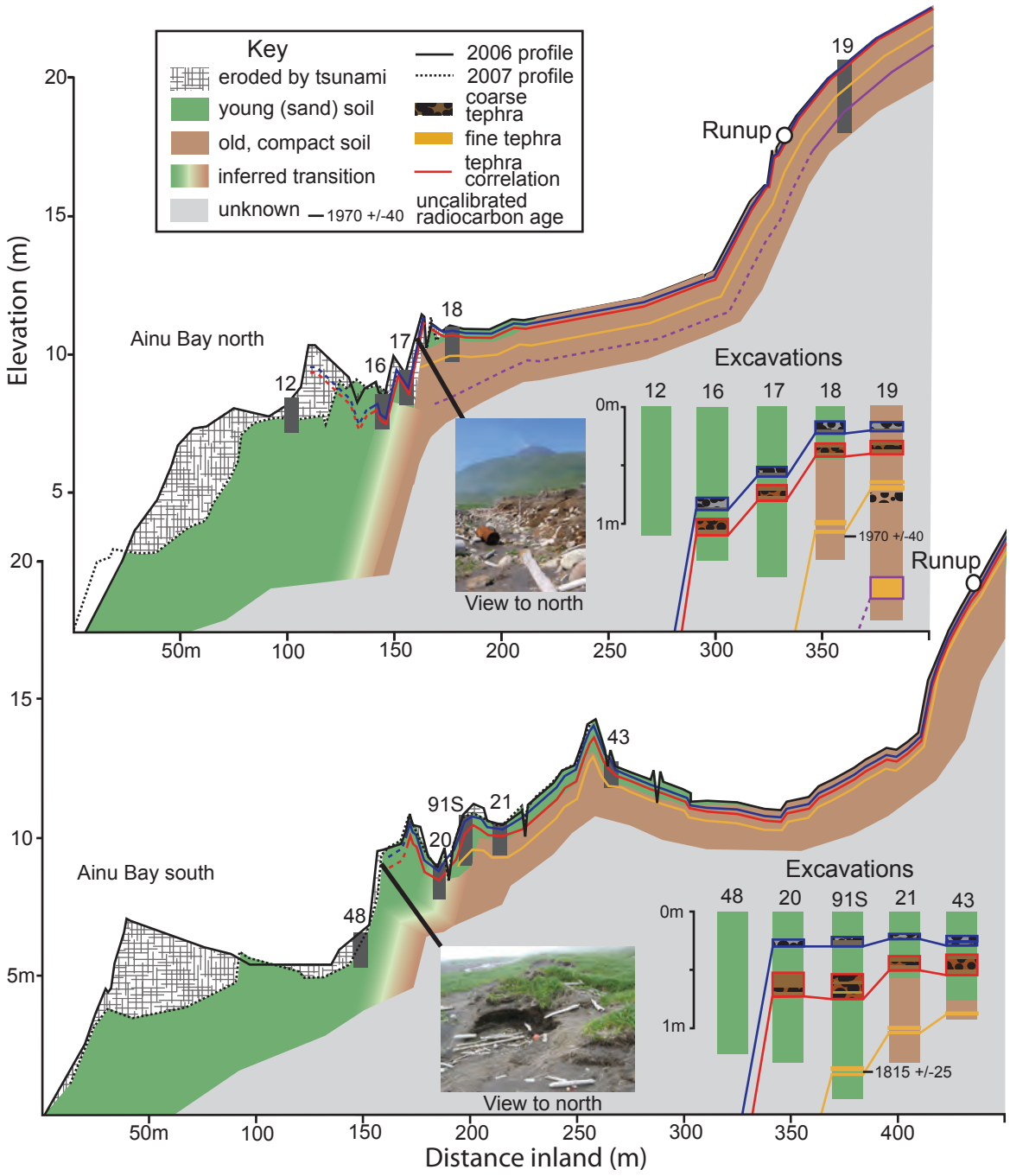

Figure 3.14: Profiles and stratigraphy from Ainu Bay, Matua (Figures 3.3, 3.4). The transition between older, well-developed soil (brown) and young sandy material (green) is interpreted from excavations and exposures. Top. Ainu Bay north (Figure 3.15). The sharp vertical contact (paleo-scarp) between young sandy soil and older compact soil between excavations 17 and 18 indicates that either large-volume erosional events have occurred in Ainu Bay in the past, or that the bay has transitioned from eroding to prograding recently. Bottom. Ainu Bay south profile (Figure 3.17) and stratigraphy are similar, though 91S is thickened by eolian sand. A distinct difference in landscape age between excavations 20 and 21 can be seen in tephra stratigraphy; 21 is tundra soil, while 20 is grassy sandy soil.

Figure 3.15. Before (summer 2006) and after (summer 2007) photoset – Ainu Bay North profile on Matua (see Figure 3.4 for location; Figure 3.3 for profile; also see Figures 3.14, 3.16). The approximate location of the profile is shown by a red line, and a red circle identifies approximately the same point in each photo. The after perspective is hard to match because of the severe erosion, lowering the surface on which the group camped for two nights in 2006. Both photos: Misty Nikula.

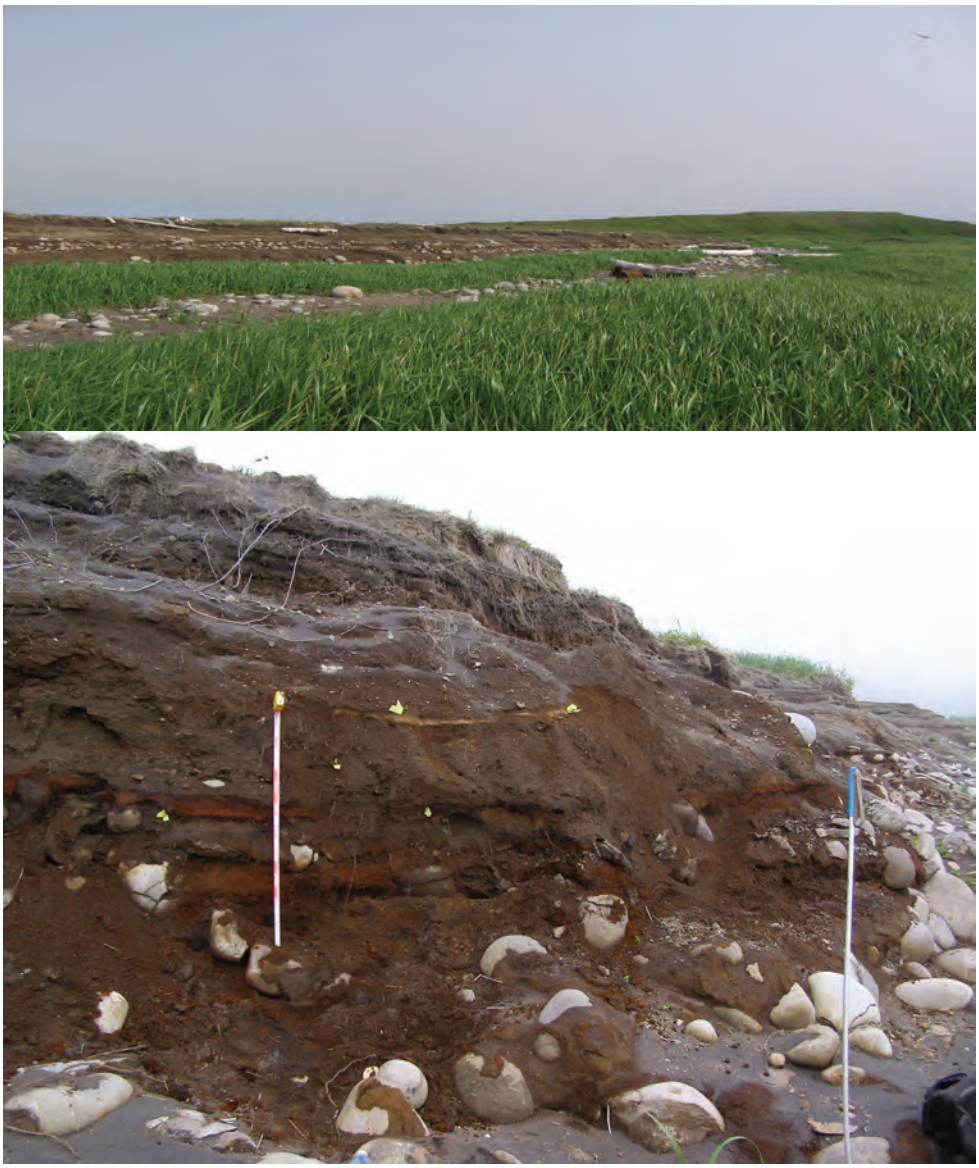

Figure 3.16. Top: View in 2007 of 100-m-long, tsunami-generated scarp crossed by Ainu Bay North profile (Figures 3.3, 3.4, 3.14). Line of bouldery sand in the foreground is another surface stripped of turf by the tsunami. Bottom: Close-up of the eroded scarp, with exposed soils and tephra. Tape on outcrop is extended to 100 cm. A light-colored tan tephra in the middle of the scarp (marked at either end by yellow flagging tape) is about 2000 years old. Both photos: J. Bourgeois.

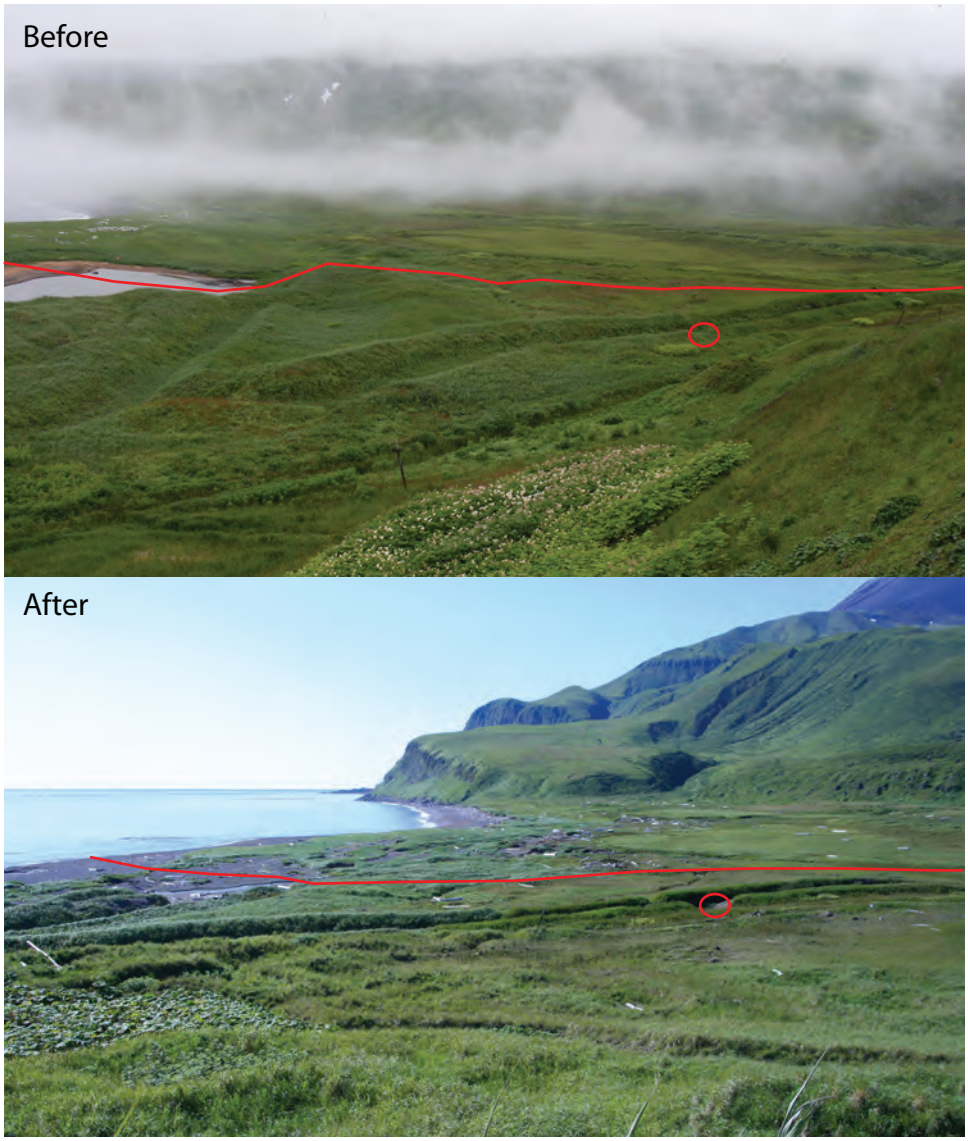

Figure 3.17. Before (summer 2006) and after (summer 2007) photoset – Ainu Bay South profile on Matua (see Figure 3.4 for location; Figure 3.3 for profile; also see Figure 3.14). The approximate location of the profile is shown by a red line, and a red circle identifies approximately the same point in each photo. The beach and proximal vegetated region suffered severe erosion, and the lake was breached, drained and filled with sand. Both photos: Misty Nikula

CHAPTER 4

Using tsunami modeling and earthquake slip distributions to interpret enigmatic runup measurements of the 2006 and 2007 Kuril Island tsunamis

Introduction

In the winter of 2006 to 2007, two tsunamis 60 days apart swept across the uninhabited beaches of the central Kuril Islands, Russia, leaving behind an enigmatic record of their passage. Post-tsunami surveys during the following two summers found and measured the location of wracklines formed by the 2006 or 2007 Kuril Island tsunamis in all of the central Kuril Islands (Chapter 2). However, without eyewitness accounts or definitive deposit records, our wrackline surveys of maximum tsunami inundation (farthest distance inland) and runup (elevation of inundation) alone cannot determine which tsunami left the record. Tsunami modeling of the two events, given accurate bathymetry and topography, may be the best available means of differentiating which tsunami(s) formed the records measured by the post-tsunami survey. Tsunami models today are capable of reproducing observed runup and inundation patterns and capturing wave behaviors, which might give clues to what happened that winter in the Kuril Islands.

Previous research on the generation and propagation of tsunamis from heterogeneous coseismic slip during great subduction-zone earthquakes shows that variations in slip amount and location play an important role in nearfield tsunami runup (Hirata et al., 2003; Geist and Dmowska, 1999; Geist, 2002; Satake et al., 2008; Borrero et al., 2009). For example, for the

1952 Kamchatka earthquake (M_w 8.8-9.0), MacInnes et al. (2010) showed that observed high runup along a specific stretch of nearfield coastline required adjacent concentrations of slip.

When tsunamis can translate locally higher slip into locally higher tsunami runup, accounting for this slip distribution in tsunami modeling is important on a human scale. Both the 2006 and 2007 Kuril Island earthquakes are well studied, but the inferred distributions of coseismic slip are quite varied, and often inconsistent. While inverting geophysical observations of an earthquake event (such as records of seismic waves, tsunamis, and GPS station motion) to a distribution of earthquake slip has become virtually an automatic response of the geophysical community after a large earthquake, results can vary significantly. The number of different ways to invert slip patterns is proliferating, and the varying inversions can give divergent results based on biases of different methods, on data selection, and on the propagation or errors and uncertainties.

In this paper, I simulate tsunami runup from many available inversions of earthquake slip distribution of 2006 and 2007 Kuril Island events and compare my simulations to field observations of wracklines, which are indicative of tsunami inundation distance and runup elevation (henceforth referred to as "field observations"). My goal is to investigate these published slip distributions in order to differentiate which tsunami (or which tsunami, where) was responsible for the records measured in post-tsunami surveys (see Chapter 2). I further investigate the implications of the spatial resolution of slip distribution on tsunami runup, and determine if slip distribution during the 2006 subduction-zone and 2007 outer-rise earthquakes can affect nearfield runup enough to be an important factor to consider in future events.

Tectonic setting

The central Kuril Island region is defined as between the Bussol and Kruzenshtern straits— a geographically complicated region with unusual bathymetry and generally smaller islands than elsewhere in the Kuril volcanic arc (Figure 4.1). Here, the 100-120 Ma Pacific plate subducts under the Okhotsk plate (Figure 4.2) at the fast rate of ~80 mm/yr (DeMets et al., 1990), excluding Okhotsk plate rotation (Apel et al., 2006). Along the Kuril Island archipelago, the submarine Vityaz Ridge fronts the volcanic arc at a depth of only a few hundred meters, except in the central Kurils where the ridge is disrupted by a forearc basin ~2 km deep (Figure 4.1). The southern boundary of the central Kurils is deeply bisected at the Bussol Strait by a submarine canyon, believed to be associated with a graben (Baranov et al., 2002; Korvachev et al., 2009). No historical earthquake is known for certain to have ruptured through this boundary, although one in 1918 is speculated to have done so (Beck and Ruff, 1987). The northern limit of the central Kurils similarly may be related to tectonic disruption of the overriding Okhotsk plate, but large transverse faults at this boundary discussed in Laverov et al. (2006) (Figure 4.1) are less geographically visible than the canyon at the southern boundary.

The central Kurils region also is defined by a character change in the velocity structure of the crust, compared to that north or south (Zlobin and Polets, 2009). The depth of the Mohorovičić discontinuity is variable along the central Kurils and is poorly defined under northern Simushir (Zlobin and Polets, 2009). The thickness of crust below central Simushir, at the southern end of the central Kurils, has been measured as 25-30 km, with a seismic

velocity boundary around 12-17 km crustal depth. The sediment carapace is generally 2-3 km thick (Zlobin and Polets, 2009).

The Kuril-Kamchatka subduction zone is strongly coupled in the central Kurils, suggesting a large potential for coseismic offsets during megathrust earthquakes. Recent analysis of motion of individual Kuril islands relative to Pacific plate motion using GPS receivers shows that interplate coupling of the subduction zone in the central Kurils extends almost to beneath the island arc, although the coupled zone narrows towards Kruzenshtern Strait (Steblov et al., 2010). The trench-parallel gravity anomaly (TPGA) in the central Kurils is positive west of the trench and essentially zero east of the trench (Raeesi and Atakan, 2009; Song and Simons, 2003). According to Song and Simons (2003), the positive TPGA in the central Kurils indicates an uncoupled subduction interface because positive TPGA means little strain accumulation. However, seismic activity in the central Kuril region since at least 1963, when a large compressional outer-rise earthquake occurred in the central Kuril region, supports the strongly coupled argument (Christensen and Ruff, 1988; Ammon et al., 2008).

Strong interplate coupling creates an environment with high slab-pull stresses enabling the possibility of large coseismic offsets during outer-rise type earthquakes. The Pacific slab in the Japan-Kuril-Kamchatka subduction zone experiences the greatest slab pull of any large subduction zone globally (Bilek et al., 2005). When a large megathrust earthquake occurs in this setting, it can completely relax compressional forces on the interface, temporarily allowing tensional forces to dominate. This scenario creates opportunity for large outer-rise earthquakes comparable to the generally larger outer-rise earthquakes on weakly coupled subduction zones, where tensional forces dominate.

Past earthquakes

Even though many large earthquakes have occurred along the Kuril-Kamchatka trench (Figure 4.2), few in the historical record are located in the central Kurils, such that the central Kurils were considered a seismic gap before the 2006 event. The last rupture near the southern boundary of the central Kurils was an M_w 8.5 event in 1963 (Beck and Ruff, 1987), while the northern Kurils and southern Kamchatka ruptured in 1952 in an M_w 9.0 event (Kanamori, 1976; Gusev and Shumilina, 2004). The earliest known central Kuril earthquake, in 1780, produced a tsunami with reports on Urup, Simushir and Ketoi islands (e.g., Solov'ev and Ferchev, 1961; Iida et al., 1967). A large earthquake (estimated M_w 7.7-8.1) in 1915 has been located to south of the 1952 rupture zone (e.g. Pacheco and Sykes, 1992; Geller and Kanamori, 1977); 1915's rupture zone may have extended into the central Kurils, but its epicenter is located geographically in the northern Kurils. No reports of a 1915 tsunami exist. Two earthquakes in 1918 occurred in the 1963 rupture area (southern Kurils) and may be very similar to 2006 subduction-zone/2007 outer-rise doublet, although the faulting geometry of the second 1918 earthquake is unknown. The first 1918 earthquake may have ruptured across the Bussol Strait into the central Kuril region (Beck and Ruff, 1987), but this is also uncertain.

2006 and 2007 Central Kuril earthquakes

The first of two tsunamigenic earthquakes in the central Kurils initiated at 11:14 UTC on 15 November 2006 (M_w 8.1-8.4). The preferred global central moment tensor (GCMT) solution of this earthquake indicates it occurred on the subduction zone, as it was a thrusting event with initiation depth at 13 km, strike of 214º, and dip of 15º. The epicenter was ESE of

Simushir Island (Figure 4.2), and propagation proceeded northward (Vallée, 2006). Henceforth, this earthquake will be referred to as "2006".

Sixty days later, at 04:23 UTC on 13 January 2007, the second tsunamigenic earthquake (M_w 7.8-8.2) initiated in the central Kurils. The GCMT solution of this earthquake indicates a normal-faulting, outer-rise event in the Pacific plate, with an epicenter approximately 100 km ESE of the 2006 event (Figure 4.2) at a crustal depth of ~10 km. Henceforth, this earthquake will be referred to as "2007". While 2007 is considered to have been triggered by 2006 (Norimatsu and Mori, 2008), 2007 is unusual for an outer-rise event both in its size and in its location closer to the trench (Figure 4.2), rather than in the outer rise itself (Ammon et al. 2008; Lay et al., 2009).

Ammon et al. (2008) and Lay et al. (2009) consider the 2006 event to have completely relaxed friction on the subduction zone, and thereby to have allowed the force of slab pull to function without hindrance; the 2007 event appears to have ruptured completely through the lithosphere of the Pacific to at least ~33 km depth (Lay et al. 2009). The few other extensional outer-rise events of comparable size (1933 Sanriku and 1977 Sumba) occurred adjacent to weak seismic coupling on the subduction zone, but are also the result of slab pull stresses rupturing through the entire oceanic lithosphere (Ammon et al. 2008). The 2007 earthquake is the third largest extensional outer-rise event recorded to date, and may be the largest in a setting with strong interplate coupling.

The geometry of the 2007 earthquake is less certain than that of 2006. The preferred fault plane of 2007 is not easily distinguished by aftershocks (Norimatsu and Mori, 2008; Lay et al., 2009; Fujii and Satake, 2008); either the northwest-dipping plane (strike ~215º; dip ~45º) or the southeast-dipping plane (strike ~42º; dip ~59º) could be valid solutions. No

compelling teleseismic evidence favors one fault plane over another (Lay et al., 2009). The depth extent of the 2007 earthquake is also poorly constrained (Steblov et al., 2008); rupture at depths below ~33 km could not be resolved robustly by seismic inversions (Lay et al., 2009). While similar uncertainties in rupture at depth are true for 2006 (Ammon et al., 2008), greater uncertainties in 2007 rupture velocity (2.6 ± 1.0 km/s) than for 2006 (1.7 ± 0.3 km/s) compound difficulties in defining the 2007 rupture zone (Lay et al., 2009). A slower velocity of rupture for 2007 would mean the earthquake had a shorter length and width (and therefore greater slip), while a faster velocity would mean the rupture covered a larger area but with lower slip.

Short-period enrichment of 2007 reflects rupture on a new or young fault plane with high rigidity, releasing a fast, short impulse of energy and resulting in stronger shaking being felt in Japan than during the 2006 earthquake (Lay et al., 2009). The 2007 earthquake released more seismic energy than 2006 (4.33×10^{16} J vs 9.63×10^{15} J), had larger body-wave spectral amplitudes, as well as larger m_b and M_s at shorter periods (Ammon et al., 2008). However, the 2006 earthquake rupture lasted longer than 2007 (around 120 s vs 60 s.) and produced a larger seismic moment (Ammon et al., 2008).

Even though 2006's moment is larger than 2007, the published values for moment from slip distribution inversions cover a range of values (Table 4.1 and 4.2). GCMT solutions record the 2006 event as M_w 8.3 (M_s 7.8, M_o 3.4×10^{21} Nm) and the 2007 event as M_w 8.1 (M_s = 8.2; M_o = 1.65×10^{21} Nm). However, seismic moments of 2006 calculated by slip distribution inversions vary from 1.6×10^{21} Nm to 5.14×10^{21} Nm, resulting in a range of moment magnitudes from 8.1 (Valleé, 2006; Yagi, 2006; Fujii and Satake, 2008) to 8.4 (Ammon et al., 2008; Steblov et al., 2008; Lay et al., 2009). The 2007 earthquake has

published seismic moments between 6.9 x 10^{20} Nm and 2.66 x 10^{21} Nm, resulting in a range of moment magnitudes from 7.8 (a variation in Fujii and Satake, 2008) to 8.2 (Yamanaka, 2007; Steblov et al., 2008; Lay et al., 2009).

Slip distributions

Calculations of slip distribution for the 2006 and 2007 Kuril earthquakes are based on teleseismic records of body (P and SH), surface (Love and Rayleigh), and W-phase waves (Yamanaka, 2006, 2007; Yagi, 2006, 2007; Vallee, 2006, 2007; Ji, 2006, 2007; Ammon et al., 2008; Raeesi and Atakan, 2009; Lay et al., 2009; Baba et al., 2009), of GPS receivers (Steblov et al., 2008; Tikhonov et al., 2008), and of tsunami waveform observations (Baba et al., 2009; Fujii and Satake, 2008). Ji (2006 and 2007), Yamanaka (2006 and 2007), Yagi, (2006 and 2007), Vallée (2006 and 2007) all performed rapid-response seismic inversions of the 2006 and 2007 earthquakes and posted their results online. The works of Ji and Yamanaka have been used by previous tsunami modelers to represent these earthquakes (Rabinovich et al., 2008 and Tanioka et al., 2008, respectively). Tables 4.1 and 4.2 catalog the characteristics of the source parameters and slip distributions used in my tsunami modeling study; additional slip distributions and more detailed description of the ones discussed in this chapter can be found in *Appendix A*.

The four seismic inversions from which I simulate tsunamis all use a different combination of seismic waves in their inversion technique. Raeesi and Atakan (2009) use only P wave, Ji (2006; 2007) uses P, SH, Rayleigh and Love waves, and Lay et al. (2009) primarily use long-period (200-1000 s) waves, referred to as the W phase, although they also use P waves and Rayleigh waves to estimate rupture velocity and fault length. Baba et al.

(2009) use P, Rayleigh and Love waves, but they also modify their solution based on inversion of tsunami records. These seismic inversions resolve slip in small subfaults, on the order of 20 by 10 km (Tables 4.1 and 4.2). Tsunami simulations discussed later in this paper based on these inversions are referred to as *JSei06* and *JSei07* for the 2006 and 2007 slip distributions of Ji (2006; 2007) (Figure 4.3), *RSei06* and *RSei07* for the 2006 and 2007 slip distributions of Raeesi and Atakan (2009) (Figure 4.4), and *LSei06* and *LSei07* for the 2006 and 2007 slip distributions of Lay et al., (2009) (Figure 4.5). The combined seismic and tsunami inversion of Baba et al. (2009) is referred to as *BSeiTs06* (Figure 4.6); Baba et al. (2009) do not analyze the 2007 earthquake.

I also simulate tsunamis from a slip distribution inversion of tsunami records (Fujii and Satake, 2008) and of GPS-measured ground motion (Steblov et al., 2008). Both of these inversions resolve slip into large subfaults, on the order of 50 by 50 km (Tables 4.1 and 4.2). Fujii and Satake (2008) invert slip into three different subfault configurations for 2006 and two for 2007. Tsunami simulations based on their solution of 2006 with 8º and 15º dip at a M_w 8.2 (Table 4.1) is referred to as *FTs06_82* and on their simulation from their southeast-dipping fault plane of 2007 (Table 4.2) as *FTs07*. I also increase the *FTs06_82* earthquake solution to a M_w 8.4, which I will refer to as *FTs06_84* (Figure 4.7). Tsunami simulations based on Steblov et al. (2008) are referred to as *SGPS06* and *SPGS07* (Figure 4.8).

Of the published slip distributions, all seismic inversions found higher maximum slip during the 2007 event— either by as little as 1 m (14 m for 2006 vs. 15 m for 2007 in Lay et al., 2009) or by more than double the value (6 m for 2006 vs. 13 m for 2007 in Raeesi and Atakan, 2009). GPS and tsunami inversions calculate a larger maximum slip during 2006. Average slip in the defined rupture zone ranged from 1.7 m to 4.6 m for 2006 (Table 4.1) and

1.3 to 7.0 m for 2007 (Table 4.2). The most common location of a slip concentration during 2006 is adjacent to Rasshua (± ~30 km NE or SW), generally at crustal depths of less than 15-20 km, although slip patches range along the whole length of the rupture (Table 4.1). Slip concentration locations for 2007 are more variable and with different studies determining maximum slip to be anywhere north or south within the rupture zone. Maximum slip depth for 2007 was shallow when permitted by inversion parameterization, i.e., when more than one down-dip subfault was used in the inversion (Table 4.2).

Why slip distributions are different

The range of slip-distribution solutions depends in part on types of data studied, on variations in Earth models employed, and on fault geometries used. Because 2006 released more energy at longer wavelengths, seismic inversions that only use higher-frequency seismic waves (such as P-waves) tend to have a smaller seismic moment than ones that include longer-period energy (such as W-phase waves). The Earth model (CRUST2, 1D-PREM, etc.) used in inversion is important because values for rigidity can vary. The standard constant rigidity for 2006 is 40 GPa and 50-52 GPa for 2007, although Tanioka et al. (2008) use 30 GPa for 2006. Earth models that have decreasing rigidity at shallower depths amplify slip at shallow depths compared to those that use a constant rigidity. Also, no Earth model currently represents the steep bathymetry near the trench, which can bias solutions, especially those based on shorter-period surface waves (cf. Lay et al., 2009). Finally, seismic moment is proportionally related to the dip of the fault; Kanamori and Given (1981) found that amplitudes of long-period surface waves excited by shallow subduction earthquakes are approximately proportional to seismic moment times the sine of twice the fault dip, but dip is

poorly resolved when earthquakes are shallower than 30 km. Steblov et al. (2008), Fujii and Satake (2008), and Baba et al. (2009) attribute the differences in seismic moment between their solutions and the GCMT solution in part to a difference in dip of the fault.

Differences among earthquake inversions can also depend as much on the limitations of methodology as on other factors. Seismic inversions resolve slip into discrete subfaults as small as 5 km by 5 km, while tsunami waveform or GPS inversions tend to use coarser subfaults, on the order of 25 or 50 km (Tables 4.1 and 4.2); finer-resolution subfaults can result in a more complicated seafloor deformation with larger-amplitude deformation if high slip is concentrated in smaller regions. GPS and tsunami inversions cannot attain the resolution of seismic inversions due, in part, to the availability of data.

Seismic inversions using only body waves (short wavelength, such as P and SH waves) distinguish pulses of energy from the earthquake, often with high precision, but not necessarily high accuracy. P-waves in particular are sensitive to fault orientation, to nearsource structure and to large-scale, heterogeneous velocity structures between the source and receiver (Baba et al. 2009); it is difficult to account for the inaccuracies in these parameters, particularly if the position of the hypocenter is poorly known. Nearsource structure is especially important for 2007 solutions, where the source fault is near steep trench slopes (Lay et al. 2009). Seismic inversions that include longer-wavelength teleseismic waves can mitigate instabilities of the shorter-period inversions but at the expense of precision, thus they appear more smoothed. Whether or not slip is actually “peaked,” as inversions of shorter wavelengths suggest, or more “smoothed,” as longer wavelengths require, is open to interpretation.

The number and location of data receivers can bias GPS and tsunami inversions. Only a few GPS receivers are located close to the 2006 and 2007 earthquake source region, and the spatial distribution is dependent on land location. Three of the eight GPS receivers in the Kuril Islands are survey-mode rather than continuous stations; a survey-mode station alone cannot distinguish effects of the 2006 earthquake from the 2007 earthquake (Steblov et al., 2008). Tsunami records are limited by locations of functioning tide gauges and DART buoys; available records used by Fujii and Satake (2008) and Baba et al. (2009) are all east of the earthquake rupture, mostly off the direct line of wave energy propagation. Tsunami inversions also depend on the bathymetry of the Pacific and therefore can be biased by bathymetric errors between the earthquake and observation locations.

Because the data used in GPS and tsunami inversions are dependent on deformation of the Earth's surface, they are less sensitive to slip at depth (Segall and Davis, 1997; Cummins et al, 1998). A given amount of slip will uplift the seafloor more if shallow than if deep. As such, a large amount of slip at great depths may have indistinguishable effect on surface deformation, and therefore cannot be accounted for in GPS and tsunami inversions. Fujii and Satake (2008) changed the depth extent (by changing down-dip width) of the 2007 fault plane by ±50% down-dip (from a maximum of 35 km depth to 20 km and 50 km) with negligible effect on the slip distribution.

Observations of the 2006 and 2007 tsunamis

Both the 2006 and 2007 tsunamis were measurable around the Pacific, with 2007 being smaller at coincident locations. Observations from 113 locations for the 2006 event, and 35 locations for 2007, are archived in the National Geophysical Data Center (NGDC),

Global Tsunami Database, and the Historical Tsunami Database for the World Ocean (HTDBWLD). Tide gauges recorded maximum tsunami water heights (positive deviation from sea level) as approximately 0.4 to 0.9 m at most stations in the southern Kurils, Japan, New Zealand, Chile, the Marquesas, Hawaii, the West Coast of the U.S.A., and the Aleutians (Table 4.3). Maximum water height on a tide gauge was 0.88 m in Crescent City, U.S.A., across the Pacific Ocean from the source. Of the records of the 2007 tsunami, maximum water heights are 0.4 at Chichijima Island, Japan, 0.36 m at Malokurilsk, Russia (Rabinovich et al., 2008), 0.32 m at Shemya in the Aleutian Islands, U.S.A. The 2007 tsunami is approximately 3.5 times smaller than 2006 in Hawaii, the closest direct path location with tide gauges recording the tsunamis (Table 4.3).

Rabinovich et al. (2008) investigated in detail records from the closest tide gauge stations to the earthquakes and modeled both the 2006 and 2007 tsunamis, using Ji (2006; 2007)'s inversion for earthquake slip. The closest functioning tide gauge to the epicenter of both events was in Malokurilsk, 600 km to the SW, which recorded a water height of 0.78 m for 2006 and 0.36 m for 2007. The sign of first-wave arrival was opposite between 2006 and 2007 for all stations studied by Rabinovich et al. (2008), and travel times were slightly longer to Japan for 2007 than for 2006. Maximum water heights from both tsunamis at stations in northern Hokkaido and the southern Kurils occurred 40 minutes to 3 hours after initial arrival, but 6 to 12 hours after initial arrival on the eastern coast of Hokkaido. Both Rabinovich et al. (2008) and Tanioka et al. (2008) attribute the late maximum wave in Japan to the tsunami reflecting off the Emperor Ridge. In modeling the two tsunamis, Rabinovich et al. (2008) determined that, based on Ji (2006; 2007)'s slip distribution, the highest tsunami

amplitudes from the simulated 2007 wave were larger than from 2006 for the entire nearfield—northern Simushir Island to Matua Island.

Post-tsunami survey teams in summers of 2007 and 2008 documented effects of the 2006 and 2007 tsunamis in the central Kurils Islands[8]. These teams surveyed 192 measurements of wracklines (interpreted as formed by a tsunami, see Chapter 2), including 97 profiles of terrestrial topography (Table 2.1) at 18 localities (Figure 2.4). Wracklines indicate maximum tsunami inundation (the maximum inland distance of tsunami penetration), and runup (elevation above mean sea level at inundation). Measurements of tsunami runup from wracklines average 10 m elevation within the surveyed area and range from 2 to 20 m. Observations are primarily on the Pacific sides of islands, but some face the Okhotsk Sea or a strait between islands.

During their survey, post-tsunami researchers inferred that the tsunami responsible for the highest elevation wrackline was 2006, with three lines of evidence in the field supporting but not confirming the inference. First, more than one wrackline was visible in some locations, the lower elevation one necessarily arriving after the largest wave (see Table 4.4). The lower line could have been made by a smaller, later wave from the same tsunami as the earlier, larger one; or the lower line could have been from the largest wave from 2007 while the higher line was the largest wave from 2006. Second, in a few localities, field parties found two separate deposits of sand and interpreted them to be one from each tsunami (Chapter 1). The extent of the younger sand corresponds roughly with the lower-elevation wrackline, and the older sand with the higher-elevation wrackline. A coherent layer of floatable vegetation debris between the two deposits suggests the passage of time after

[8] The post-tsunami survey team assumed that the highest measured wrackline was generated by the 2006 tsunami in every location (see Chapters 2 and 3).

deposition of the first sand layer (and of a vegetation-debris veneer) and before the second layer. If the lower wrackline was from the same tsunami as the higher, the second wave would have easily re-entrained the floatable vegetation. Instead, the vegetation debris was likely protected from erosion by a cover such as snow or ice. Third, the field team never saw merging or crossing wracklines, indicating that, at least as far as a wrackline was traced in one location, the highest wave was consistently from the same event.

These field observations are evidence that can help differentiate tsunami behavior in the central Kuril Islands. I can compare these observational data to results from tsunami simulations based on slip distributions of the earthquakes. I do not intend to dispute the validity of slip-distribution calculations, but rather to discover what type of slip-inversion approaches more accurately recreate the most important factors in the formative process of the tsunamis.

Methods

To generate and propagate a tsunami from earthquake slip-distribution patterns, I use the MOST code (Method of Splitting Tsunami; Titov and Synolakis, 1995, 1998; Titov and Gonzales, 1997), the standard forecasting model in the NOAA Center for Tsunami Research. MOST has been tested against analytical solutions of the canonical problem (cf. Hall and Watts, 1953), against results of experimental studies, and against field observations of tsunamis (Titov and Synolakis, 1997; 1998; Borrero et al. 2009). MOST numerically solves the non-linear shallow-water wave equations for the water dynamics off- and near-shore (Titov and Synolakis, 1998; Gica et al., 2008). To compute inundation, a moving boundary is implemented for the shoreline; the MOST code has the ability to handle weakly breaking

waves (Titov and Synolakis, 1995). The accuracy of the computed runup depends on bathymetric and topographic grid resolution and accuracy, as well as the time step used in computation.

I converted bathymetric and topographic data for the Kuril region into a 0.0245º (1.7 - 2.7 km) grid covering the entire study region, and within the larger grid, a series of 0.0035º (240 - 390 m) grids for regions of interest, and 0.0005º (35 - 55 m) grids to cover field areas (Figure 4.9). Telescoping grids decrease run time and allow for computation in complicated areas (Titov and Synolakis, 1998). Bathymetric grids are a combination of ETOPO1 1 Arc-Minute Global Relief Model[9] and 1 arc-second SRTM data[10]. Using Arc-GIS software, I modified ETOPO1 and STRM data with local shipping charts and coastal topographic profiles measured by the post-tsunami surveyors.

Using Okada (1985)'s equations for the deformation of a homogeneous half-space, I converted the earthquake slip distributions previously discussed into seafloor deformation patterns that define the initial tsunami. Okada (1985)'s equations are the standard method for generating initial conditions in tsunami modeling studies (Gica et al., 2008). I calculated seafloor deformations for each of the slip distributions in Tables 4.1 and 4.2: Ji (2006; 2007) (Figure 4.3), Raeesi and Atakan (2009) (Figure 4.4), Lay et al. (2009) (Figure 4.5), Baba et al. (2009) (Figure 4.6), Fujii and Satake (2008) (Figure 4.7), and Steblov et al. (2008) (Figure 4.8). I linearly increased one of Fujii and Satake (2008)'s solutions for 2006 to a M_w 8.4 when it became apparent that any 2006 earthquakes smaller than M_w 8.4 were not capable of

[9] Amante, C. and B. W. Eakins, 2008. Procedures, Data Sources and Analysis, National Geophysical Data Center, NESDIS, NOAA, U.S. Department of Commerce, Boulder, CO, http://www.ngdc.noaa.gov/mgg/global/global.html (last accessed December 2010)

[10] Shuttle Radar Topography Mission, 1 Arc Second scene SRTM_u03_n008e004, Unfilled Unfinished 2.0, Global Land Cover Facility, University of Maryland, College Park, Maryland, http://www2.jpl nasa.gov/srtm/ (last accessed December 2010)

producing tsunami runup of the observed magnitude (Table 4.1 and Figure 4.7). I also created additional slip-distribution scenarios, discussed in more detail below.

In addition to using the seafloor deformation pattern as the input for the initial tsunami in my tsunami simulations, I also used seafloor deformation as a means of comparing relative size of the tsunamis created by different earthquake slip distributions, before the simulated tsunamis became modified by bathymetry and topography (Table 4.5). In particular, I calculated the average land-level change and the volume of seafloor deformed— determined by integrating the amount of land-level change over the surface area of deformation— for any part of the seafloor that moved more than (an arbitrary) 0.25 m up or down. Finally, I calculated the potential energy of the initial tsunami by multiplying together seafloor deformation, the mass of water moved, and gravity (Table 4.5).

Methodological assumptions

The methodology for simulating tsunamis includes two important assumptions that could affect my analysis. First is that MOST assumes rupture occurred instantaneously. In the Kuril earthquake cases, rupture timing is not an important factor because the relatively brief rupture duration of both earthquakes—2006 rupture lasted 120 seconds and 2007 around 60 seconds—would have negligible impact on tsunami generation and propagation. Tsunami propagation velocity is at most 0.3 km/s in the deepest waters over the trench, and is much smaller than rupture velocities of around 2 km/s for the 2006 earthquake and around 3.5 km/s for the 2007 earthquake (Ammon et al., 2008; Raeesi and Atakan, 2009; Lay et al., 2009).

The other major assumption in my methodology is that the initial tsunami waveform is identical to surface deformations calculated using Okada (1985)'s equations, because the wavelength of ocean-bottom deformation is much larger than the water depth (cf. Tanioka et al., 2008). Tanioka et al. (2008), Rabinovich et al. (2008) and Baba et al. (2009) argue that this procedure might not be valid for 2007's high-angle-dip, narrow-wavelength, outer-rise rupture in deep water, as the fault width is only a few times greater than water depth. Tanioka et al. (2008) and Rabinovich et al. (2008) use other methods for transferring the deformation of the 2007 earthquake to the surface, such as Kajiura (1963)'s equations or the three-dimensional Laplace equation, but I did not attempt this in my tsunami-modeling technique. However, our computations indicate that the width of deformation is at least 60 km, showing that the wavelength is still many times water depth, and therefore that transformations are not necessary. Width of deformation (indicated in Tables 4.1 and 4.2 and on Figures 4.3-4.8) for this comparison is measured perpendicular to the trench axis, and includes only the deformed seafloor that moved vertically more than 0.25 m.

Comparison methods

I compared field observations with simulated tsunamis after calculating the simulated inundation/runup points closest to a field observation in our highest-resolution bathymetric grids (Figure 4.9). A grid point in a simulation was considered to be a location of maximum tsunami inundation if (a) it was once considered "dry" but became "wet" at some point during the simulation and (b) one of the four bordering grid points to the north, south, east, or west remained "dry" for the entire simulation. The elevation of inundation plus the maximum water-depth cover is the simulated runup elevation (see *Appendix B* for all results). Whether

or not simulated tsunami behavior reproduced a similar pattern of runup as field observations was a qualitative judgment based on the simulated runup in an entire high-resolution grid and all field observations therein (see Figures 4.10-4.14). For making a direct, quantitative comparison, I used only the inundation grid point in a tsunami simulation closest to a field observation.

Direct comparisons of simulated runup with field observation were considered a "good match" if simulated runup was within 25% of an observation. The value of 25% was chosen based on an estimate of the uncertainties or errors associated with simulating tsunamis in the Kuril Islands using MOST. Uncertainty in tsunami models is very complicated to assess because the error of a model varies with grid resolution, time step, bathymetry, etc. (R. Weiss, pers. comm.). While there is as yet no uncertainty assessment of MOST, Shuto, 1991 suggest a 15% error for well-defined numerical simulations. The MOST model is more complicated than tsunami models available in 1991 and bathymetry in the Kuril Islands has known errors, thus an error of 25% was deemed reasonable.

To determine which methodologies of slip-distribution inversion best reflect characteristics of an earthquake to which tsunamis are most sensitive, I also combined results for both 2006 and 2007 simulations from the same inversion methodology (Table 4.6). Because the two tsunamis can be differentiated in field observations only such that wracklines are continuous intra-site, but not inter-site, the combinations only included the higher runup values of the two simulations in any one named field site. Cases that were considered a better match had more simulated runup values within 25% of field observations, as well as a median percent match closer to 100%, with low values for standard deviation (see Table 4.6).

Analysis and results

No simulation matched field observations everywhere, but all simulations provide opportunities to study the behavior and impact of slip distribution on tsunamis from 2006-style and 2007-style earthquakes. In the following sections, I show that both 2006 and 2007 tsunamis are necessary to explain all our field observations, and some published slip distributions are better able to match these observations. However, inverting a slip distribution based solely on nearfield observations would be non-unique because the observed wracklines appear to have been a combination of both events. I also present examples of simulations that suggest the distribution of slip in a 2007-style, outer-rise earthquake is a less important factor in generating nearfield tsunami runup patterns than for a 2006-style, subduction-zone event. Differences in slip resolution can have a varied impact on tsunami runup; the size of subfaults used in earthquake inversion is most important when such resolution affects the volume of water displaced by the initial tsunami.

2006 and 2007 are fundamentally different tsunamis

Distinct differences between simulated 2006 and 2007 tsunamis are due to fault mechanics, as expected, and as discussed in earlier work by Tanioka et al. (2008), Rabinovich et al. (2008), Fujii and Satake (2008), Baba et al. (2008), etc. The normal-faulting 2007 earthquake results in a dominantly trough-shaped pattern of seafloor deformation, rather than the more common ridge-shaped pattern associated with thrust earthquakes, like 2006 (Figures 4.3-4.8). As a result, the initial tsunami is dominantly negative (below sea level) for 2007 and positive (above sea level) for 2006 (Table 4.5). The higher-angle dip of 2007 produces a noticeably narrower zone of seafloor deformation than

that of 2006 (Tables 4.1-4.2; Figures 4.3-4.8). The result is a narrower-wavelength tsunami for 2007, which behaves differently than 2006, especially when shoaling into bays or entering narrow passages. This narrower-wavelength, simulated tsunami created zones of "splash," defined as limited zones of inundation with distinctly higher runup compared to surrounding zones (see examples in Figure 4.15).

Even though the 2007 slip distributions have a smaller moment magnitude than 2006 distributions (generally M_w 8.2 vs. 8.4), and usually have less coseismic seafloor deformation, they still displace a comparable amount of water (Table 4.5). The 2007 earthquake ruptured near the Kuril-Kamchatka trench so that most seafloor deformation occurred where the overlying water column was 6-7 km, whereas 2006 deformation occurred primarily in 2-5-km-deep water. The maximum and average amounts of seafloor deformation are generally bigger for 2007 earthquakes (Table 4.5), but deformation is usually confined to a smaller area. Potential energy of each initial tsunami is a good indicator of how tsunami runup will be in the nearfield for 2007-style events, but not for 2006-style events. In simulations for both earthquake cases, high maximum seafloor deformation correlates with high maximum nearfield runup (Table 4.5). This correlation supports the idea that heterogeneous slip is an important consideration for determining nearfield runup.

Slip distributions during outer-rise events and their impact on tsunami runup

Variations in slip distribution for 2007 have less of an impact on simulated tsunami runup than for 2006. This difference could occur because 2007 is a smaller earthquake than 2006, or because 2007, as an outer-rise event, is farther away from the central Kuril Islands than 2006. I simulated theoretical distributions with disparate but reasonable differences in

slip, and with slip concentrations located at the ends of the 2006 and 2007 rupture zones (Figure 4.16). Slip concentrations from 2006-style earthquakes produced tsunamis with adjacent runup differences of 5-20 m, but of only 2-3 m for 2007-style (Figure 4.16). Such small differences in 2007-style tsunami runup imply that when modeling nearfield runup for similar-style events it may not be necessary to account for non-uniform slip distributions. The 2-3 m differences in 2007-style runup can easily be detected in our modeling method, but such a small difference between potential tsunamis might be insignificant when planning for the tsunami hazard potential of future outer-rise earthquakes.

Island-by-island analysis of tsunami runup and comparison with field observations

Investigating simulations of tsunami runup island by island from all slip distributions enables us to see that, with given data and assumptions, both 2006 and 2007 tsunamis are needed to reproduce/match all field observations. Tsunamis from larger (M_w 8.4) 2006-style earthquake scenarios (*LSei06, FTs06_84, SGPS06,* and *BSeiTs06*) more consistently match observations regionally, but on Matua Island and parts of Rasshua Island 2007 simulations better explain our surveyed wracklines than any 2006 simulation. The 2007 tsunami is more susceptible to dissipation; therefore a 2006 tsunami is also necessary to explain our field observations outside the nearfield.

The 2006 tsunami was almost universally larger than 2007 to the north or south of the rupture zone. While simulated runup was almost never as large as observed wracklines, the simulations suggest that wracklines in field sites outside the nearfield were all formed by the 2006 tsunami. The simulated 2007 tsunami is smaller than 2006 outside the nearfield because the narrower, farther-offshore 2007 tsunami experiences greater effects of dissipation than

the wider, closer 2006 tsunami. Only the 2007 simulation from *JSei07* was larger than its 2006 counterpart outside the nearfield. In general the *JSei07* simulation was larger than the *JSei06* simulation by a greater amount than any other 2007 simulation was larger than its paired 2006 simulation by the same inversion methodology. The tsunami simulations of Rabinovich et al. (2008) from the same slip distributions (based on Ji, 2006; 2007) show 2007 as being similarly larger at comparable sites south of the rupture zone, but not north. Most likely, the difference between their and my simulations is due to their use of the Laplace equations to transform seafloor deformation to surface deformation, whereas I used a 1:1 transfer of seafloor to surface deformation.

Tsunami simulations cannot distinguish whether 2006 or 2007 formed the observed wracklines on Simushir Island, possibly due to inaccurate bathymetric data (see further discussion in the *Limitations* section below). Some 2006 and 2007 simulations can produce runup in the same elevation range as field observations of wracklines in Spaseniya and Opasnaya bays, but neither tsunami can match the pattern of field observations in Dushnaya Bay (Table 4.7, Figure 4.10). In Spaseniya and Opasnaya bays, some simulated runup results from 2006-style earthquakes are virtually identical to simulated runup from 2007-style earthquakes. For example, the *JSei07* simulation and the *SGPS06* simulation are both 4-5 m in Spaseniya Bay and 5-6 m in Opasnaya Bay (Figure 4.10) and are generally within 25% of runup.

On Ketoi Island, both 2006 and 2007 simulated tsunamis also can generate runup in the elevation range of field observations and can approximate the runup pattern (Table 4.7, Figure 4.11). Therefore, the more likely source for the tsunami generating the observed wracklines on Ketoi cannot presently be determined. The *FTS06_84* and *LSei06* simulations

are both good matches in 60-80% of Ketoi sites, as are *JSei07*, *LSei07*, and *RSei07* (Table 4.7). It might be possible to differentiate between 2006 and 2007 if we had observed a wrackline in the cove between the western (Yuzhni Bay) and eastern (SE Coast) sites (see Figures 4.11 for location). Simulated runup from the three best-matching 2007 examples is highest in the cove, whereas the maximum simulated runup in the cove from 2006 tsunamis is equivalent to the maximum of nearby field observations (Figure 4.11). Unfortunately, the cove is backed by a steep cliff, which did not permit the generation and/or preservation of a wrackline for us to measure. For Ketoi runup, the two best-matching simulations from 2006 earthquakes both have concentrations of slip adjacent to Rasshua, but the location of slip concentration for best-matching simulations from 2007 slip concentrations is variable (*JSei07* = Rasshua-Matua and N. Simushir; *LSei07* = Rasshua; *RSei07* = Ketoi; Table 4.2). Variable locations of slip concentration for 2007 earthquakes that result in tsunamis with similar simulated runup on Ketoi give further indication that slip location is not an important factor in determining runup patterns in 2007-style events.

Simulations suggest that the 2006 tsunami was more likely than 2007 to have left the wrackline record on the two Ushishir islands (Table 4.7, Figure 4.12). The runup patterns from simulated tsunamis from 2006 slip distributions better match field observations than from 2007 distributions. The 2006-style *BSeiTs06*, *LSei06*, and *FTs06_84* simulations all produce a better match with field observations and with the overall field-observation pattern than any 2007 tsunami. No simulated 2007 tsunami matches more than 20% of Ushishir field measurements, while *BSeiTs06*, and *FTs06_84* can reproduce field observations 60-70% of the time (Table 4.7).

On Rasshua Island, tsunami simulations based on 2006 slip distributions match field observations better than those based on 2007 (53-58% of sites vs. 47-53% of sites, Table 4.7), but only simulated 2007-style tsunamis matched the 20 m wrackline surveyed at the very north end of Rasshua. Tsunami simulations from either 2006 or 2007 can mimic field observations equally well in southern and southeastern Rasshua (Figure 4.13). The simulated 2006 tsunami is larger on the Okhotsk coast, although simulations show both tsunamis come within 25% of field observations there. In northern Rasshua, simulated 2007 tsunamis (particularly *JSei07*, *RSei07*, and *LSei07*) produced amplification at the very northern cape of the island, a scenario that is realistic based on field observations (Figure 4.13).

On Matua Island, 2006 tsunami simulations do not produce the surveyed wrackline pattern and are rarely within the elevation range of field observations on most of the island; some 2007 runup simulations match the observed pattern and elevation range much better (Table 4.7, Figure 4.14). Only in Yuzhnaya Bay is simulated 2006 tsunami runup within close comparison of observed values (Figure 4.14). The 2007 simulations based on seismic inversions (*LSei07*, *JSei07,* and *RSei07*) better match observed wracklines in Ainu Bay and Northeast Matua in general, but neither a 2006 nor 2007 simulated tsunami is able to match the overall pattern of field observations well. Dvoynaya Bay shows extreme amplification, or "splash," in the center of the bay, most noticeably from *LSei07*, and *RSei07* simulations of 2007. The splash correlates with a location of higher observed wracklines. The *LSei07* simulation overshoots this splash; however, if the *LSei07* slip distribution in its entirety is moved down-dip by 5 km, the "splash" is markedly reduced, and this deeper-seated simulation more closely agrees with the high Dvoynaya Bay wracklines. Errors in the bathymetric grids used in simulations are the most likely explanation for the poor overall

pattern match in Ainu Bay and Northeast Matua, and potentially also for the anomaly that 2006 simulations better match field observations in Yuzhnaya Bay even though 2007 would be larger there (see *Limitations* section for further discussion).

The best-matching tsunami simulation(s)

To determine the overall best match between tsunami simulations and field observations, the two events cannot be considered in isolation of each other because both tsunamis produced runup in the Kuril Islands. Thus I combine both 2006 and 2007 simulations from each inversion methodology while using only the higher runup of the two simulations in any one named field site (see Figures 4.10-4.14 for named sites) because wracklines were continuous per named site. Since 2006 and 2007 were fundamentally different events, it is likely that one inversion methodology or geophysical data type may be better at representing the tsunami-forming characteristics of one earthquake than the other. However, for the purposes of determining the best-matching simulations, I assume that one methodology is equally sensitive to the same aspects of an earthquake, regardless of whether it was a subduction-zone or outer-rise event.

Of any intra-methodology combination, the 2006 and 2007 simulated runup based on Lay et al. (2009)'s published slip distributions (*LSei06* and *LSei07*) produced the best match with field observations (Figure 4.17; Table 4.6). Lay et al. (2009)'s combination had the most number of simulated runup points within 25% of field observations, a higher median percent match between simulation and field, and a lower median difference (Table 4.6). However, the standard deviation suggests a wider range than other simulations in the extreme high and low values of poorly matching locations (Figure 4.17).

In simulations using Lay et al. (2009)'s scenario, 2007 had a more local effect while 2006 was a regional event. That Lay et al. (2009)'s distributions are the best-match supports the hypothesis that only Matua and parts of Rasshua islands are better explained by 2007 (see previous *Island-by-island analysis of tsunami runup and comparison with field observations* section). The 2007 tsunami based on their slip distribution was large throughout the central Kurils, but not as large as for their 2006. The simulated 2007 tsunami most strongly affected coastlines directly adjacent to the location of maximum slip for the 2007 earthquake. Simulations in Dushnaya Bay (Simushir Island) and on Ketoi Island could not be differentiated as to whether *LSei06* or *LSei07* would have been the tsunami that formed the observed wracklines. Relative to tsunamis simulated from many other slip distributions, *LSei06* has consistently higher runup (Figure 4.17). The seafloor deformation from *LSei06* generates such a large tsunami because the deformation occurs over a greater area than almost all other slip distributions, with the exception of the comparable *BSeiTs06* and *FTs06_84*. Maximum slip from the *LSei06* earthquake is adjacent to Ushishir-to-Rasshua islands; the other slip concentrations that simulate equally large 2006 tsunamis are roughly similar— either just to the south (*BSeiTs06*) or just to the north (*FTs06_84*).

Other simulations using intra-methodology combinations of 2006 and 2007 indicate different relative contributions of either event to overall runup distribution (see *Appendix B*). The combined simulation of *SGPS06* and *SGPS07*, based on the GPS inversion of Steblov et al. (2008), would indicate that wracklines were formed by a roughly equal combination of the two tsunamis. Although generally smaller, simulated tsunamis based on Steblov et al. (2008) were similar to Lay et al. (2009), in that 2006 was larger outside the nearfield and on most of Simushir Island, and 2007 was larger on Rasshua and most of Matua islands. Simulations

based on Steblov et al. (2008) are different from those based on Lay et al. (2009) in that *SGP07* was larger than *LSei07* on Ushishir, and that the 2006 and 2007 tsunamis could not be distinguished on parts of Matua.

Intra-method simulation combinations based on Fujii and Satake (2008) would indicate that 2006 was the only wave that formed high wracklines in the Kurils, regardless of whether the *FTs06_82* or *FTs06_84* simulation is used in the combination. Conversely, the *JSei06* and *JSei07* combination of simulations from slip distributions of Ji (2006; 2007) would indicate that 2007 was the only tsunami forming the wracklines, even in the farthest field sites from the source. Results from tsunami simulation combination based on Raeesi and Atakan (2009), *RSei06* and *RSei07*, were similar to Ji (2006; 2007), with higher runup in the nearfield being exclusively from 2007, although simulated 2006 produced higher runup outside the central Kurils for most field sites.

The effect of slip resolution on the tsunami

The discussions above consider only focal mechanism and slip location to be primary factors in generating inter-simulation differences in nearfield runup, but differences in subfault resolution among inversion methodologies also could be important. For example, even if higher-resolution inversions have the same average slip as lower-resolution inversions, higher-resolution inversions tend to have higher maximum slip and smaller-area concentrations of higher slip. If tsunamis are less sensitive to maximum slip than to average slip, then earthquakes with closer-to-the-average slip covering a greater area of the rupture would generate a larger tsunami than earthquakes with the same average slip value but a higher maximum slip.

As a test of the effect of slip-distribution resolution on the tsunami, I manipulated the spatial resolution of a few seismic inversions. The different methodologies employed in inverting geophysical data to earthquake slip distributions for the 2006 and 2007 tsunamis used essentially two different subfault resolutions. Inversions that incorporated seismic data used subfault lengths and widths generally of 10 to 20 km, while inversions without seismic data used subfault lengths and widths generally of 40 to 50 km (Table 4.1 and 4.2). For my test, I decreased the spatial resolution (length and width of subfaults) of seismic inversions (in the example presented here, of *LSei06* and *LSei07*) to resemble more closely the inversions based on tsunami or GPS data, and I averaged the original slip distribution into the new larger areas (Figure 4.18 and 4.19).

When spatial resolution of slip patches decreased, simulated nearfield runup increased in the 2007 case, but stayed approximately the same in the 2006 case (Figure 4.20). Maximum deformation increased by 50% for the 2006 case but decreased by 40% for 2007, even though the average amount of seafloor deformation stayed the same in both cases (Table 4.5). Width of deformation decreased slightly for 2006 but almost doubled for 2007. Total seafloor deformation and potential energy increased in both cases, although 2007 increased by 50-60% while 2006 by only 10-20% (Table 4.5).

The simulations tested suggest that width and amount of deformation, as well as potential energy of the initial tsunami are the important factors for generating nearfield runup; peak or average deformation and maximum or average slip do not correlate with the differences observed in the nearfield tsunami. Width of deformation increases if coarser subfaults redistribute a concentration of slip or cause closer-to-average slip in the up-dip and down-dip extent of the rupture zone. If these two parameters remain similar (such is the 2006

case, Table 4.5, Figure 4.18), there will not be a significant effect on tsunami runup. Potential energy increases if coarser subfaults result in more slip occurring in deeper water and at the shallowest extent of the rupture. In the case of 2006 and southwest-dipping 2007 earthquakes, deeper water and shallower slip are synonymous, but deeper water is associated with deeper slip for northwest-dipping 2007 earthquakes. The *LSei07* simulation is a northwest-dipping earthquake; consequently, slip averaged into larger areas extended more slip deeper, and the associated deeper deformation moved a larger water column.

Predicting what would happen in all cases if earthquake slip resolution were to be standardized can be problematic because seafloor deformation depends on the original distribution of slip. My general conclusion from changing the resolution of the *LSei06* and *LSei07* simulations is that finer-resolution subfaults are necessary in tsunami modeling if concentrations of slip are located at the edges of a rupture zone. If slip is more centrally located in a rupture area, finer- and coarser-resolution distributions can generate similar nearfield tsunamis. Alternately, if subfault resolution in an inversion is already "coarse," the number of finer-resolution slip configurations is too great to tell in what way resolution biases the simulations.

Inverting a slip distribution based solely on nearfield runup

I had originally planned to manipulate 2006 or 2007 slip distributions in an attempt to match field observations more thoroughly, and thus to understand better the formative properties of the two tsunamis, but it is apparent that this goal is unattainable. Results discussed previously show that runup in some sites is better matched by 2006, some by 2007, but either could be equally likely on Simushir and Ketoi islands (see *Island-by-island*

analysis of tsunami runup section). Because I cannot discriminate wholesale between the tsunamis with our nearfield observations of tsunami wracklines, further attempts at producing or modifying a slip distribution to better match field observations encounter a problem of non-uniqueness. That is, more than one combination of specific waveforms from either event could combine to reproduce our field observations.

Limitations

All hydrodynamic numerical models are limited because they must approximate complex flow dynamics, and tsunamis are particularly complex. Accurate bathymetry and high-resolution bathymetric grids are necessary to successfully simulate realistic patterns of runup. Errors in, or too low resolution of, nearshore bathymetry can cause inaccurate wave setup and shoaling, resulting in too high or too low runup, and in inaccurate representations of resonance or edge waves. Too-small tsunami runup is a more common situation than too-high when using tsunami models due in part to nearshore grid resolution. Coarse grid resolutions underestimate runup heights (Titov et al., 1997; Pan et al., 2010); refined grids are more able to resolve higher frequency waves because they better capture energy preservation (Myers and Baptista, 2001). Pan et al. (2010) showed that >5-m differences in simulated runup over 20 m can occur between simulations on grids with 0.0003º and 0.0006º resolution. Their conclusion is a likely explanation for why most field observations greater than 15 m were rarely reproduced by tsunami simulations (see Figure 4.17); appropriate nearshore grid resolution needed to produce field observations of the highest runup in the central Kurils may be finer than my 0.0005º grids.

Publicly available bathymetry in the Kuril Islands has known errors; I attempted to account for shallow-water errors by merging the publicly available bathymetry with shipping charts. Baba et al. (2009) compare bathymetry from the (publicly available) GEBCO dataset with bathymetry from an ocean-bottom-seismographic survey by Japanese oceanographers; GEBCO bathymetry deviated from survey measurements by up to 600 m in some locations. The downloadable ETOPO1 bathymetry I used is similar to GEBCO bathymetry, since little has changed in the collection of new datasets for the Kurils in recent years. The shipping charts I used are based on nearshore maps from World War II; thus our grids are more accurate in areas with human occupation in the war, and are less reliable where volcanic or other processes may have altered the coastal zone since the war.

Additional problems with bathymetry occur due to our methodologies of extrapolating gridded bathymetry from contour lines from shipping charts using Arc-GIS, and combining ETOPO1 with shipping charts. While much care was taken to reduce the number of extrapolation errors between topographic lines, small inconsistencies still exist, especially at the apex of convex and concave slopes. Errors associated with the combination of ETOPO1 and shipping charts are due to the disagreement of water depth in the combination zone. All water deeper than 1000 m is solely from the ETOPO1 dataset, and water shallower than 100 m water depth is from shipping charts. Between those depths, the bathymetry is a merge of the two. If both the charts and ETOPO1 are accurate and consistent with each other, I assume the result agrees with reality. However, more often than not, these two datasets did not agree, and I forced the combination to change smoothly from one dataset to the other. The largest disagreements were, unfortunately, on the continental slope between the trench and the islands.

As a result of the problems with bathymetric accuracy, up to one third of our locations may be overly affected by bathymetric irregularities or may require a higher resolution to produce reliable results. Two grids in the nearfield, *aisb* and *dush* (see location in Figure 4.9), had severe problems with simulated runup producing the pattern of field observations. In the *aisb* grid on Matua Island, our field observations record a wrackline in Ainu Bay (13-20 m) that was more than twice as large as that in adjacent Yuzhnaya Bay to the east (4-8 m). However, simulations always produced runup that was approximately the same between the two bays (at most, a difference of 2-3 m) (Figure 4.14). Either the simulations were affected by inaccurate or low-resolution bathymetry, or a secondary process such as a landslide generated a locally amplified wave in Ainu Bay. In the *dush* grid on Simushir Island, 2007 tsunamis amplify in the center of the bay even though observed wracklines are lowest there. Either 2007 did not have large runup in Dushnaya Bay, or our bathymetric grid is incorrectly affecting the shoaling of the 2007 wave. The latter is more likely the case because 2006 tsunamis also do not match the observed pattern, even though simulated 2006 tsunamis do not amplify in the center of the bay.

Tsunami simulations in many of the grids to the north or south of the rupture zone (*kast*, *pesc*, *vosk*, *musl* and *blak* grids in Figure 4.9) almost never generate runup as large as field observations. Explanations include (a) dissipation in MOST was greater than in reality, (b) MOST unrealistically represented energy transfer along the island chain, (c) the wavelengths of all simulated 2006 earthquakes were too narrow and therefore dissipated too quickly, (d) all slip distributions of 2006 were too small, or (e) all 8 grids outside the nearfield had bathymetric errors or too coarse a grid resolution that acted to reduce tsunami energy and runup.

Besides resolution, bathymetry and dissipation, simulated tsunami behavior is also constrained by a model's constitutive equations. When the MOST model calculates runup, it cannot mimic a breaking wave; MOST is considered to reliably reproduce runup when a wave is weakly breaking, but runup associated with strongly breaking waves could be over- or under-estimated by MOST depending on the situation (Vasily Titov and Diego Arcas, pers. comm.). Weakly nonlinear, nonbreaking waves have larger runup on gentle nearshore slopes (Lynett, 2007), which is definitely not the case in the central Kurils, where the highest runup values are often associated with the steepest slopes (Chapter 2).

Conclusions

The general conclusion of our modeling efforts is that the 2007 tsunami alone is not capable of reproducing all field observations, that a 2006 tsunami might be able to, but that a combination of the largest runup of each of the two tsunamis is more likely responsible for the surveyed wracklines. Runup on Matua Island and northernmost Rasshua Island were better matched by simulations of 2007 tsunamis, whereas a 2006 tsunami is necessary to explain runup measurements outside the central Kurils and in the Ushishir islands. Which tsunami was responsible for wracklines on Simushir, Ketoi and parts of Rasshua Island cannot be distinguished based solely on existing field observations; some simulated tsunamis from slip distributions of the 2006 earthquake matched observations equally well as some 2007 slip-distribution simulations.

As judged by the ability to match field observations, the best tsunami simulations of 2006 all have earthquake slip located in the north-central part of the rupture zone (approximately adjacent to Rasshua or Matua islands). The best tsunami simulations of 2007

have variable locations of slip concentrations. Additionally, I show that extreme but reasonable differences in slip-concentration location have less of an impact on nearfield tsunami runup for a 2007 tsunami than for a 2006 tsunami. The difference may be an artifact of 2007 being a smaller earthquake than 2006 or may be because 2007 was an outer-rise event, and therefore farther away from the Kuril Islands than 2006.

Looking only at the nearfield runup (wrackline) data, I conclude that Lay et al. (2009)'s inversions of P, surface and W-phase teleseismic waves for 2006 and 2007 combined to reproduce field observations of runup better than other combinations. Simulated tsunamis using their earthquake slip distribution predict that tsunami runup was primarily from 2006, but that 2007 was the larger wave on Matua Island— a similar result as our earlier conclusion. Other M_w 8.4 2006 slip distributions also show that a subduction-zone tsunami is capable of explaining most of the field observations in the nearfield, with the exception of Matua Island. Simulations of 2007 alone can generate tsunami runup of comparable magnitude to field observations at some sites, but in fewer locations than can M_w 8.4 2006 simulations.

I am unaware of any previous tsunami modeling based on inversions of W-phase seismic waves, but our conclusions indicate that W-phase inversions are sensitive to similar aspects of the earthquake as that of tsunamis. Kanamori and Rivera (2008) similarly suggest that amplitudes of long-period waves better represent the tsunami potential of an earthquake, and they further propose that W-phase inversions are effective for very large earthquakes and for slow tsunami earthquakes. Rapid W-phase source inversions also can be used for rapid tsunami-warning purposes because they more accurately estimate moment magnitude than short-period seismic waves (Kanamori and Rivera, 2008). It remains to be seen if all

inversions based on W-phase data should be preferred for modeling the nearfield runup of a tsunami; a future test using only one well-observed tsunami will likely constrain more variables and enable further investigation of this hypothesis.

Seismic inversions resolve slip at a much higher resolution (length and width of subfaults) than tsunami or GPS inversions do; resolution of slip plays an important role in determining the overall seafloor deformation pattern, which then affects tsunami runup in the nearfield. By decreasing the slip resolution of two seismic inversions, I show that tsunamis are more sensitive to the total amount of seafloor deformation than to peak amplitude of deformation or maximum slip, any of which depend on the scale at which slip is inverted. In the particular example I examined, averaging slip over a larger area had the greatest effect when it caused an increase in the width and total volume of deformation. The effect of subfault size on the tsunami depends on how those subfaults allocate slip to the shallow and deep reaches of the rupture zone.

The case of the 2006 and 2007 Kuril Island tsunamis is an excellent example of a situation where farfield records—of one tsunami consistently larger than another—do not necessarily indicate what the nearfield runup pattern and magnitude will be. Understanding nearfield runup is an important consideration for evaluating potential tsunami hazards. Additionally, numerical modeling of both the 2006 and 2007 earthquakes and tsunamis is capable of untangling two unobserved events (cf. Martin et al., 2008), an indication that this method is a potentially useful tool for paleo-tsunami studies.

Table 4.1: Overview of earthquake parameters, different interpretations of the 2006 earthquake slip distribution used in tsunami simulation, and parameters of the intial tsunami in simulations

		Fujii and Satake (2008)	**Baba et al. (2009)**	**Steblov et al. (2008)**	**Lay et al. (2009)**	**Raeesi and Atakan (2009)**	**Ji (2006)**
	method	tsunami inversion (tide gauges, DART and cabled tsunami sensors)	seismic (P, Rayleigh and Love waves) and tsunami (bottom pressure records)	GPS inversion (continuous and survey)	seismic (W phase, surface and P waves)	seismic (P waves)	seismic (P, SH, Raleigh, Love waves)
model parameters	along-strike length (km)	200	400	230	240	280	400
	along-dip width (km)	100	140	150	100	150	137.5
	subfault length (km)	50	20	57.5	20	20	20
	subfault width (km)	50	20	50	10	15	12.5
	strike	214º	220º	221º	220º	220º	220º
	dip	8º (shallow) and 15º (deep)	10º	9º, 16º, 22º	15º	15º	14.89º
	rake	92º	calculated (90 ± 45); avg. 109º	calculated; avg. 114º	calculated; avg. 96º	calculated; avg. 100º	calculated; avg. 91º
earthquake parameters	hypocenter depth	-	20 km below sea level	30 km below sea level	12 km in crust	28.5 km below sea level	27 km in crust
	M_o (Nm)	2.5 x 10^21	5.0 x 10^21	5.14 x 10^21	5.0 x 10^21	2.78 x 10^21	3.9 x 10^21
	M_w	8.2 *(or increased to 8.4)*	8.4	8.4	8.4	8.23	8.3
slip distribution	total avg. slip/avg. slip if > 0.25 m (m)	8.2 = 3.1/4.1 8.4 = 5.4/7.2	2.6/2.8	3.6/5.4	4.6/4.6	1.9/1.9	1.7/2.3
	maximum slip (m)	8.2 = 7.4 8.4 = 13	11.8	12.1	14.0	5.6	8.9
	location of maximum slip perpendicular to[#]	Rasshua - Matua	Ketoi - Ushishir	N Simushir - Ketoi	Ushishir - Rasshua	N Simushir; Kruzenshtern Strait; Rasshua	Ushishir - Rasshua
	size of slip patch(es)[$] (length x width) (km)	50 - 100 x 50 - 100	140 x 10	57.5 x 100	80 (or 60) x 50 (or 10)	60 (or 30) x 30; 45 (or 30) x 60; 20 x 15	80 x 37.5
	approximate depth in crust of maximum slip (km)	5 - 31	6.5 - 10	0.5 - 22	3 - 13	13 - 20; 31 - 42; 9	8 - 19
	average slip within patch(es)[$] (m)	8.2 = 6.3 8.4 = 11.1	10.3	11.2	11.1	4.8; 4.5; 4.1	7.5
	number of subfaults in slip patch(es)[$]	3	7	2	8	5; 8; 1	12

= see Figure 4.1 for island names and locations
$ = "patch" defined as subfaults with at least 2/3 of maximum slip

Table 4.2: Overview of earthquake parameters, different interpretations of the 2007 earthquake slip distribution used in tsunami simulation, and parameters of the intial tsunami in simulations

		Fujii and Satake (2008)	**Steblov et al. (2008)**	**Lay et al. (2009)**	**Raeesi and Atakan (2009)**	**Ji (2007)**
	method	tsunami (tide gauges, DART, and cabled tsunami sensors)	GPS (continuous and survey)	seismic (W phase, surface and P waves)	seismic (P waves)	seismic (P, SH, Raleigh, and Love waves)
model parameters	along-strike length (km)	240	230	300	240	200
	along-dip width (km)	40	50	60	40	35
	subfault length (km)	40	57.5	20	20	8
	subfault width (km)	40	50	10	10	5
	strike	42º	41º	220º	40º	42º
	dip	58º	59º	47º	45.5º	57.89º
	rake	-114º	calculated; avg. -125º	calculated; avg. -106º	calculated; avg. -97º	calculated; avg. -114º
earthquake parameters	hypocenter depth	-	30 km below sea level	4 km in crust	14 km in crust	18 km in crust
	M_o (Nm)	1.1 x 10^21	2.66 x 10^21	2.6 x 10^21	1.73 x 10^21	1.9 x 10^21
	M_w	8.0	8.22	8.2	8.1	8.1
slip distribution	total avg. slip/avg. slip if > 0.25 m (m)	2.7/4.4	4.4/4.4	2.3/2.7	3.8/4.1	7.0/7.3
	maximum slip (m)	3.5	8.3	15.0	13.3	20.3
	locationof maximum slip perpendicular to[#]	Rasshua - Matua	N Simushir - Ketoi	Rasshua	Ketoi	Rasshua-Matua; N Simushir
	size of slip patch(es)[$] (length x width) (km)	80 x 40	57.5 x 50	100 x 10	80 x 20	48 (or 16) x 15 (or 5); 8 x 15
	depth in crust of maximum slip (km)	7 - 41	0.5 - 44	4 - 10	11 - 25	3 - 16; 3 - 16
	average slip within patch(es)[$] (m)	3.3	8.3	12.6	11.3	16.6; 17.3
	number of subfaults in slip patch(es)[$]	2	1	5	7	13; 3

= see Figure 4.1 for island names and locations

$ = "patch" defined as subfaults with at least 2/3 of maximum slip

Table 4.3: Tide-gauge locations with records of the maximum water heights of both 2006 and 2007 tsunamis; 2006 is always larger. Records from the National Geophysical Data Center Global Tsunami Database, the Historical Tsunami Database for the World Ocean and Rabinovich et al. (2008).

Location	2006 max. height (m)	2007 max. height (m)	Times 2006 is bigger by
ABASHIRI, JAPAN	0.24	0.09	2.8
ADAK, SWEEPER COVE, AK, USA	0.15	0.05	3.0
ANTOFAGASTA, CHILE	0.23	0.10	2.3
ARENA COVE, CA, USA	0.59	0.25	2.4
CALLAO-LA PUNTA, PERU	0.37	0.14	2.6
CHARLESTON, OR, USA	0.19	0.04	4.8
CHICHIJIMA ISLAND, JAPAN	0.50	0.40	1.3
CRESCENT CITY, CA, USA	0.88	0.23	3.8
HACHINOHA, JAPAN	0.53	0.15	3.7
HANASAKI, JAPAN	0.40 or 0.37	0.13 or 0.14	2.6 to 3.1
HILO, HI, USA	0.49	0.11	4.5
HONOLULU, HI, USA	0.17	0.06	2.8
IQUIQUE, CHILE	0.32	0.09	3.6
KAHULUI, HI, USA	0.76	0.17	4.5
KUSHIRO, JAPAN	0.20 or 0.27	0.10 or 0.13	2.0
KWAJALEIN, MARSHALL ISLANDS	0.14	0.11	1.3
LA PUSH, WA, USA	0.16	0.13	1.2
MALOKURILSK, RUSSIA	0.78	0.36	2.2
MIDWAY ISLANDS	0.48	0.19	2.5
NAWILIWILI, HI, USA	0.44	0.10	4.4
NEAH BAY, WA, USA	0.05	0.03	1.7
OFUNATO, JAPAN	0.42	0.22	1.9
PAGO PAGO, AMERICAN SAMOA	0.22	0.11	2.0
POINT REYES, CA, USA	0.31	0.12	2.6
PORT ORFORD, OR, USA	0.56	0.27	2.1
PORT SAN LUIS, CA, USA	0.57	0.11	5.2
RAROTONGA, COOK ISLANDS	0.09	0.04	2.3
SAN FRANCISCO, CA, USA	0.15	0.05	3.0
SANTA BARBARA, CA, USA	0.40	0.10	4.0
SHEMYA ISLAND, AK, USA	0.46	0.32	1.4
SITKA, AK, USA	0.13	0.08	1.6
TALCAHUANO, CHILE	0.49	0.08	6.1
TOKACHIKO, JAPAN	0.37	0.14	2.7
URAKAWA, JAPAN	0.59	0.18	3.4
WAKE ISLAND	0.11	0.08	1.4
WAKKANAI, JAPAN	0.16	0.04	3.9
YAKUTAT, AK, USA	0.06	0.05	1.2
YUZHNO-KURILSK, RUSSIA	0.28	0.06	5.0

Table 4.4: Parameters of lower elevation tsunami wrackline compared to higher-elevation wrackline at observed locations

Island	Site	Longitude (ºE)	Latitude (ºN)	Lower-elevation wrackline		Higher-elevation wrackline	
				Runup* (m)	Inundation (m)	Runup* (m)	Inundation (m)
Simushir	dush103	152.20214	47.07818	3.2	15	10.8	49
Simushir	dush012	152.17726	47.06393	3.6	75	6.9	120
Simushir	dush106	152.19476	47.07537	4.1	32	13	70
Simushir	dush006	152.16650	47.05628	4.4	32	4.4	106
Simushir	dush102	152.20566	47.07835	4.4	32	7.7	51
Simushir	dush101	152.20884	47.07880	4.6	23	8.8	44
Simushir	dush110	152.18429	47.06960	5.2	56	8.8	114
Simushir	dus2_06	152.17549	47.06201	5.6	70	6.7	122
Simushir	dush007	152.16878	47.05807	7.4	105	6.3	139
Simushir	dus1_06	152.18614	47.06971	7.6	140	10.6	100
Matua	aisb001	153.22497	48.04412	10.3	175	17.1	327

* corrected for tides

Table 4.5: A comparison of the seafloor deformation (intial tsunami equivalent) calculated for each earthquake slip distribution, compared to the on-land simulated tsunami in the central Kuril Islands.

model	maximum deformation (m)	width of deformation[$] (km)	average deformation[$]			total seafloor deformation[$]			potential energy[$#]			nearfield inundation	
			absolute value (m)	only positive (m)	only negative (m)	absolute value (m^3*10^{10})	only positive (m^3*10^{10})	only negative (m^3*10^{10})	absolute value ($J*10^{17}$)	only positive ($J*10^{17}$)	only negative ($J*10^{17}$)	average runup[&] (m)	sum of all runup[^] (m)
BSeiTs06	4.0	140	0.7	0.9	-0.4	2.4	1.6	-0.7	12.1	10.6	-1.5	9.6	1287
FTs06_84	4.0	210	0.9	1.2	-0.7	2.8	1.9	-0.9	9.2	7.7	-1.5	7.7	1035
LSei06	4.3	200	0.9	1.3	-0.5	2.1	1.6	-0.5	7.4	6.4	-1.0	7.4	989
FTs06_82	2.3	140	0.7	0.8	-0.5	1.5	1.0	-0.4	4.9	4.2	-0.7	5.5	731
SGPS06	4.0	175	0.8	1.0	-0.6	2.5	1.8	-0.8	10.1	8.0	-2.1	5.1	677
RSei06	1.5	230	0.5	0.5	-0.5	1.9	1.3	-0.5	7.5	6.6	-1.0	3.8	504
JSei06	2.8	200	0.7	1.0	-0.4	1.6	1.4	-0.3	9.9	9.2	-0.8	3.5	469
JSei07	-7.4	110	1.0	0.6	-1.4	1.6	0.5	-1.1	10.9	3.0	-7.9	9.5	1271
LSei07	-6.4	60	1.1	0.4	-1.5	1.4	0.2	-1.2	9.2	1.1	-8.1	9.5	1269
RSei07	-4.1	110	1.2	0.3	-1.4	1.5	0.1	-1.4	9.3	0.5	-8.8	9.2	1232
SGPS07	-1.5	60	0.6	0.0	-0.6	1.2	0.0	-1.2	7.2	0.0	-7.2	6.5	869
FTs07	-0.7	75	0.4	0.0	-0.4	0.3	0.0	-0.3	2.0	0.0	-2.0	2.6	344
coarse *LSei06*	6.3	180	0.9	1.3	-0.5	2.5	1.8	-0.7	8.3	6.9	-1.3	8.4	1127
coarse *LSei07*	-3.6	110	1.1	0.3	-1.3	2.1	0.2	-2.0	15.0	0.8	-14.2	11.5	1541

[$] only calculated for seafloor deformation greater than 0.25 m

[#] potential energy calculated using mass of water column x gravity x seafloor deformation

[&] field observation average is 10.6

[^] field observation sum is 1422

Table 4.6: Overview of match between maximum simulated tsunamis (combined 2006 and 2007) compared to observations from only the central Kuril Islands

slip distribution	Fujii and Satake (2008)*	Fujii and Satake (2008)	Lay et al. (2009)	Ji (2006; 2007)	Raeesi and Atakan (2009)	Steblov et al. (2008)	Baba et al. (2009)[$]
combined tsunami models	*FTs06_84 FTs07*	*FTs06_82 FTs07*	*LSei06 LSei07*	*JSei06 JSei07*	*RSei06 RSei07*	*SGPS06 SGPS07*	*BSeiTS06*
# above	35	9	56	52	43	20	63
# below	99	125	78	82	91	114	71
# within 25% (out of 134)	54	20	62	53	53	41	52
median location agreement	76%	50%	90%	87%	83%	66%	94%
standard deviation of agreement	37%	27%	53%	47%	44%	39%	54%
median runup difference	-2.2	-4.8	-0.8	-1.1	-1.7	-3.0	-0.4
standard deviation of runup	3.9	3.8	4.6	4.6	4.0	4.4	4.8

* using 2006 as an Mw 8.4
$ = only 2006 modeled

Table 4.7: Percentage of sites by location that have good match (within 25%) with observed runup

location		grids^	total observations	2006							2007				
				FTs06_84	*FTs06_82*	*LSei06*	*JSei06*	*RSei06*	*SGPS06*	*BSeiTs06*	*FTs07*	*LSei07*	*JSei07*	*RSei07*	*SGPS07*
S. Kurils (Urup and Chirpoi)		Kast, Pesc	7	0%	0%	0%	0%	0%	57%	0%	0%	0%	0%	0%	0%
Central Kuril Islands	Simushir	Spas, Opas, Dush	36	31%	6%	19%	8%	14%	36%	44%	0%	28%	33%	25%	19%
	Ketoi	Keto	15	67%	27%	80%	0%	13%	20%	27%	0%	47%	60%	80%	20%
	Ushishir	Rypo	10	70%	10%	30%	0%	0%	0%	60%	0%	20%	20%	20%	10%
	Rasshua	Rass, Rasi, Nepr, Rasn	19	53%	11%	58%	11%	26%	16%	58%	11%	47%	53%	47%	47%
	Matua	Aisb, Sary, Mane	54	30%	20%	30%	0%	0%	11%	28%	0%	46%	37%	39%	33%
N. Kurils (Shiashkotan, Kharimkotan, Onekotan)		Vosk, Land, Seve, MuslM, MuslL, Blak	19	37%	21%	0%	0%	0%	42%	0%	0%	0%	5%	0%	0%

^ See Figure 4.9 for locations

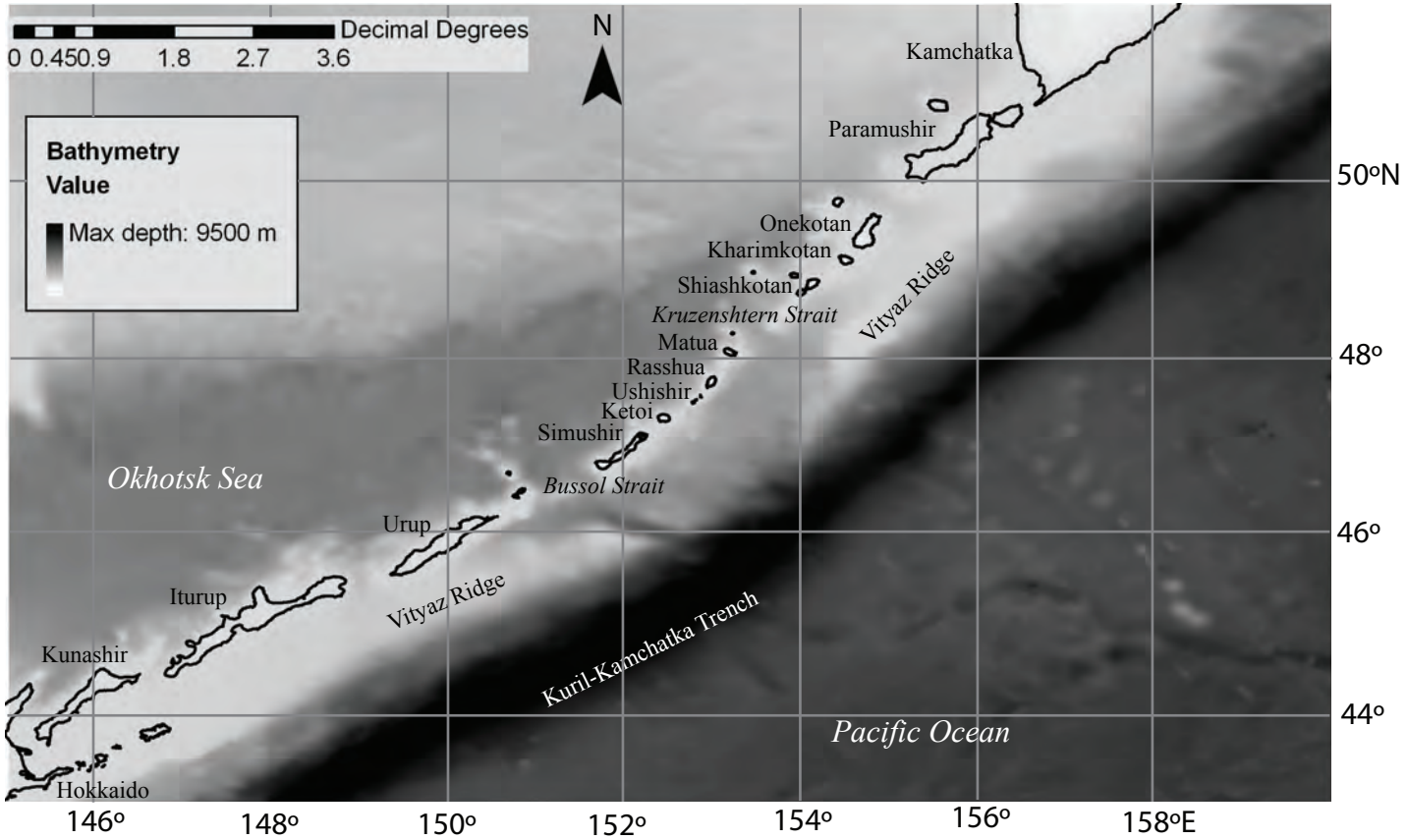

Figure 4.1: Location, bathymetry and geographic features of the Kuril Islands, Russia. Bathymetry is from ETOPO1 1 Arc-Minute Global Relief Model (www.ngdc.noaa.gov/mgg/global/global.html). The central Kuril Islands extend from the Bussol Strait to the Kruzenshtern Strait.

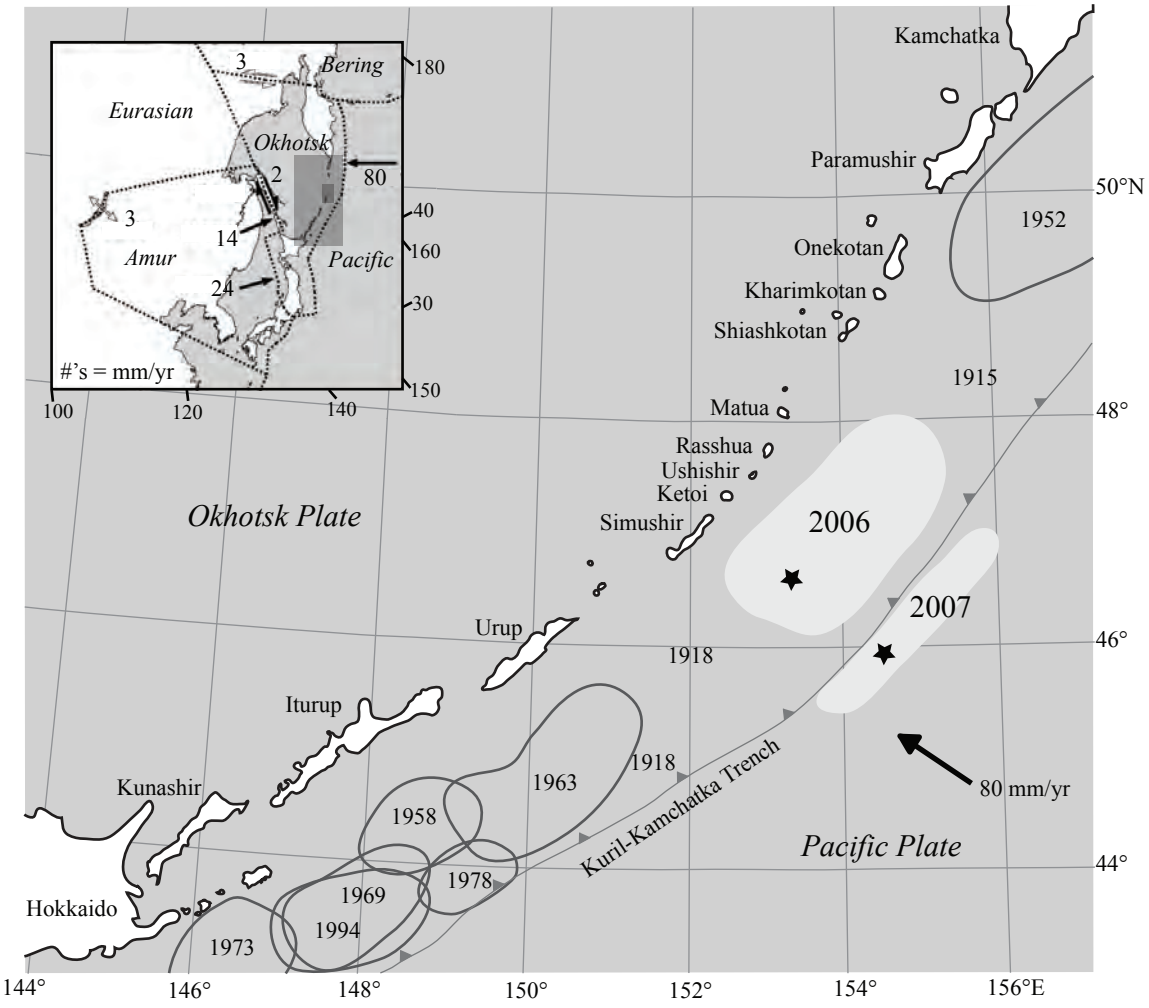

Figure 4.2: Tectonic setting (inset) and past earthquakes (after Fedotov et al., 1982) in the Kuril Islands. Stars indicate the GCMT epicenters of 2006 and 2007 earthquakes. Rupture zones for historical earthquakes are outlined in gray and for 2006 and 2007 in white. Rupture zones for the 1915 and two 1918 earthquakes are unknown. Plate motions in inset are in mm/yr.

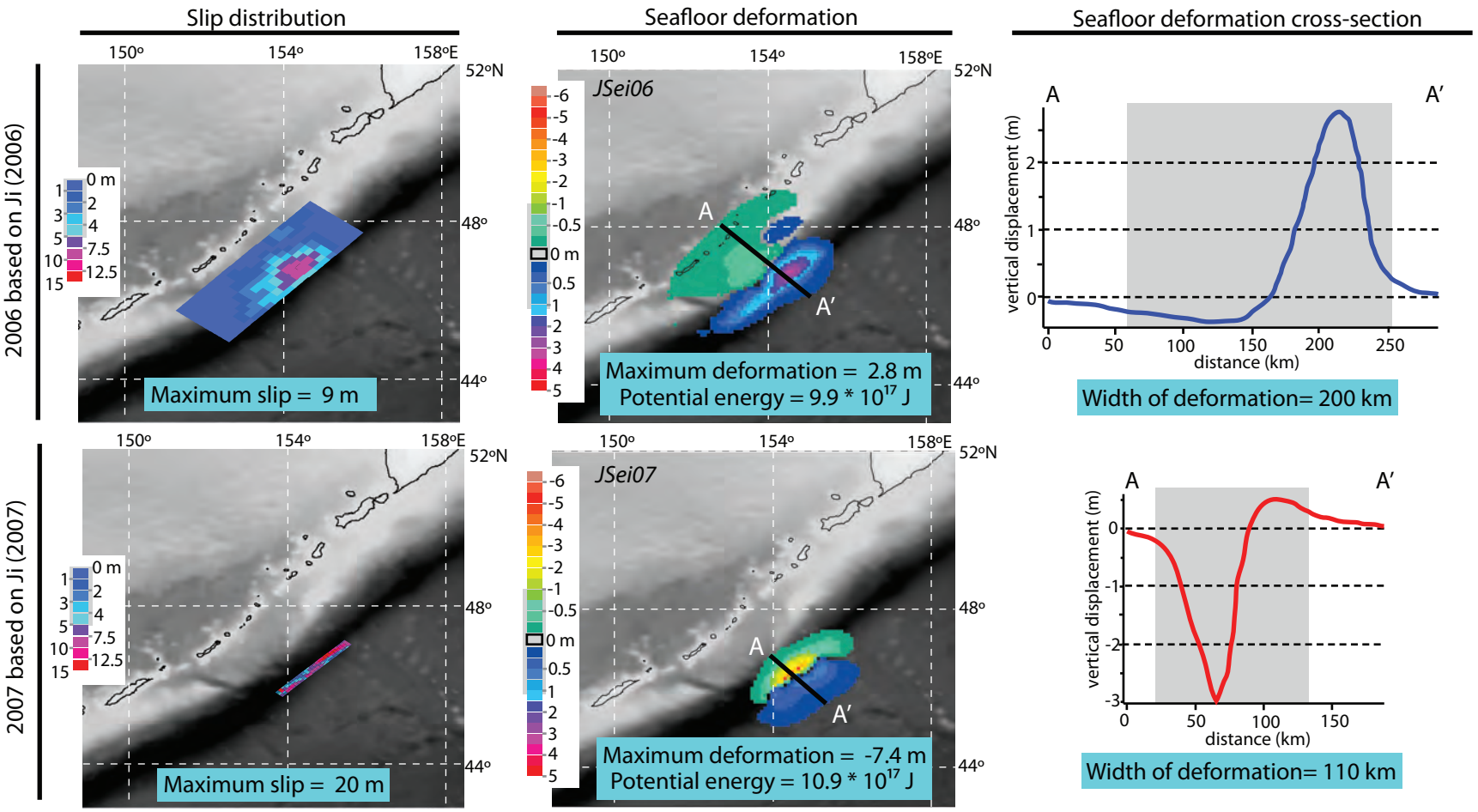

Figure 4.3: Ji (2006; 2007)'s slip distributions for both the 2006 and 2007 earthquake, the resulting seafloor deformation patterns (and therefore initial tsunami waveforms) produced by Okada (1985)'s equations, and a cross-section through each initial tsunami. Names for tsunami simulations based on the slip distributions (*JSei06* and *JSei07*) are indicated.

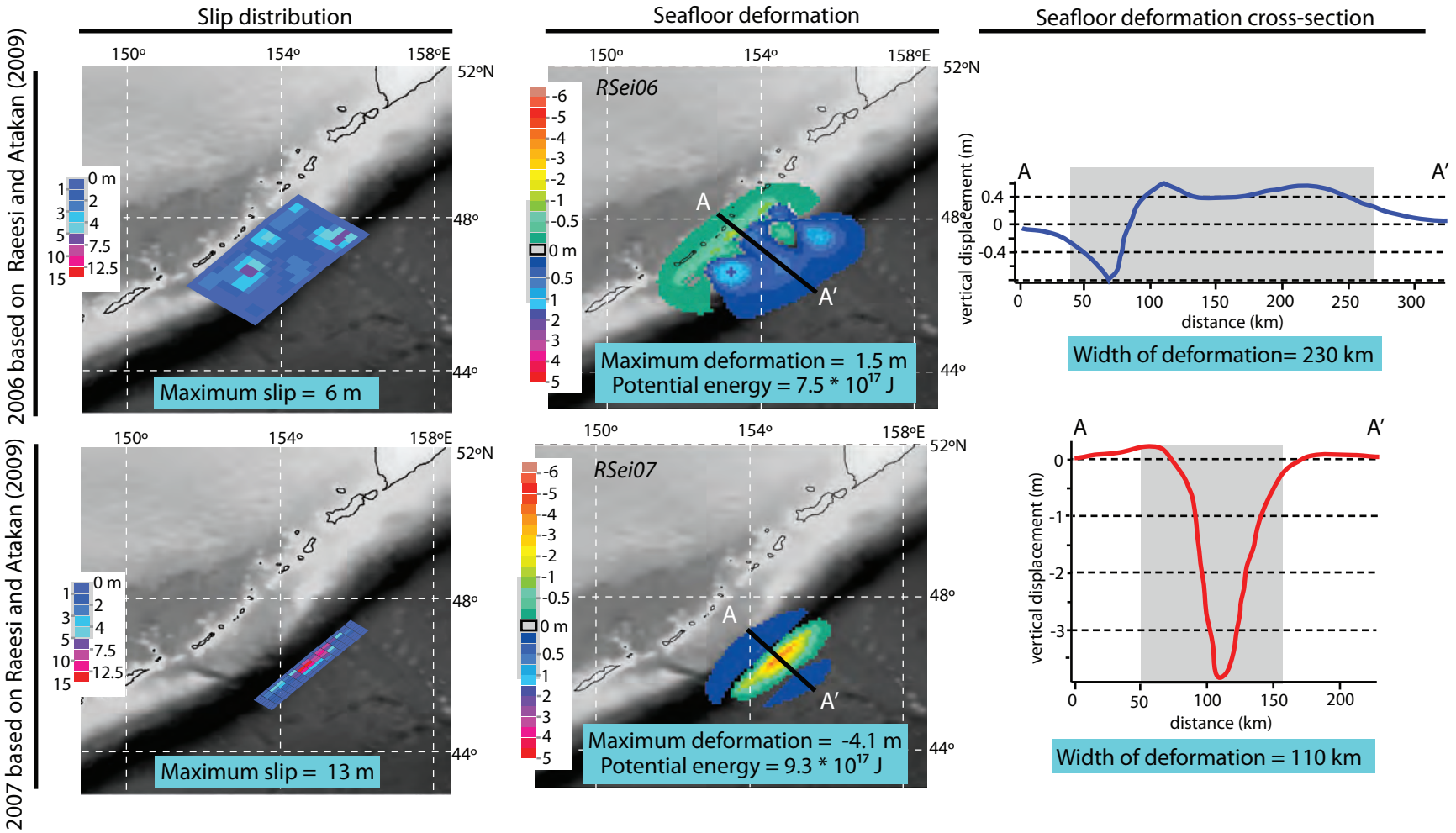

Figure 4.4: Raeesi and Atakan (2009)'s slip distributions for both the 2006 and 2007 earthquake, the resulting seafloor deformation patterns (and therefore initial tsunami waveforms) produced by Okada (1985)'s equations, and a cross-section through each initial tsunami. Names for tsunami simulations based on the slip distributions (*RSei06* and *RSei07*) are indicated.

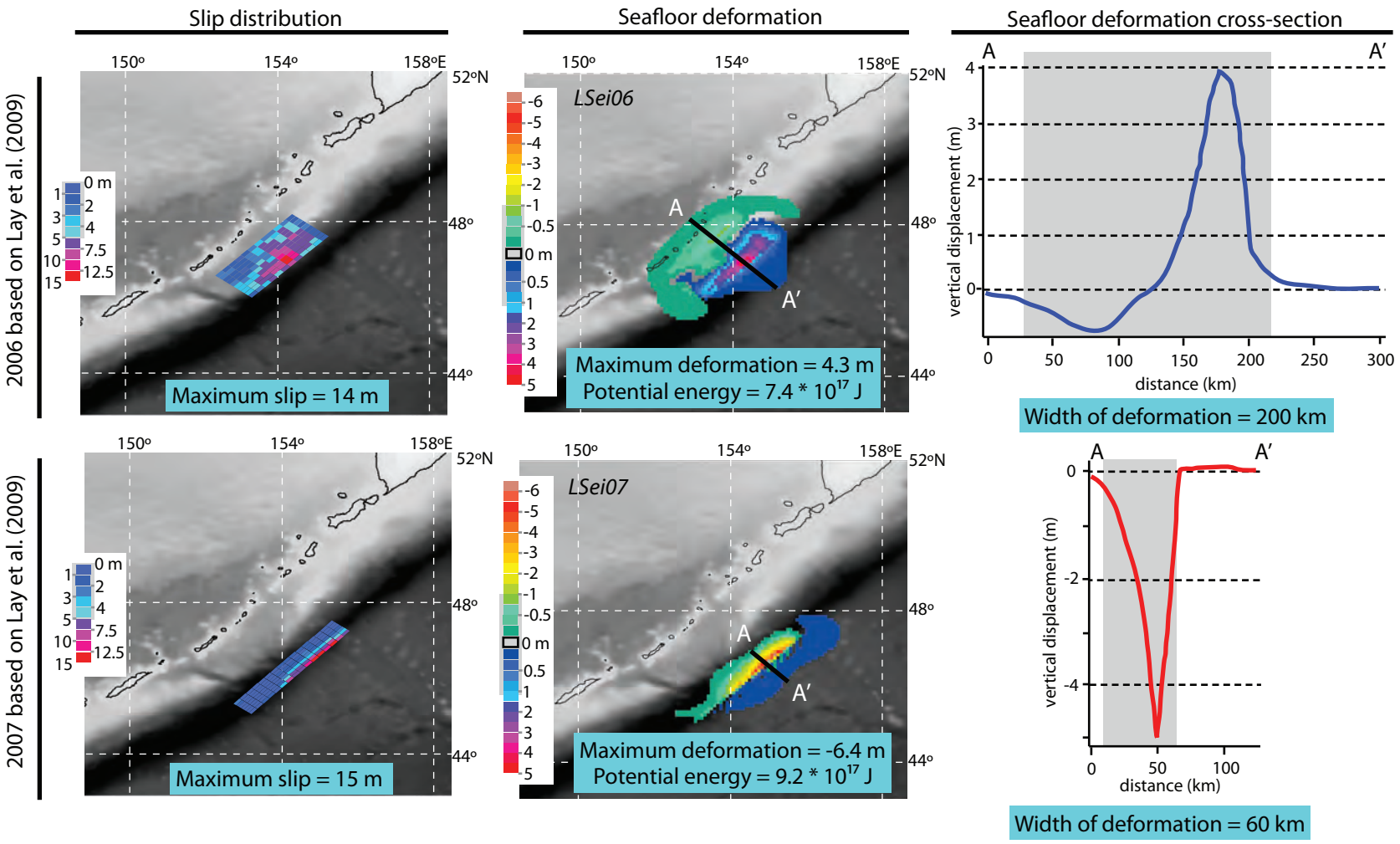

Figure 4.5: Lay et al. (2009)'s slip distributions for both the 2006 and 2007 earthquake, the resulting seafloor deformation patterns (and therefore initial tsunami waveforms) produced by Okada (1985)'s equations, and a cross-section through each initial tsunami. Names for tsunami simulations based on the slip distributions (*LSei06* and *LSei07*) are indicated.

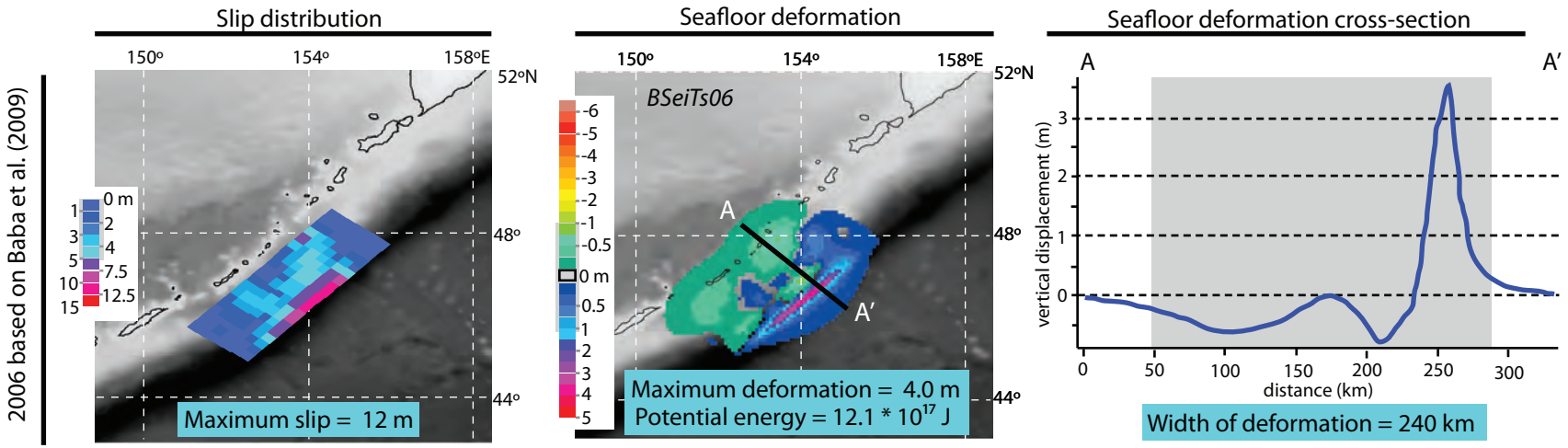

Figure 4.6: Baba et al. (2009)'s slip distributions for the 2006 earthquake, the seafloor deformation pattern (and therefore initial tsunami waveform) produced by Okada (1985)'s equations, and a cross-section through the initial tsunami. Baba et al. (2009) did not solve for a 2007 slip distribution. The name for the tsunami simulation based on their 2006 slip distribution (*BSeiTs06*) is indicated.

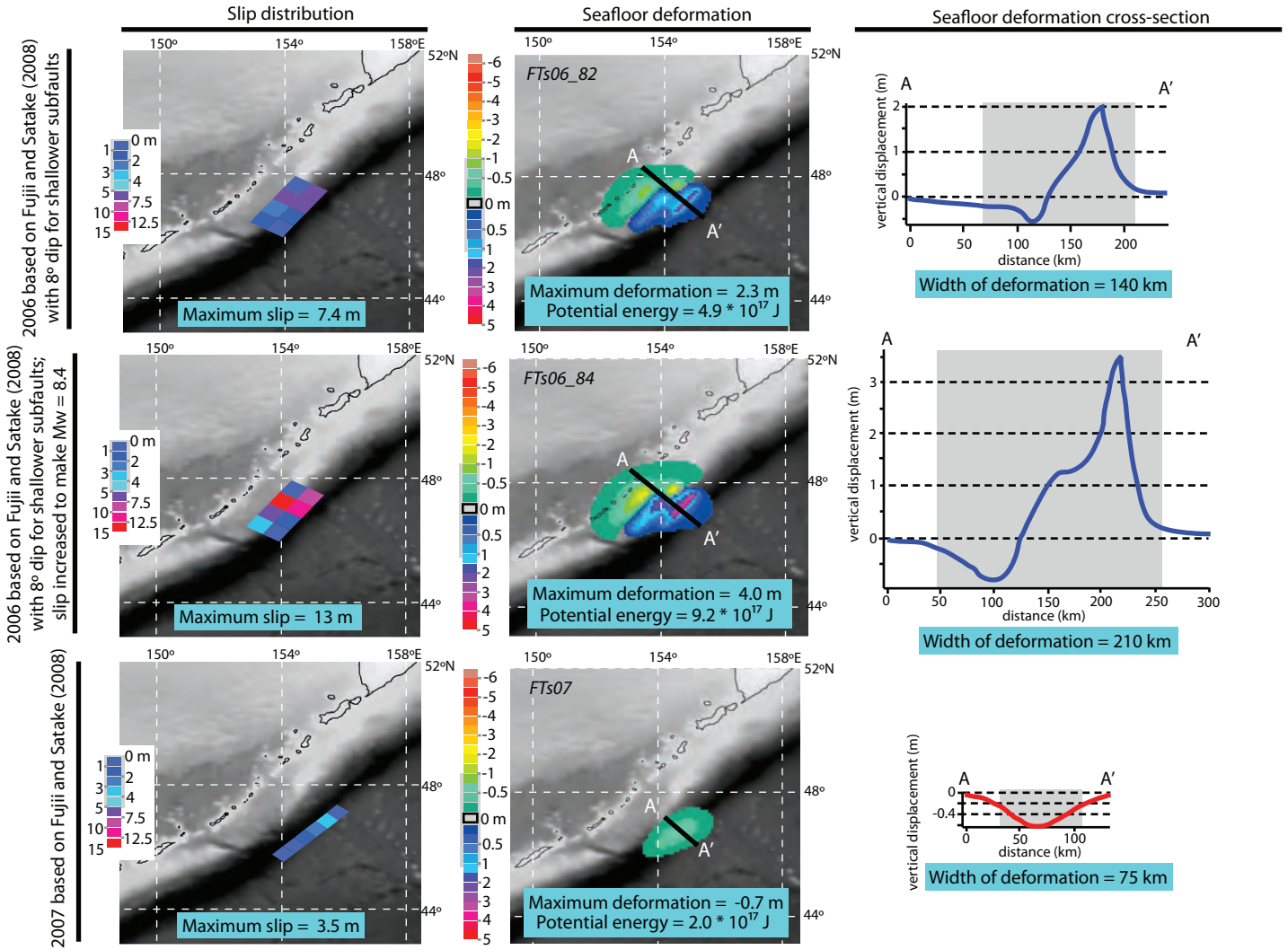

Figure 4.7: Fujii and Satake (2008)'s slip distributions for both the 2006 and 2007 earthquake, the resulting seafloor deformation patterns (and therefore initial tsunami waveforms) produced by Okada (1985)'s equations, and a cross-section through each initial tsunami. Only their slip distributions used in this paper are shown. Names for tsunami simulations based on the slip distributions (*FTs06_82, FTs06_84* and *FTs07*) are indicated. The *FTs06_84* model is a modification of the *FTS06_82* model.

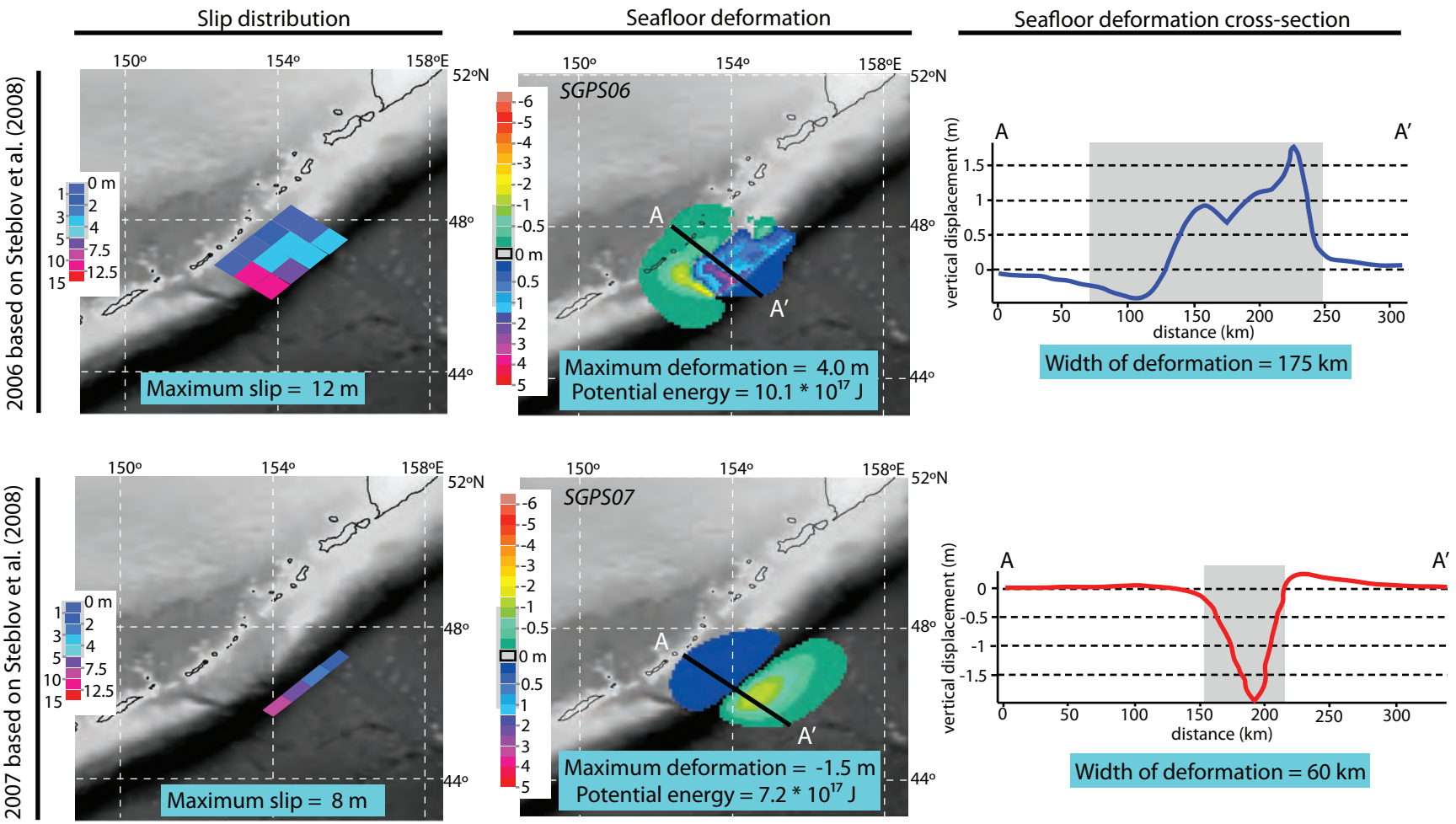

Figure 4.8: Steblov et al. (2008)'s slip distributions for both the 2006 and 2007 earthquake, the resulting seafloor deformation patterns (and therefore initial tsunami waveforms) produced by Okada (1985)'s equations, and a cross-section through each initial tsunami. Names for tsunami simulations based on the slip distributions (*SGPS06* and *SPGS07*) are indicated.

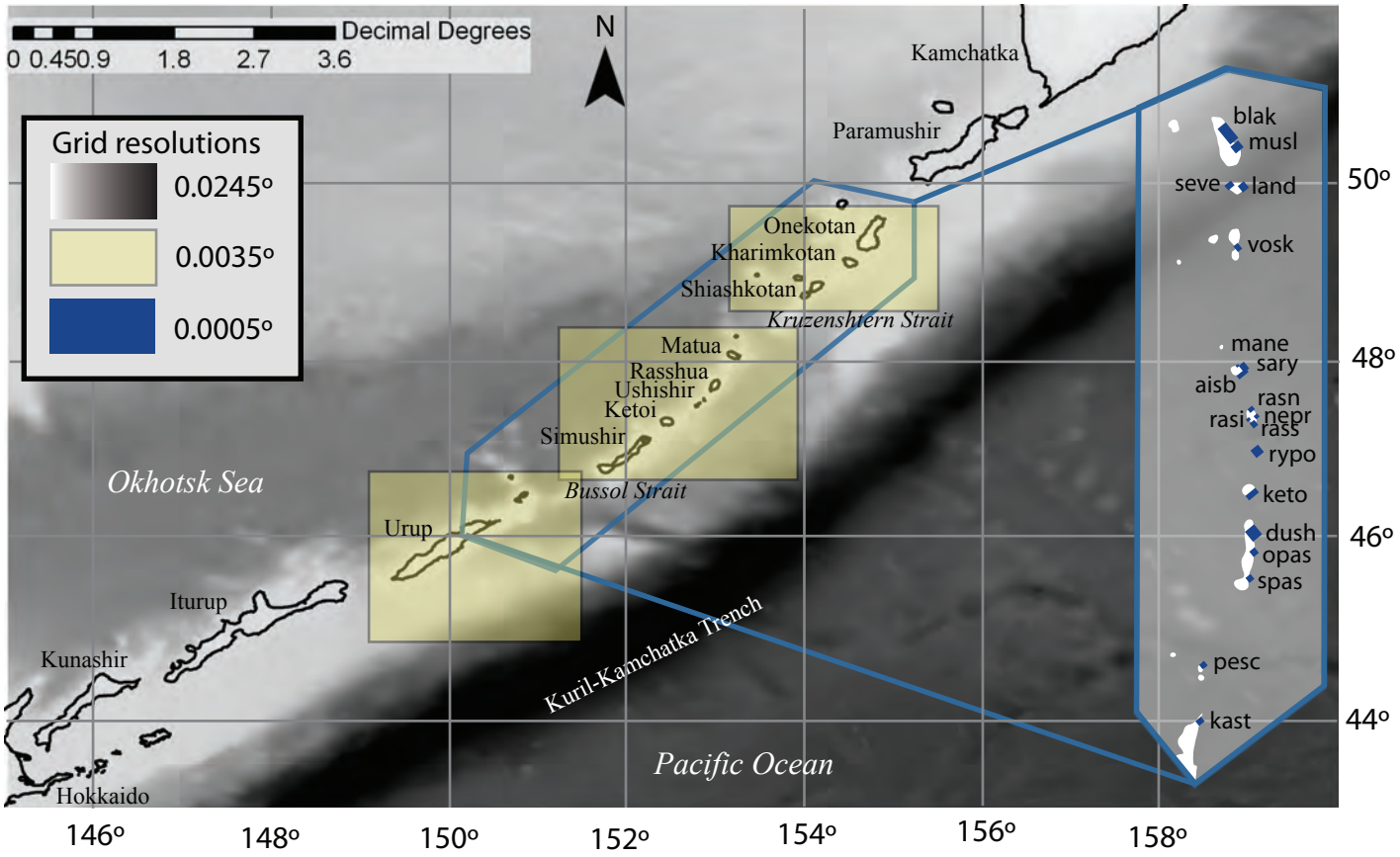

Figure 4.9: Layout of bathymetric grids used in simulating tsunamis in MOST. The black and white grid is the coarsest resolution, followed by yellow, then blue grids. Runup and inundation were calculated in the highest resolution (blue) grids. The names of each high-resolution grid are noted for reference.

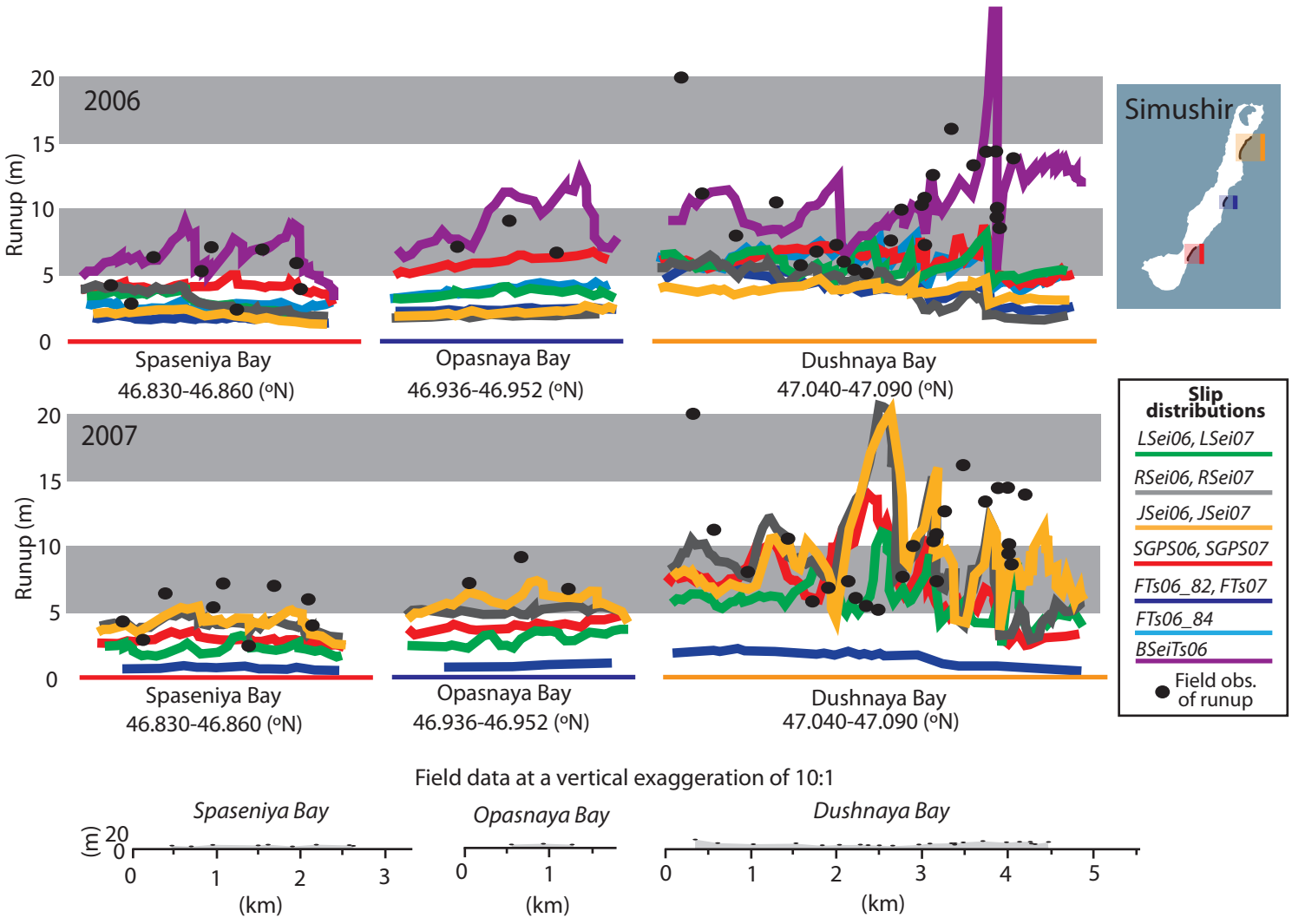

Figure 4.10: Simulated tsunami runup for the entire stretch of coastline that has high-resolution bathymetric grids on Simushir Island. Location of grids on the island is indicated by the inset. Field observations are included at the bottom with only 10:1 vertical exaggeration to illustrate that the field observations are noisy, as suggested by the upper plots.

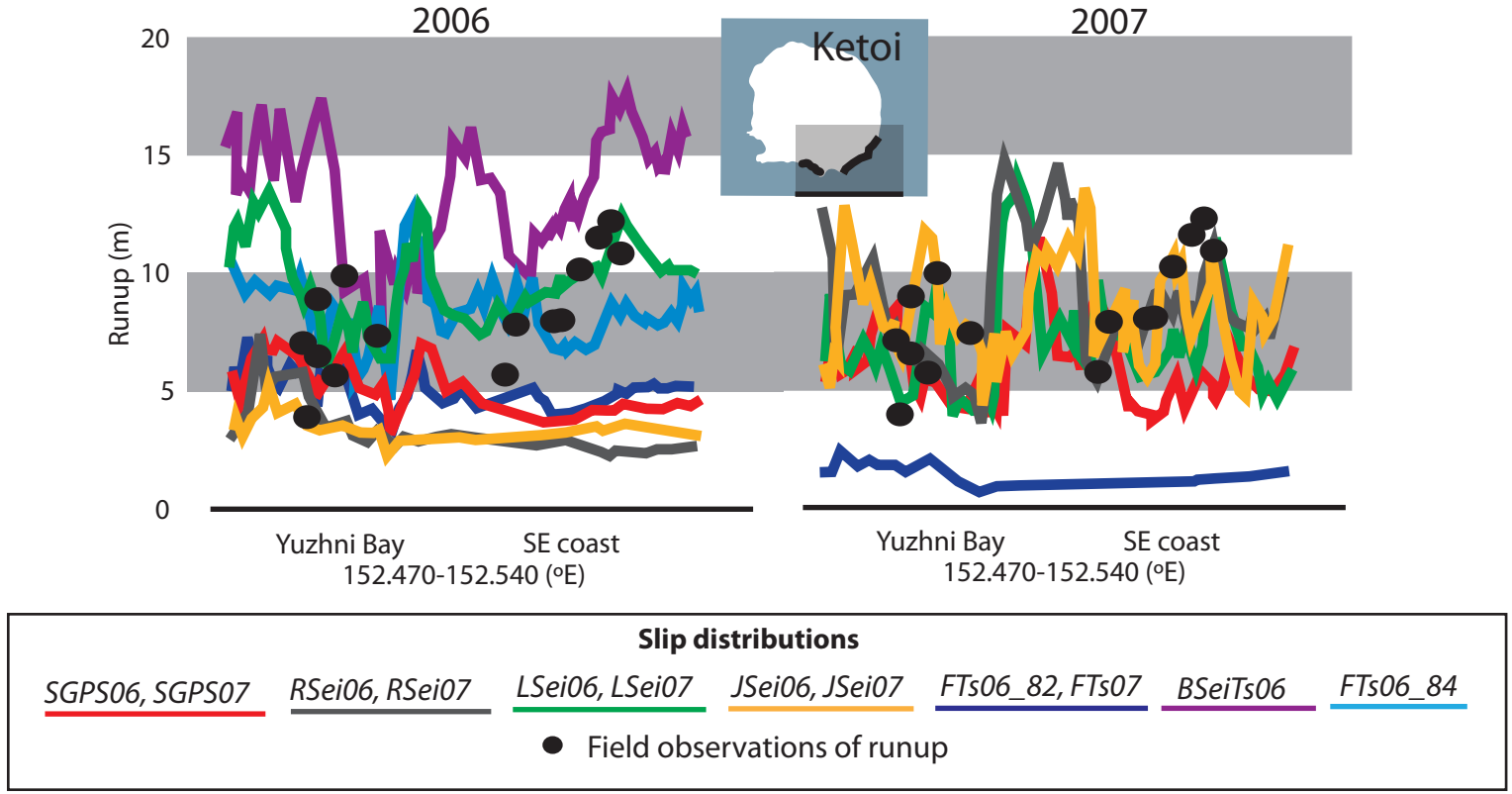

Figure 4.11: Simulated tsunami runup for the entire stretch of coastline that has a high-resolution bathymetric grid on Ketoi Island. Location of the grid on the island is indicated by the inset.

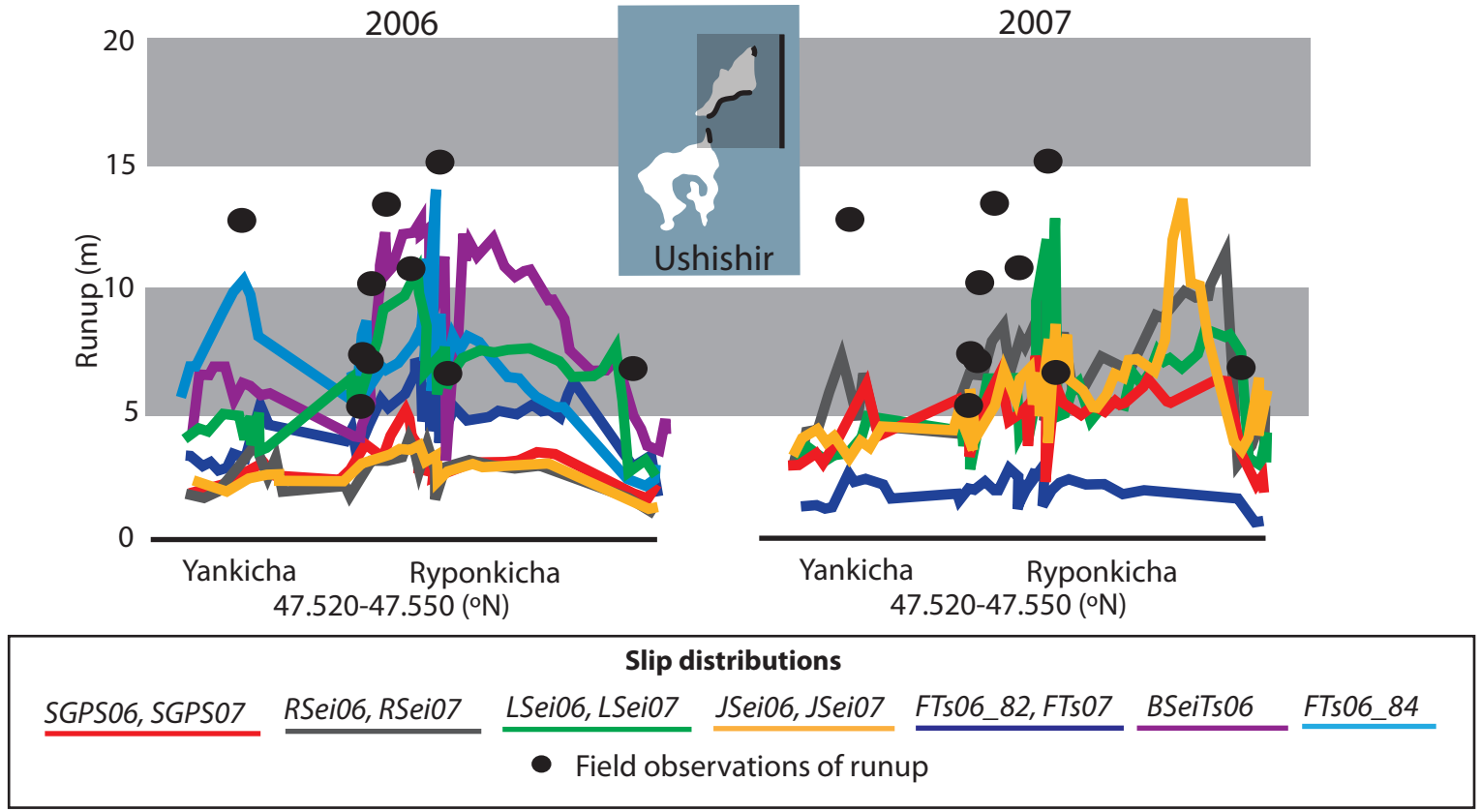

Figure 4.12: Simulated tsunami runup for the entire stretch of coastline that has a high-resolution bathymetric grid in the Ushishir islands. Location of the grid on the islands is indicated by the inset.

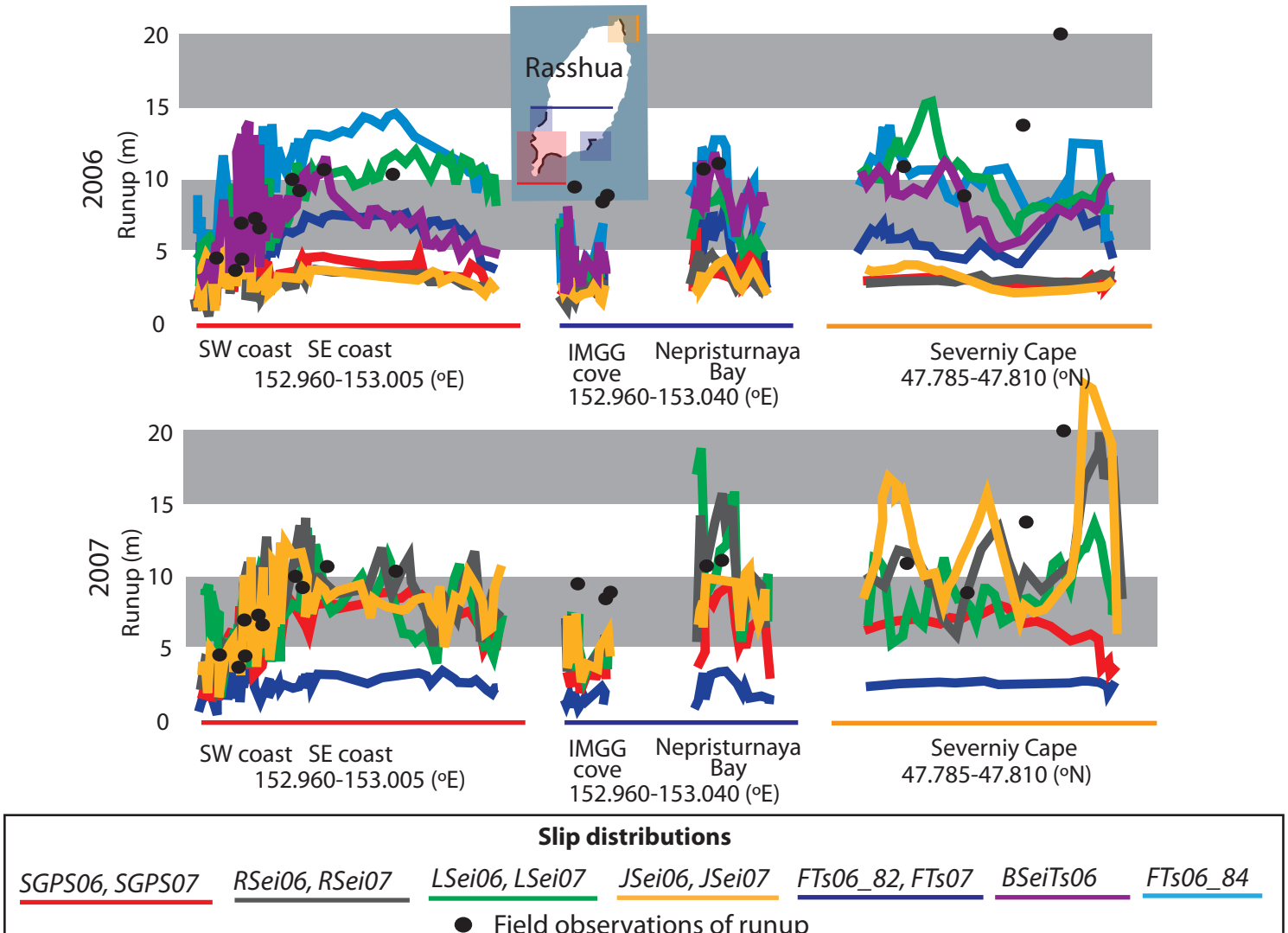

Figure 4.13: Simulated tsunami runup for the entire stretch of coastline that has high-resolution bathymetric grids on Rasshua Island. Location of grids on the island is indicated by the inset.

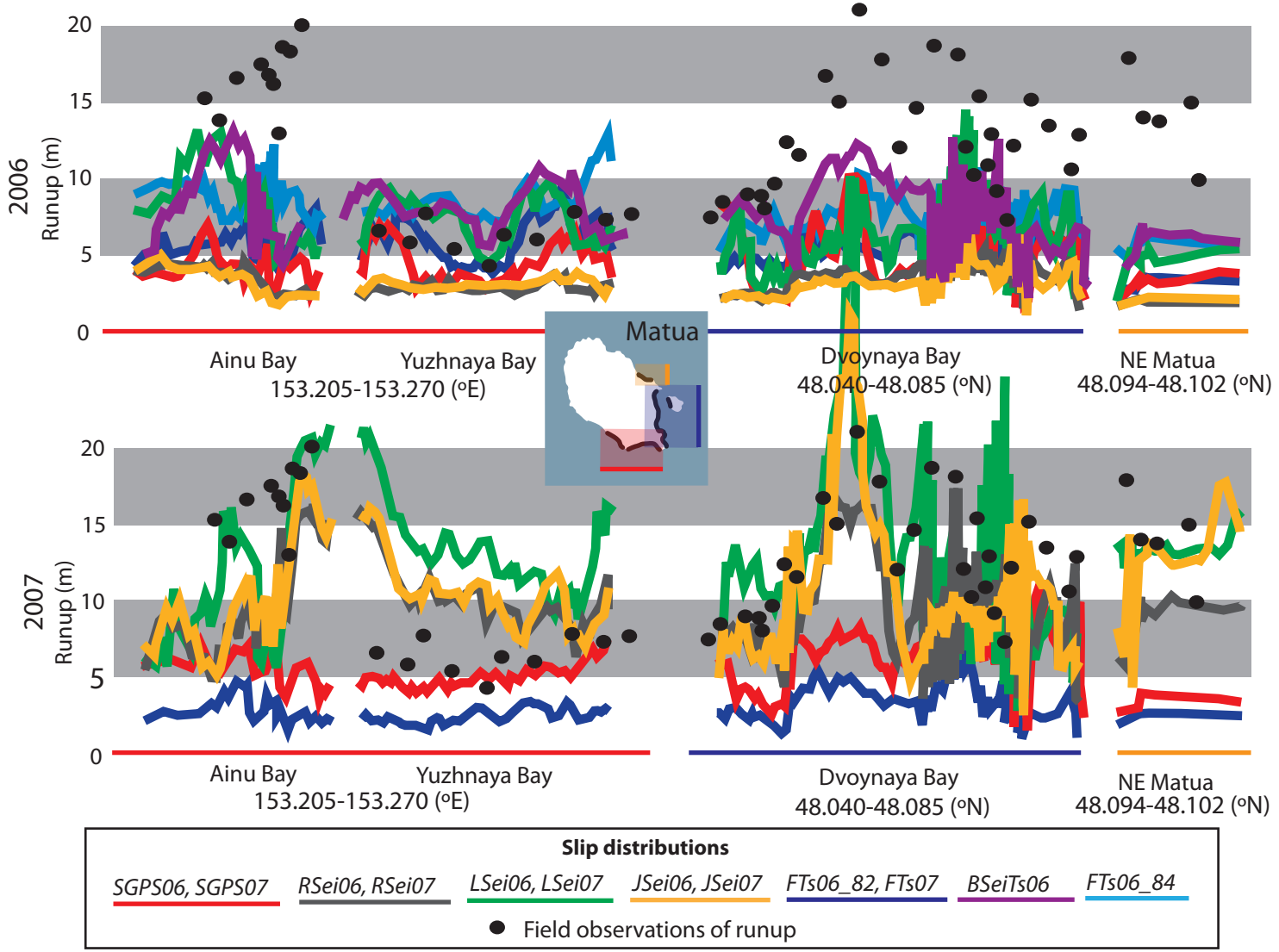

Figure 4.14: Simulated tsunami runup for the entire stretch of coastline that has high-resolution bathymetric grids on Matua Island. Location of grids on the island is indicated by the inset.

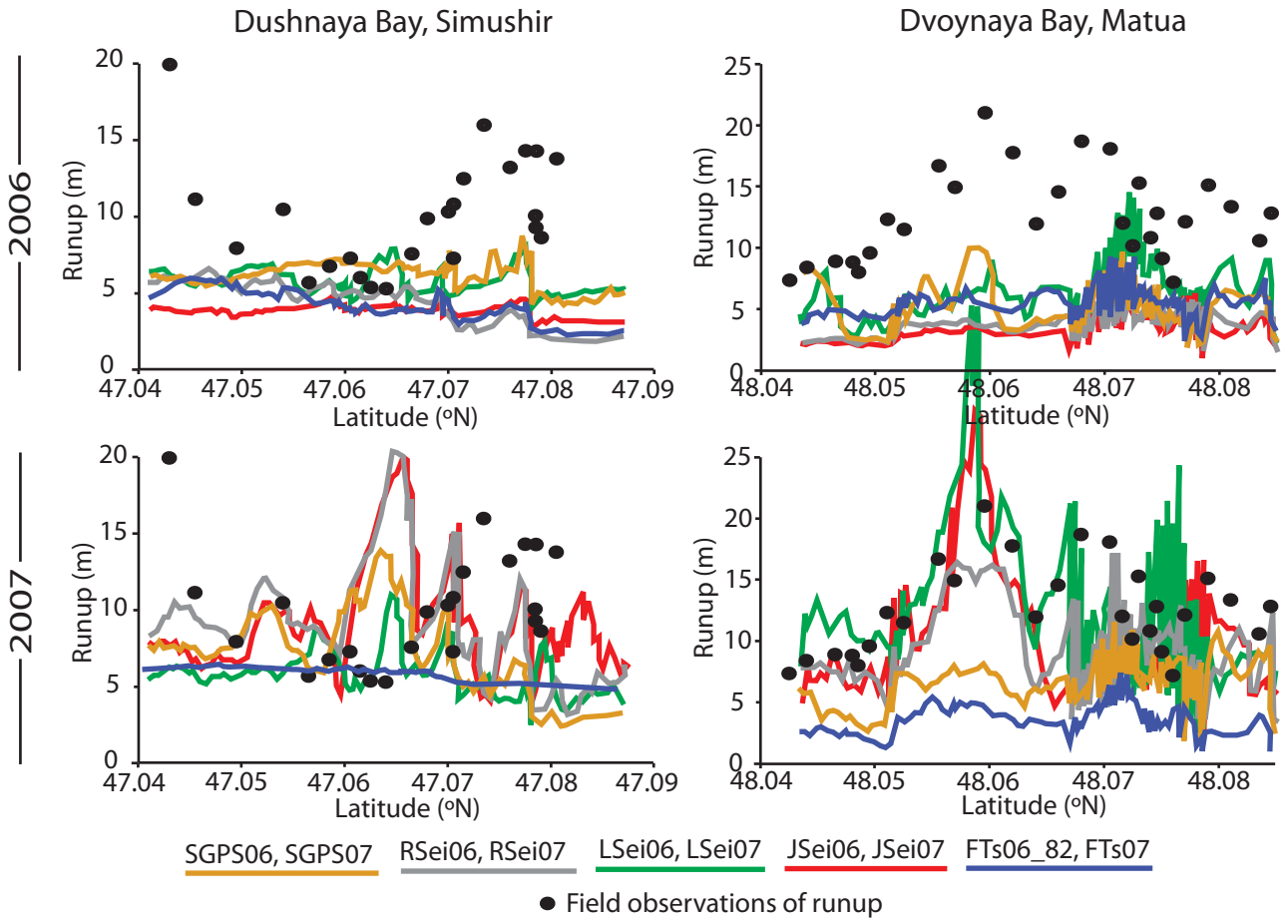

Figure 4.15: Runup distribution for both 2006 and 2007 simulated tsunamis from published slip distributions for Dushnaya and Dvoynaya Bays (dush and sary grids in Figure 4.9). The narrower wavelength 2007 tsunami experiences amplification where 2006 does not. Similar amplification in Dvoynaya Bay is needed to explain observed runup, but not in Dushnaya Bay.

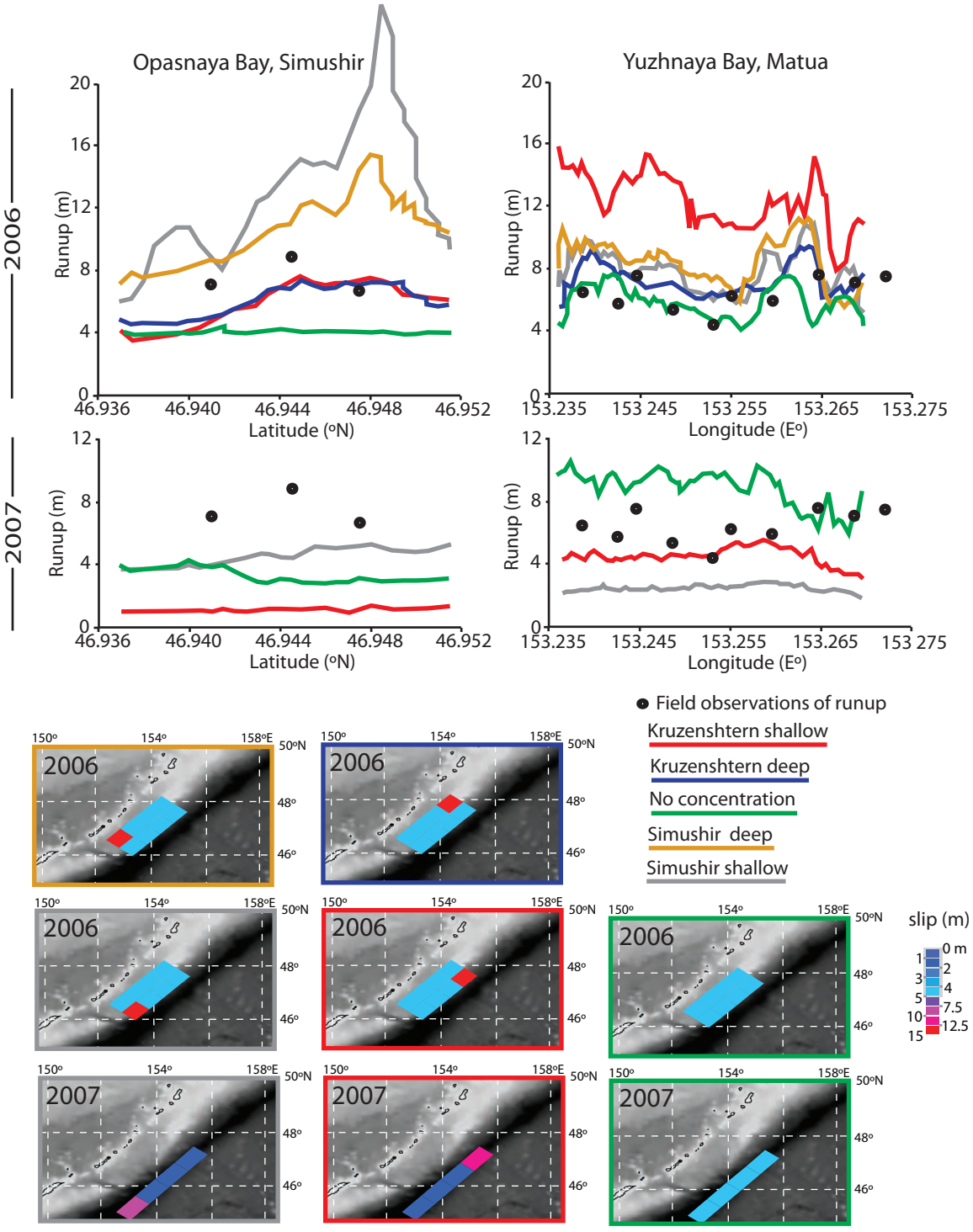

Figure 4.16: Runup distribution for simulated tsunamis with large differences in slip distribution within 2006 and 2007 rupture-zone and seismic-moment limits. Earthquakes have slip of 15 m (2006) or 8 m (2007) adjacent to Simushir Island or Kruzenshtern Strait. Opasnaya Bay is located at the southern end and Yuzhnaya Bay at the northern end of the rupture zone.

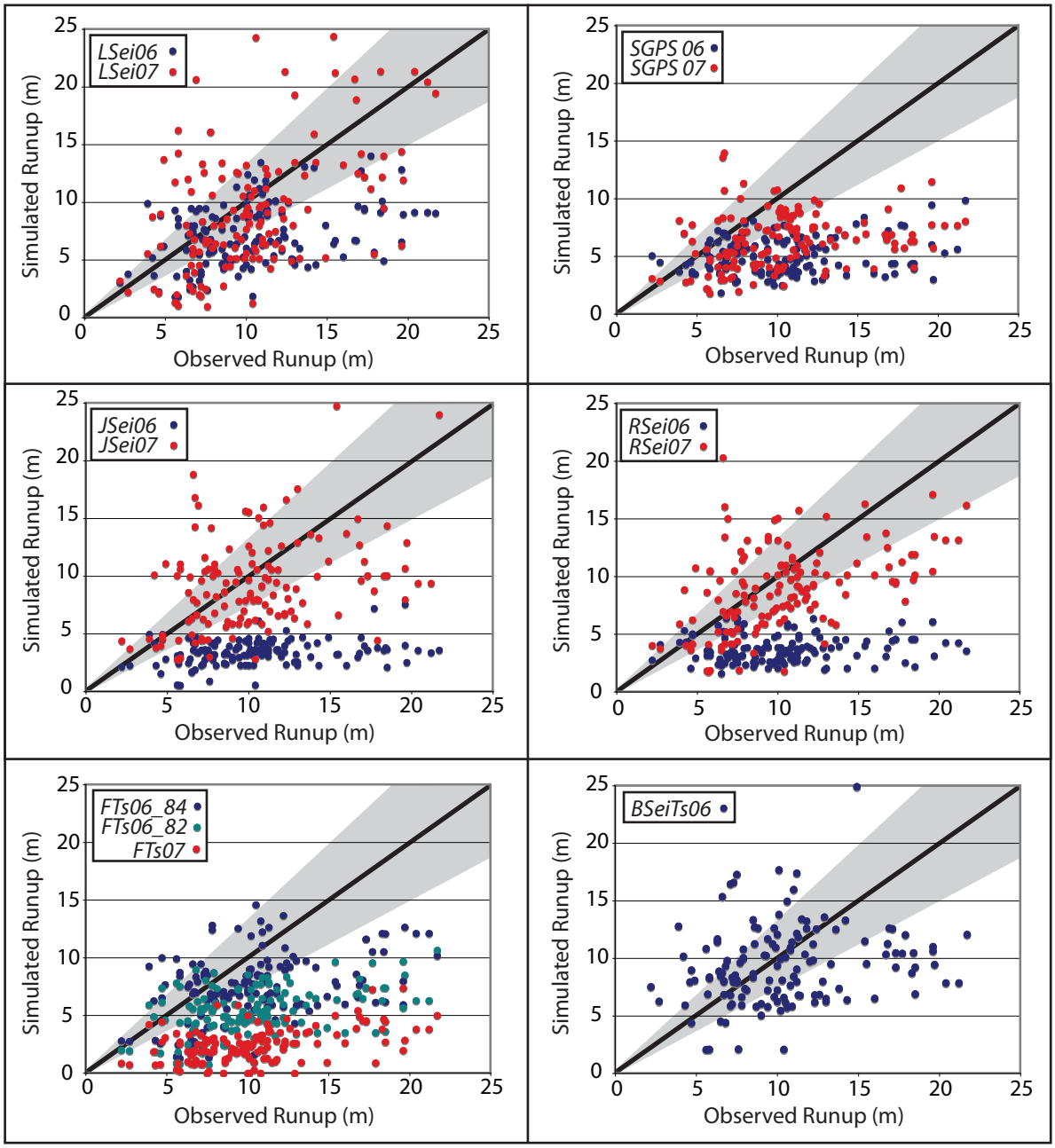

Figure 4.17: The distribution of observed field observations compared to simulated runup for the slip distributions indicated. The diagonal line indicates what would be a perfect match; the gray area is within 25% of observed runup.

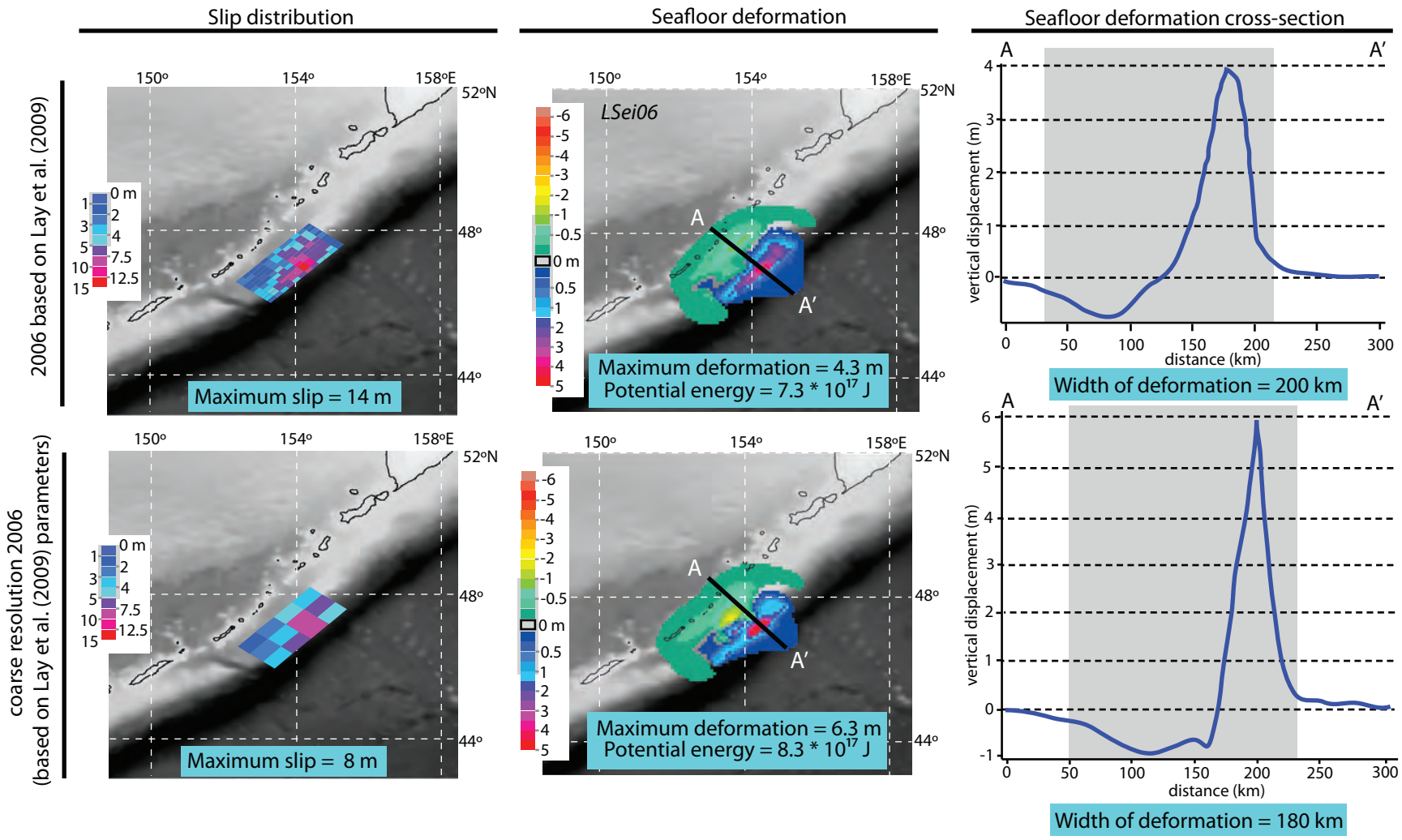

Figure 4.18: The *LSei06* slip distribution and seafloor deformation shown at the published subfault resolution, and at a subfault resolution similar to tsunami or GPS inversions.

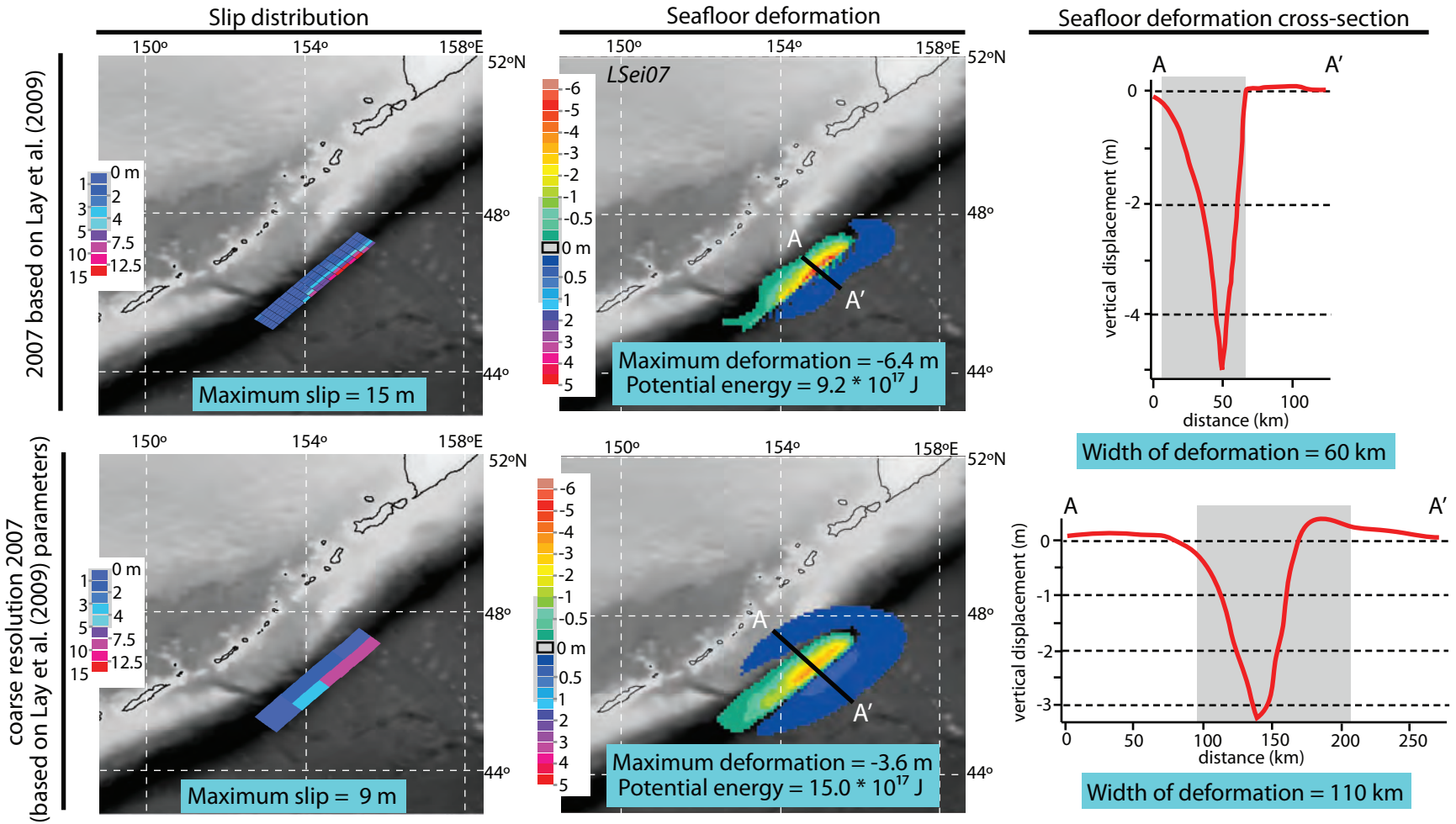

Figure 4.19: The *LSei07* slip distribution and seafloor deformation shown at the published subfault resolution, and at a subfault resolution similar to tsunami or GPS inversions.

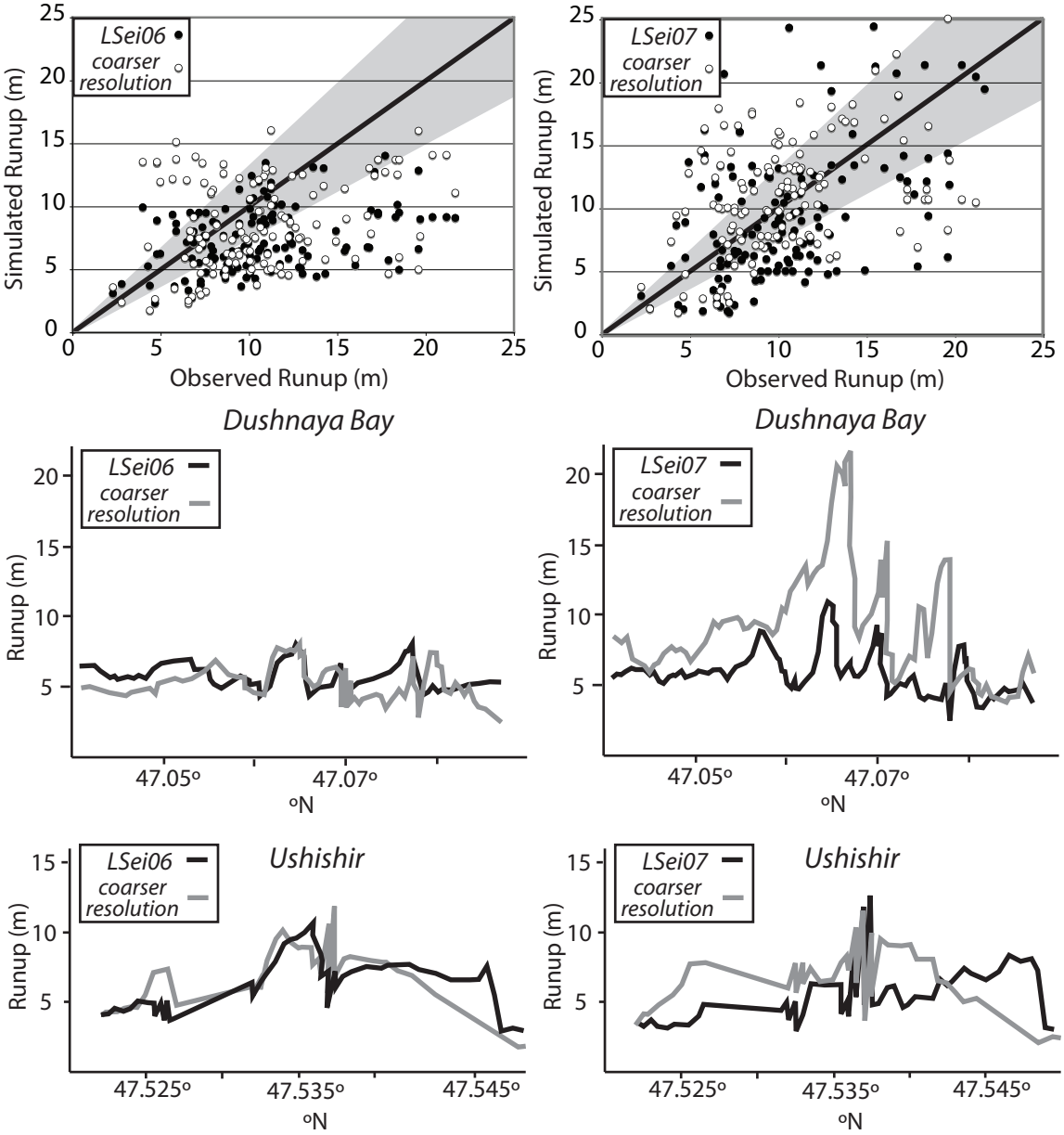

Figure 4.20: **Top**: The distribution of observed field observations compared to simulated runup for the *LSei06*, *LSei07*, and the same slip distributions at a subfault resolution similar to tsunami or GPS inversions (see Figure 4.18 and 4.19). The diagonal line indicates what would be a perfect match; the gray area is within 25% of observed runup. **Middle and Bottom**: Comparison of maximum simulated runup from the high-resolution bathymetric grids from Dushnaya Bay (middle) and Ushishir (bottom) shows that simulated runup from the 2007 example generally increased with coarser subfault resolution, while it stayed similar in the 2006 example.

CHAPTER 5

Conclusion

The combination of a dense network of geophysical and geological observations of the 15 November 2006 and 13 January 2007 Kuril Island earthquake doublet and associated tsunamis allows us to take a first step linking seismological characteristics of an earthquake to the effect of a tsunami on a coastline. As is often observed but rarely measured in post-tsunami surveys, the response of Kuril coastlines to the Kuril Island tsunami(s) was dominantly erosional, more so where there was higher tsunami runup. The nearfield expression of the tsunami(s) in the central Kuril Islands, including runup of up to 20 m, remained unknown until we conducted post-tsunami surveys in the summers of 2007 and 2008 (Chapter 2). Tsunami runup over a distance of 600 km averaged ~10 m in 192 locations surveyed and was typically between 5 and 15 m. Local topography had a strong effect on inundation and some effect on runup. Higher runup generally occurred along steep, protruding headlands, whereas longer inundation distances occurred on lower, flatter coastal plains. Sediment transport was ubiquitous where sediment was available—deposit grain size was typically sand, but ranged from mud to large boulders. Wherever there were sandy beaches, a more or less continuous sand sheet was present on the coastal plain. The tsunami eroded the beach landward, stripped vegetation, created scours and trim lines, cut through ridges, and plucked rocks out of the coastal plain.

In conjunction with our paleo-tsunami-related fieldwork 3-5 months prior to the 2006 and 2007 tsunami(s), we have collected a compelling data set of quantitative coastal geomorphic change (Chapter 3). Pre- and post-tsunami surveys of the islands, including four

topographic profiles measured in 2006 and reoccupied in 2007, provide the confidence to attribute many changes to the tsunami, and in some cases quantify these changes, in spite of an absence of eyewitness accounts in the central islands. Areas with low runup (<8 m) experienced limited geomorphic change, primarily confined to the beach or stream channels. Regions with high runup (>15 m) experienced massive erosion that dramatically altered the coastline. Tsunami deposits corresponded within ~90% to the extent of tsunami runup and inundation. The amount of sediment eroded by the tsunami far outweighed the amount deposited on land in all cases studied. The tsunami was dominantly erosive in the Kuril Islands because the high-relief topography of the coastline accelerated tsunami outflow.

The post-tsunami survey (Chapters 2 and 3) primarily found and measured only one tsunami wrackline, indicative of the largest onshore wave, with few clues as to which of the two tsunamis formed it. To clarify the responsible event, tsunamis were simulated using the numerical MOST (Method of Splitting Tsunamis) tsunami model from earthquakes based on published slip distributions of the 2006 and 2007 earthquakes inverted from teleseismic waves, tsunami waveforms and/or GPS-measured ground motion. Analyses presented in Chapter 4 suggest that the tsunami responsible for the wrackline in most places was probably the 2006 tsunami, but that 2007 was more likely responsible for the largest wave on Matua Island and on parts of Rasshua Island. Simulations of either tsunami could produce runup within the range of field observations in the central Kurils depending on different earthquake scenarios, although none could match all the data to within 25%.

The number and diversity of available inversions of earthquake slip distribution provide an opportunity to investigate the effect of slip distribution on the nearfield tsunami runup pattern. The distribution of slip in outer-rise earthquakes similar to the 2007 Kuril

Islands event causes less variation in nearfield runup patterns than is the case for subduction-zone earthquakes similar to the 2006 Kuril Island event. Differences in slip resolution (length and width of subfaults) used in inversion techniques can also have a considerable impact on simulated tsunami runup patterns when these differences affect the up-dip or down-dip distribution of slip. Slip resolutions that average slip over a larger area can increase or decrease width and maximum amplitude of seafloor deformation, causing changes in the tsunami waveform and leading to measurable differences in runup values.

How tsunami-modeling conclusions could change interpretations about tsunami geomorphology

Results from tsunami simulations show that runup from the 2007 tsunami could be as high or higher than the 2006 tsunami in some locations. Our post-tsunami survey assumed that the largest tsunami was 2006 in all cases. Tsunami modeling had not been completed at the time of publication of Chapters 2 and 3, thus the implications of the combined effect of two tsunamis (rather than one) on tsunami geomorphology was not fully explored in these earlier chapters. While it is not unusual for one tsunami to have multiple waves inundating and combining their effects on a coast, the main difference in the 2006/2007 case is that the time between potentially inundating waves is 2 months, rather than tens of minutes.

I can deduce that in coastal plains where our post-tsunami survey observed a traceable continuous wrackline (all locations measured in 2007 and ~half in 2008), one tsunami was consistently larger; in no place did one wrackline cross another or two wracklines merge. If the dominant tsunami was 2006, then the 2007 tsunami was likely small with correspondingly limited opportunities to erode and deposit sediment. At most, this

tsunami rose to the lower wrackline observed in Dushnaya and Ainu bays (Table 4.4). This scenario is the case previously assumed for any interpretations about tsunami geomorphology made in Chapter 2 and 3. Conversely, if the dominant tsunami affecting a coastal plain was 2007 (such as simulations show on Matua Island), the later 2007 tsunami would overprint records of the earlier 2006 tsunami, leaving little evidence of the 2006 tsunami's passage.

Two tsunamis closely spaced in time can easily have additive geomorphic effects; especially in the Kuril Island winter when vegetation is naturally dormant and there is no time for ecological recovery of the coastal plain. If 2006 was comparable to 2007 (but still smaller), it would have been capable of removing vegetation, eroding soil, and depositing sediment on the coastal plain. Other conditions being equal (see next paragraph about snow and ice), the newly exposed surface would enable a larger 2007 to have more opportunity for erosion, and provide more sediment for entrainment. In this case, the cumulative amount of erosion and deposition from 2006/2007 could be more than double similar tsunamis occurring in isolation of each other. This scenario of a sizable 2006 tsunami followed by a larger 2007 tsunami is not dramatically different than a smaller train of waves followed by a larger train in the same tsunami. However, in a normal tsunami scenario, one might expect water from an early wave still outflowing from the landscape when a later wave arrives; this would probably not be the case if 2 months had passed.

Due to freezing and snow-armoring of the soil in the Kuril winter, the 2007 tsunami could have had a limited geomorphic effect regardless of its size. Snow, ice and cold weather dominate the winter, and 2006/2007 was no exception. Frozen coastal conditions affect not only the ability of a tsunami to erode vegetation, sediment and soil, but they also might make less available the large number of driftwood logs, marine refuse and dead vegetation

extensively found in the tsunami wracklines. A satellite image of the central Kuril Islands shows no snow in low elevations on November 22nd, 2006, but a layer of snow or ice covers the entire islands on December 1st, 2006[11]. Weather records between the two tsunamis indicate daily average temperatures in the range of -3 to -6 ºC, based on four-times daily temperature records[12].

While such conditions probably would not create a completely solidified landscape before the 2007 tsunami, they could make terrestrial sediment difficult to erode, especially if ice increases the relative cohesion of coastal soils. Of note, if 2007 was incapable of generating a wrackline due to winter conditions, it could have unobserved higher runup than 2006. In this situation, erosive capability of 2007 would be similarly limited, but the inundating waves could extend the inland penetration distance of a tsunami deposit because sediment is always available for entrainment in unfrozen, sandy nearshore environments typical at these latitudes. If the landscape was covered in ice, this hard layer may be capable of surviving tens of minutes of tsunami flow (Bretwood Higman, pers. comm.). If the landscape was covered in looser snow—a more likely scenario because a warm, loose base to a snow/ice winter cover is more common in northern maritime climates (Bretwood Higman, pers. comm.)— the snow's effect on the tsunami could be minimal. These ideas about how a tsunami behaves differently in the winter are speculations; eyewitnesses or post-tsunami surveys in the future are needed immediately after tsunamis that occur in winter conditions to provide more concrete arguments.

---

[11] The November 22nd, 2006 Digital Globe satellite image and the December 1st, 2006 ASTER satellite image are the only available images with low cloud cover between the 2006 and 2007 earthquakes.

[12] NCEP Reanalysis data provided by the NOAA/OAR/ESRL PSD, Boulder, Colorado, USA, from their Web site at http://www.cdc noaa.gov/

Directions for future research

Countless opportunities for future research are prompted by the studies presented in this dissertation. The post-tsunami surveys provide a foundation that future field studies can use to document changes as Kuril Island coastlines re-equilibrate from the erosion and deposition of the 2006 and 2007 tsunamis. Analyses of our post-tsunami survey observations of tsunami wracklines can be used to build stronger links between paleo-tsunami studies and modern tsunami surveys. Future testing the effects of earthquake slip distributions on other tsunamis can expand our predictions of inversion methodologies that are more useful to implement in future tsunami modeling of earthquakes in the nearfield. Finally, additional exploration of the link between characteristics of earthquake rupture (as expressed in tsunamis) and tsunami geomorphology can help us improve interrogation of the influence of the subduction zone cycle on coastal landscape evolution.

The studies presented in this dissertation provide a solid basis for future long-term research into recovery of natural systems from tsunamis. After the destruction caused by the tsunami(s), new vegetation has been re-growing on the coastal plain. Field surveys conducted in 2010 on Matua Island collected extensive records of new vegetation types, the fate of vegetation whose survival was uncertain in 2007, and rate of decomposition of once-coherent tsunami wracklines. Comparison of the old and new data can help address questions such as whether plant communities can help identify zones of erosion, or how long recognizable wracklines survive. Three summers of beach surveys have tracked profile changes with the goal of determining the fate of sediment that was removed from the coastal plain, but it is too soon to answer the questions of whether the sediment return to the island as new beach ridges, or if it been removed from the islands' littoral systems forever.

A major goal of tsunami geology is to calibrate what we can learn from modern tsunami deposits, using known modern tsunami characteristics, in order to relate paleo-tsunami deposits to characteristics of the unknown event that created those deposits. Future returns to the locations studied in this dissertation can provide a key benchmark for understanding how modern tsunami deposits change as they evolve into "paleo-tsunami deposits." Deposits that extended at least 90% as far as water penetration when measured in 2007 and 2008 are already becoming preserved as vegetation duff, soils and volcanic tephra cover them. By returning to the Kuril Islands to observe the tsunami deposits through time, tsunami geologists will be able to track the preservation or disappearance of sand layers with known thicknesses. Understanding how the recognizable deposit extent inland changes with time will be an invaluable tool for paleo-tsunami studies.

Tsunami geomorphology is a fledgling topic in tsunami geology; the results presented in this dissertation are only a first step for learning (1) how to recognize paleo-examples of tsunami-induced geomorphic features and (2) how tsunamis affect coastal-plain development and landscape evolution. An important hypothesis that has stemmed from my observations of tsunami erosion is that erosional features in areas with high (>~15m) tsunami runup may become permanent alterations of the coastline. For example, features visible for decades or centuries might include the breaching of a beach ridge in Dushnaya Bay, the removal of the seaward beach ridges in Ainu Bay, the breaching of a lake in Ainu Bay, and the development of inland scours in general. Further comparison with geomorphology of other tsunami-prone regions can provide supporting evidence that these newly eroded features will be preserved (cf. MacInnes et al., 2005). Additionally, comparisons of Kuril Island coastal geomorphology with similar coastlines in non-tsunami-prone regions can help answer questions about the

role of tsunamis in coastal evolution and help determine if tsunami geomorphology is a useful topic for paleo-tsunami studies to pursue.

The tsunami simulations presented in this dissertation are a first-order attempt to understand the utility of slip-distribution inversion for forward-modeling tsunami studies in the nearfield. Better bathymetry, especially in the poorly surveyed and remote Kuril Islands, is needed to improve a model's forecasting ability. Other earthquakes that have many inversions for slip distribution and dense nearfield runup measurements, such as 2009 Samoa Islands or 2010 Chile, should be tested with the same methods used in this dissertation. Tsunami simulations from a particular type of inversion technique might be more reliable at simulating tsunamis that match nearfield observations than other inversion techniques. While my conclusion is that the W-phase inversion (Lay et al., 2009) matched field observations slightly better than other inversions, it remains to be seen if W-phase waves are equally sensitive to the tsunami-generating characteristics of other earthquakes.

Tsunamis produce coastal change, but what aspect or characteristic of a tsunami does the coastline respond to? This question is the ultimate link between seismology and geomorphology— where one day we may be able to relate erosion observations in a field location to tsunami behaviors caused only by tsunamis from earthquakes with heterogeneously distributed slip. This dissertation presents the hypothesis that backflow on steeper shorelines, such as those in the Kuril Islands, is more erosive than inflow. Numerical models that can simulate erosion can test the relative erosive capacity of tsunami inflow vs. outflow in the Kurils and elsewhere. Onshore tsunami modeling of tsunami behavior is a newly developing tool that can produce simple 3-D simulations of realistic tsunami flow with initiation parameters of grain motion (Huntington et al., 2007; Jaffe and Gelfenbaum et al.,

2007; Lynett, 2007). The extensive observations of erosion style and volume presented in Chapters 2 and 3, and the tsunami simulations calculated for Chapter 4, provide benchmarks for further investigating tsunami behavior. In particular, erosional features not dominated by local variations in tsunami outflow provide individual case studies that can clarify the range of tsunami behavior caused by slip distribution in the tsunami's source earthquake.

LIST OF REFERENCES

Alonso C.V., Bennet, S.J., and Stein, O.R., 2002, Predicting head cut erosion and migration in concentrated flows typical of upland areas: Water Resources Research v. 38, p. 1303-1318, doi: 10.1029/2001WR001173.

Ammon, C.J., Kanamori, H., and Lay, T., 2008, A great earthquake doublet and seismic stress transfer cycle in the central Kuril islands: Nature, v. 451, p. 561-566.

Andrade, C., 1992, Tsunami generated forms in the Algarve Barrier Islands: Science of Tsunami Hazards. v. 10, p. 21-34.

Apel, E.V., Bürgmann, R., Steblov, G., Vailenko, N., King, R., and Prytkov, A., 2006, Independent active microplate tectonics of northeast Asia from GPS velocities and block modeling: Geophysical Research Letters, v. 33, L11303, doi: 10.1029/2006GL026077.

Baba, T., Cummins, P.R., Thio, H.K., and Tsushima, H., 2009, Validation and joint inversion of teleseismic waveforms for earthquake source models using deep ocean bottom pressure records: A case study of the 2006 Kuril megathrust earthquake, Pure and Applied Geophysics, v. 166, p. 55-76, doi: 10.1007/s00024-008-0438-1.

Baranov, B., Wong, H.K., Dozorova, K., Karp, B., Lüdmann, T., and Karnaukh, V., 2002, Opening geometry of the Kurile Basin (Okhotsk Sea) as inferred from structural data: Island Arc, v. 11, p. 206-219, doi: 10.1046/ j.1440-1738.2002.00366.x.

Beck, S.L., and Ruff, L.J., 1987 Rupture process of the great 1963 Kurile Islands earthquake sequence: Asperity interaction and multiple event rupture: Journal of Geophysical Research, v. 92, p. 14,123-14,138, doi: 10.1029/JB092iB13p14123.

Bilek, S.L., Conrad, C.P., and Lithgow-Bertelloni, C., 2005, Slab pull, slab weakening, and their relation to deep intra-slab seismicity: Geophysical Research Letters, v. 32, L14305, doi: 10.1029/2005GL022922.

Borrero, J.C., Weiss, R., Okal, E.A., Hidyat, R., Suranto, Arcas, D., and Titov, V.V., 2009, The tsunami of 2007 September 12, Bengkulu province, Sumatra, Indonesia: post-tsunami field survey and numerical modeling: Geophysical Journal International, v. 178, p. 180-194.

Bourgeois, J., 2009, Geologic effects and records of tsunamis, in Bernard, E.N. and Robinson, A.R., eds., The Sea: Volume 15, Tsunamis: Cambridge, Massachusetts, Harvard University Press, p. 55-91.

Bourgeois, J., and MacInnes, B.T., 2010, Tsunami boulder transport and other dramatic effects of the 15 November 2006 central Kuril Islands tsunami on the island of Matua: Zeitschrift für Geomorphologie, v. 54, no. 3, p. 175-195.

Bourgeois, J., Petroff, C., Yeh, H., Titov, V., Synolakis, C. E., Benson, B., Kuroiwa, J., Lander, J., and Norabuena, E., 1999, Geologic setting, field survey and modeling of the Chimbote, northern Peru, tsunami of 21 February 1996: Pure and Applied Geophysics, v. 154, no. 3/4, p. 513-540.

Briggs, M.J., Synolakis, C.E., Kanoglu, U., and Creen, D.R., 1996, Runup of solitary waves on a vertical wall, in Yeh, H., Liu, P., and Synolakis C., eds., Long-Wave Runup Models: Proceedings of the International Symposium, Friday Harbor, USA, 12-17 September 1995, World Science, p. 375-383.

Choowong, M., Murakoshi, N., Hisada, K., Charusiri, P., Daorerk, V., Charoentitirat, T., Chutakositkanon, V., Jankaew, K., and Kanjanapayont, P., 2007, Erosion and

Deposition by the 2004 Indian Ocean Tsunami in Phuket and Phang-nga Provinces, Thailand: Journal of Coastal Research, v. 23, p. 1270-1276.

Cook, D.B., Fujita, K., and McMullen, C.A., 1986, Present-day plate interactions in northeast Asia - North-American, Eurasian, and Okhotsk plates: Journal of Geodynamics, v. 6, p. 33-51.

Cummins, P.R., Hirano, S., and Kaneda, Y., 1998, Refined coseismic displacement modeling for the 1994 Shikotan and Sanriku-oki earthquakes: Geophysical Research Letters, v. 25, no. 17, p. 3219-3222.

Dawson, A.G., 1994, Geomorphological effects of tsunami run-up and backwash: Geomorphology, v. 10, p. 83-94.

Dawson, A.G., and Shi, S., 2000, Tsunami deposits: Pure and Applied Geophysics, v, 157, p. 875-897.

De Mets, C., Gordon, R.G., Argus, D.F., and Stein, S., 1990, Current plate motions: Geophysical Journal International, v. 101, p. 425-478, doi: 10.1111/j.1365-246X.1990.tb06579.x.

Dengler, L., Uslu, B., Barberopoulou, A., Yim, S.C., and Kelly, A., 2009, The November 15, 2006 Kuril Islands-Generated Tsunami in Crescent City, California: Pure and Applied Geophysics, v. 166, p. 37-53.

Farreras, S.F., 2000, Post-tsunami field survey procedures: An outline: Natural Hazards, v. 21, p. 207-214.

Fedotov, S.A., 1965, Regularities of the distribution of large earthquakes of Kamchatka, the Kuril Islands and north-eastern Japan: Akad. Nauk SSSR Inst. Fiziki Zemli Trudy, v. 36, no. 203, 66-93. [in Russian]

Fedotov, S.A., Chernyshev, S.D., and Chernysheva, G.V., 1982, The Improved Determination of the Source Boundaries for Earthquakes of M>7.75, of the Properties of the Seismic Cycle, and of Long-term Seismic Prediction for the Kurile-Kamchatka Arc: Earthquake Prediction Research, v. 1, p. 153-171.

Fritz, H.M., Synolakis, C.E., and McAdoo, B.G., 2006, Maldives field survey after the December 2004 Indian Ocean tsunami: Earthquake Spectra, v. 22, no. S3, p. S137-S154.

Fujii, Y., and Satake, K., 2008, Tsunami Sources of the November 2006 and January 2007 Great Kuril Earthquakes: Bulletin of the Seismological Society of America, v. 98, doi: 10.1785/0120070221.

Geist, E.L., 2002, Complex earthquake rupture and local tsunamis: Journal of Geophysical Research, v. 107, doi: 10.1029/2000JB000139.

Geist, E.L., and Dmowska, R., 1999, Local tsunamis and distributed slip at the source: Pure and Applied Geophysics, v. 154, p. 485-512.

Gelfenbaum, G., and Jaffe, B., 2003, Erosion and Sedimentation from the 17 July 1998 Papua New Guinea Tsunami: Pure and Applied Geophysics, v. 160, p. 1969-1999, doi: 10.1007/s00024-003-2416-y.

Geller, R.J., and Kanamori, H., 1977, Magnitudes of great shallow earthquakes from 1904 to 1952: Bulletin of the Seismological Society of America, v. 67, p. 587-598.

Gica, E., Spillane, M., Titov, V.V., Chamberlin, C., and Newman, J.C., 2008, Development of the forecast propagation database for NOAA's short-term inundation forecast for tsunamis (SIFT): NOAA Technical Memo, OAR PMEL-139, 89 pp.

Goff, J., Liu, P.L.-F., Higman, B., Morton, R., Jaffe, B.E., Fernando, H., Lynett, P., Fritz, H., Synolakis, C., and Fernado, S., 2006, Sri Lanka field survey after the December 2004 Indian Ocean tsunami: Earthquake Spectra, v. 22, no. S3, p. S155-S172.

Gorshkov G.S., 1970, Volcanism and the Upper Mantle; Investigations in the Kurile Island Arc: New York, Plenum Publishing Corporation, 385pp.

Gusev A.A., and Shumilina, L.S., 2004. Recurrence of Kamchatka strong earthquakes on a scale of moment magnitudes: Fizika Zemli, v. 40, no. 3, p. 34-42.

Harada, T. and Ishibashi, K., 2007, Two parallel trench-normal fault planes within the Pacific slab associated with the 1994 and 2000 Kurile earthquakes as revelated by simultaneous relocation of their main shocks and aftershocks: Earth Planets Space, v. 59, p. e25-e28.

Higman, B., and Bourgeois, J., 2008, Deposits of the 1992 Nicaragua Tsunami, in Shiki, T., Tsuji, Y., Yamazaki, T., and Minoura, K., eds., Tsunamiites: Features and Implications: San Francisco, Elsevier, p. 81-104.

Hirata, K., Geist, E., Stake, K., Tanioka, Y., and Yamaki, S., 2003, Slip distribution of the 1952 Tokachi-Oki earthquake (M 8.1) along the Kuril Trench from tsunami waveform inversion: Journal of Geophysical Research, v. 108, doi: 10.1029/2002JB001976.

Huntington, K., Bourgeois, J., Gelfenbaum, G., Lynett, P., Jaffe, B., Yeh, H., and Weiss, R., 2007, Sandy signs of a tsunami's onshore depth and speed: Eos, (Transactions, American Geophysical Union), v. 88, no. 52, p. 577-578, doi: 10.1029/2007EO520001.

Iida, K., Cox, D.C., and Pararas-Carayannis, G., 1967, Preliminary catalog of tsunamis occurring in the Pacific Ocean: Hawaii Institute of Geophysics, University of Hawaii, Honolulu, Data Report Number 5, HIG-67-10, 261 pp.

Jaffe, B., and Gelfenbaum, G., 2007, A simple model for calculating tsunami flow speed from tsunami deposits: Sedimentary Geology, v. 200, no. 3-4, p. 347-361, doi: 10.1016/j.sedgeo.2007.01.013.

Jaffe, B.E., Borrero, J.C., Prasetya, G.S., Peters, R., McAdoo, B., Gelfenbaum, G., Morton, R., Ruggiero, P., Higman, B., and Dengler, L., 2006, Northwest Sumatra and Offshore Islands Field Survey after the December 2004 Indian Ocean Tsunami: Earthquake Spectra, v. 22, p. S105.

Ji, C., 2006, Rupture process of the 2006 Nov 15 Magnitude 8.3 - Kuril Island Earthquake (Revised): http://www.geol.ucsb.edu/faculty/ji/big_earthquakes/2006/11/15/kuril.html, Accessed Nov 6, 2008.

Ji, C., 2007, Rupture process of the 2007 Jan 13 Magnitude 8.1 - Kuril Island Earthquake (Revised): http://www.geol.ucsb.edu/faculty/ji/big_earthquakes/2007/01/13/kuril.html, Accessed Nov 6, 2008.

Johnson, J.M., and Satake, K., 1999, Asperity distribution of the 1952 great Kamchatka earthquake and its relation to future earthquake potential in Kamchatka: Pure and Applied Geophysics, v. 154, no. 3/4, 541–553.

Kajiura, K., 1963, The leading wave of a tsunami: Bulletin of the Earthquake Research Institute, v. 41, p. 535–571.

Kanamori, H., 1976, Re-examination of the Earth's free oscillations excited by the Kamchatka earthquake of November 4, 1952: Physics of the Earth and Planetary Interiors, v. 11, no. 3, p. 216-226.

Kanamori, H. and Given, J.W., 1981, Use of long-period surface waves for rapid determination of earthquake-source parameters: Physics of the Earth and Planetary Interiors, v. 27, p. 8-31.

Kanamori, H., and Rivera, L., 2008, Source inversion of W-phase: speeding up seismic tsunami warning: Geophysical Journal International, v. 175, p. 222-238.

Kaistrenko, V.M., 1997, Concrete tsunami manifestation: Tsunamis of 1993 and 1994 on the Russian coast: Geodynamics of Tectonosphere of the Pacific Eurasia Conjunction Zone Volume VII, Yuzhno-Sakhalinsk, 193 pp. [in Russian]

Kato, Y., and Kimura, M., 1983, Age and origin of so-called “Tsunami-ishi”, Ishigaki Island, Okinawa Prefecture: Journal of the Geological Society of Japan, v. 89, p. 471-474.

Kench, P.S., McLean, R.F., Brander, R.W., Nichol, S.L., Smithers, S.G., Ford, M.R., Parnell, K.E., and Aslam, M., 2006, Geological effects of tsunami on mid-ocean atoll islands: The Maldives before and after the Sumatran tsunami: Geology, v. 34, p. 177-180, doi: 10.1130/G21907.1.

Kench, P.S., Nichol, S.L., Smithers, S.G., McLean, R.F., and Brander, R.W., 2008, Tsunami as agents of geomorphic change in mid-ocean reef islands: Geomorphology, v. 95, p, 361-383.

Kikuchi, M., and Kanamori, H., 1982, Inversion of complex body waves: Bulletin of the Seismological Society of America, v. 72, p. 491-506.

Kikuchi, M., and Kanamori, H., 1991, Inversion of complex body waves-III: Bulletin of the Seismological Society of America, v. 81, p. 2335-2350.

Kikuchi, M., Kanamori, H., and Satake, K., 1993, Source complexity of the 1988 Armenian earthquake: Evidence for a slow after-slip event: Journal of Geophysical Research, v. 98, p. 15,797-15,808, doi: 10.1029/93JB01568.

Konno, E., Iwai, J., Tkayanagi, Y., Nakagawa, H., Onuki, Y., Shiata, T., Mii, H., Kitamura, S., Kodaka, T., and Kataoka, J., 1961, Geological survey on the Chile Earthquake Tsunami affected areas in the Sanriku coast, northeast Japan: Contributions of the Institute of Geology and Palaeontology, Tohoku University, v. 52, p. 1-40. [in Japanese with English abstract]

Korvachev, S.A., Kuzin, I.P., and Lobkovskii, L.I., 2009, Marine Seismological Observations in the Central Kurile Segment before Catastrophic Earthquakes on November, 2006 (M = 8.3) and January, 2007 (M = 8.1): Izvestiya, Physics of the Solid Earth, v. 45, no. 9, p. 777-793.

Kurian, N.P., Pillai, A.P., Rajith, K., Murali Krishnan, B.T., and Kalaiarasan, P., 2006, Inundation characteristics and geomorphological impacts of December 2004 tsunami on Kerala coast: Current Science, v. 90, p. 240-249.

Kuzin, I.P., Lobkovsky, L.I., and Solov'eva, O.N., 2001, Characteristics of seismicity in the central Kurile region: Izvestiya - Russian Academy of Sciences, Physics of the Solid Earth, v. 37, no. 6, p. 464-473.

Laverov, N.P., Lappo, S.S., Lobkovsky, L.I., Baranov, B.V., Kulinich, R.G., and Karp, B.Y., 2006, The Central Kuril "Gap": Structure and seismic potential: Doklady Earth Science, v. 409, p. 787-790, doi : 10.1134/ S1028334X06050254.

Lay, T., Kanamori, H. Ammon, C.J., Hutko, A.R., Furlong, K. and Rivera, L., 2009, The 2006–2007 Kuril Islands great earthquake sequence: Journal of Geophysical Research, v. 114, B11308, doi: 10.1029/2008JB006280.

Levin, B.V., Kaistrenko, B.M., Rybin, A.B., Nosov, M.A., Pinegain, T.K., Razhigaeva, N.G., Sassorova, E.V., Ganzei, K.S., Ivelskaya, T.N., Kravchunovskaya, E.A., Kolesov, C.V., Evdokimov, Y.V., Bourgeois, J., MacInnes, B., and Fitzhugh, B., 2008, Manifestations of the tsunami on November 15, 2006, on the Central Kuril Islands and results of the runup heights modeling: Transactions (Doklady) of the Russian Academy of Sciences, Earth Science Section, v. 419, no. 2, p. 335-338.

Lynett, P., 2007, The effect of a shallow water obstruction on long wave runup and overland flow velocity: Journal of Waterway, Port, Coastal, and Ocean Engineering, v. 133, no. 6, p. 455-462.

MacInnes, B.T., Bourgeois, J., Pinegina, T., Martin, M.E., and Kravchunovskaya, E., 2005, Geomorphic effects of tsunamis in Asacha and Mutnaya Bays, Southern Kamchatka Peninsula, Russia: Eos, (Transactions, American Geophysical Union), v. 86, no. 52, Fall Meeting Supplement, abstract T11A-0360.

MacInnes, B.T., Pinegina, T.K., Bourgeois, J., Razhegaeva, N.G., Kaistrenko, V.M., and Kravchunovskaya, E.A., 2009a, Field survey and geological effects of the 15 November 2006 Kuril tsunami in the middle Kuril Islands: Pure and Applied Geophysics, v. 166, doi 10.1007/s00024-008-0428-3.

MacInnes, B.T., Bourgeois, J., Pinegina, T.K., and Kravchunovskaya, E., 2009b. Tsunami geomorphology: erosion and deposition from the 15 November 2006 Kuril Island tsunami: Geology, v. 37, p. 995-998.

MacInnes, B.T., Weiss, R., Bourgeois, J. and Pinegina, T.K., 2010, Slip Distribution of the 1952 Kamchatka Great Earthquake Based on Near-Field Tsunami Deposits and Historical Records: Bulletin of the Seismological Society of America, v. 100, no. 4, p. 1695-1709, doi: 10.1785/0120090376.

Maheshwari, B.K., Sharma, M.L., and Narayan, J.P., 2006, Geotechnical and structural damage in Tamil Nadu, India, from the December 2004 Indian Ocean tsunami: Earthquake Spectra, v. 22, no. S3, p. S475-S493.

Malik, J.N., Murty, C.V.R., and Rai, D.C., 2006, Landscape changes in the Andaman and Nicobar islands (India) after the December 2004 great Sumatra earthquake and Indian Ocean tsunami: Earthquake Spectra, v. 22, no. S3, p. S43-S66.

Maramai, A., and Tinti, S., 1997, The 3 June 1994 Java Tsunami: A Post-Event Survey of the Coastal Effects: Natural Hazards, v. 15, p. 31-49.

Martin, M.E., Weiss, R., Bourgeois, J., Pinegina, T.K., Houston, H., and Titov, V.V., 2008, Combining constraints from tsunami modeling and sedimentology to untangle the 1969 Ozernoi and 1971 Kamchatskii tsunamis: Geophysical Research Letters, v. 35, L01610, doi: 10.1029/2007GL032349.

Melekestev, I.V., 1980, Volcanism and Relief Formation: Moscow, Nauka, 212 pp. [in Russian]

Minoura, K., Gusiakov, V.G., Kurbatov, A., Takeuti, S., Svendsen, J.I., Bondevik, S., and Oda, T., 1996, Tsunami sedimentation associated with the 1923 Kamchatka earthquake: Sedimentary Geology, v. 106, p. 145-154.

Myers E.P., and Baptista, A.M., 2001, Analysis of Factors Influencing Simulations of the 1993 Hokkaido Nansei-Oki and 1964 Alaska Tsunamis: Natural Hazards, v. 23, no. 1, p. 1-28.

Nakanishi, A., Smith, A.J., Miura, S., Tsuru, T., Kodaira, S., Obana, K., Takahashi, N., Cummins, P.R., and Kanada, T., 2004, Structural factors controlling the coseismic rupture zone of the 1973 Nemuro-Oki earthquake, the southern Kuril Trench seismogenic zone: Journal of Geophysical Research, v. 109, doi: 10.1029/2003JB002574.

Nanayama, F., 2008, Sedimentary Characteristics and Depositional Processes of Onshore Tsunami Deposits: An Example of Sedimentation Associated with the 12 July 1993 Hokkaido-Nansei-oki Earthquake Tsunami, in Shiki, T., Tsuji, Y., Yamazaki, T., and Minoura, K., eds., Tsunamiites: Features and Implications: San Francisco, Elsevier, p. 63-80.

Norimatsu, K., and Mori, J.J., 2008, Fault plane determination and possible triggering of the 2007 Kuril Island earthquake (Mw 8.1): Eos, (Transactions, American Geophysical Union), v. 89, no. 53, Fall Meeting Supplements, Abstract S23B-1886.

Okada, R., 1985, Surface deformation due to shear and tensile faults in a half-space, Bulletin of the Geological Society of America, v. 75, no. 4, p. 1135-1154.

Okal, E.A., Sladen, A., and Okal, E.A.-S., 2006, Rodrigues, Mauritius, and Réunion islands; Field survey after the December 2004 Indian Ocean tsunami: Earthquake Spectra, v. 22, no. S3, p. S241-S261.

Pacheco, J.F., and Sykes, L.R., 1992, Seismic moment catalog of large shallow earthquakes, 1900 to 1989: Bulletin of the Seismological Society of America, v. 8, p. 1306-1349.

Pan, W., Wang, S., and Cai, S., 2010, Numerical simulations of the coastal effects of tsunami waves caused by the 1993 Hokkaido-Nansei-Oki earthquake: Chinese Journal of Oceanology and Limnology, v. 28 no. 5, p. 1029-1039.

Pelinovsky, E., Troshina, E., Golinko, V., Osipenko, N., and Petrukin, N., 1999, Runup of tsunami waves on a vertical wall in a basin of complex topography: Physics and Chemistry of the Earth (B), v. 24, no. 5, 431-436.

Rabinovich, A.B., Lobkovsky, L.I., Fine, I.V., and Thomson, R.E., 2008, Source observations and modeling of the Kuril Islands tsunamis of 15 November 2006 and 13 January 2007: Advances in Geosciences, v. 14, p. 105-116.

Raeesi, M., and Atakan, K., 2009, On the deformation cycle of a strongly coupled plate interface: The triple earthquakes of 16 March 1963, 15 November 2006, and 13 January 2007 along the Kurile subduction zone: Journal of Geophysical Research, v. 114, B10301, doi: 10.1029/2008JB006184.

Satake, K., Nanayama, F., and Yamaki, S. 2008, Fault models of unusual tsunamis in the 17th century: Earth Planets Space, v. 60, p. 925-935.

Segall, P., and Davis, J., 1997, GPS Applications for geodynamics and earthquake studies: Annual Review of Earth and Planetary Science, v. 25, p. 301-336.

Shepard, F.P., MacDonald, G.A., and Cox, D.C., 1950, The tsunami of April 1, 1946, Hawaii: California University, Scripps Institute of Oceanography Bulletin, v. 5, p. 391-528.

Shi, S., Dawson, A.G., and Smith, D.E., 1995, Coastal sedimentation associated with the December 12th 1992 tsunami in Flores, Indonesia: Pure and Applied Geophysics, v. 144, p. 525-536.

Shuto, N., 1991, Numerical Simulation of Tsunamis- Its Present and Near Future: Natural Hazards, v. 4, p. 171-191.

Soloviev, S.L., and Ferchev, M.D., 1961, Summary of data on tsunamis in the USSR: Bulletin of the Council for Seismology, v. 9, p. 1-37. [in Russian]

Soloviev, S.L., 1972, Recurrence of earthquakes and tsunamis in the Pacific Ocean: Volny Tsunami, Trudy Sakhnii, v. 29, p. 7-47. [in Russian]

Song, T.A., and Simons, M., 2003, Large trench-parallel gravity variations predict seismogenic behavior in subduction zones: Science, v. 301, p. 630–633, doi: 10.1126/science.1085557.

Srinivasalu, S., Thangadurai, N., Switzer, A.D., Ram Mohan, V., and Ayyamperumal, T., 2007, Erosion and sedimentation in Kalpakkam (N Tamil Nadu, India) from the 26th December 2004 tsunami: Marine Geology, v. 240, p. 65-75.

Steblov, G.M., Kogan, M.G., Levin, B.V., Vasilenko, N.F., Prytkov, A.S., and Frolov, D., 2008, Spatially linked asperities of the 2006-2007 great Kuril earthquakes revealed by GPS: Geophysical Research Letters, doi: 10.1029/2008GL035572.

Steblov, G.M. Vasilenko, N.F., Prytkov, A.S., Frolov, D.I., and Grekova, T.A., 2010, Dynamics of the Kuril-Kamchatka Subduction Zone from GPS Data: Physics of the Solid Earth, v. 46, no. 5, p. 440-445.

Tanioka, Y., Hasegawa, Y. and Kuwayama, T., 2008, Tsunami waveform analysis of the 2006 underthrust and 2007 outer-rise Kurile earthquakes: Advances in Geosciences, v. 14, p. 129-134.

Tikhonov, I.N., Vasilenko, N.F. Zolotukhin, D.E. Ivelskaya, T.N. Poplavsky, A.A. Prytkov, A.S. and Spirin, A.I., 2008, Simushir Earthquakes and Tsunami of November 15, 2006, and January 13, 2007: Russian Journal of Pacific Geology, v. 2, no. 1, p. 1-14.

Titov, V.V. and Gonzales, F.I., 1997, Implementation and testing of the methods of splitting tsunami (MOST) model: Technical Report NOAA Technical Memo, ERL PLEL-112 (PB98-122773), NOAA/Pacific Marine Environmental Laboratory, Seattle, WA.

Titov, V.V. and Synolakis, C.E., 1995, Modeling of breaking and nonbreaking long-wave evolution and runup using VTCS-2: Journal of Waterways, Ports and Ocean Engineering, v. 121, p. 308-316.

Titov, V.V. and Synolakis, C.E., 1998, Numerical modeling of tidal wave runup: Journal of Waterway, Port, Coastal and Ocean Engineering, v. 124, p. 157-171.

Titov, V.V., Mofjeld, H.O., Gonzales, F.I., and Newman, J.C., 2001, Offshore forecasting of Alaskan tsunamis in Hawaii, in: Hebenstreit, G.T., ed., Tsunami Research at the End of a Critical Decade. Birmingham, England, Kluwer Academic Publishers, p. 75-90.

Titov, V.V., Gonzales, F.I., Bernard, E.N., Eble, M.C., Mofjeld, H.O., Newman, J.C., and Venturato, A.J., 2005, Real-time tsunami forecasting: challenges and solutions: Natural Hazards, v. 35, p. 41-58.

Umitsu, M., Tanavud, C., and Patanakanog, B., 2007, Effects of landforms on tsunami flow in the plains of Banda Aceh, Indonesia, and Nam Khem, Thailand: Marine Geology, v. 242, p. 141-153, doi: 10.1016/j.margeo.2006.10.030.

Valleé, M., 2006, Séisme des Kuril, http://geoazur.oca.eu/spip.php?article110, Accessed Oct 25, 2010.

Valleé, M., 2007, Séisme des Kurill, http://geoazur.oca.eu/spip.php?article109&var_%20recherche=kuril, Accessed Oct 25, 2010.

Yagi, Y., 2006, 2006年11月15日 千島列島沖で発生した地震の断層破壊のイメージング（暫定）: http://www.geo.tsukuba.ac.jp/press_HP/yagi/EQ/Chishima/, Accessed Nov 6, 2008.

Yagi, Y., 2007, 2007年1月13日 千島列島沖で発生した地震の断層破壊のイメージング（暫定）: http://www.geo.tsukuba.ac.jp/press_HP/yagi/EQ/2007Chishima/, Accessed Nov 6, 2008.

Yamanaka, Y., 2006, 06/11/15 11:14(UT) Kuril Islands: EIC Seismological Note, no. 183, http://www.eri.u-tokyo.ac.jp/sanchu/Seismo_Note/2006/EIC183e.html, Accessed Nov 6, 2008,

Yamanaka, Y., 2007, 07/01/13 04:23(UT) Kuril Islands: EIC Seismological Note, no. 184, http://www.eri.u-tokyo.ac.jp/sanchu/Seismo_Note/2007/EIC184e.html, Accessed Nov 6, 2008.

Yeh, H., Titov, V., Gusiakov, V., Pelinovsky, E., Kharmushin, V. and Kaistrenko, V., 1995, The 1994 Shikotan earthquake tsunamis: Pure and Applied Geophysics, v. 144, no. 3/4, p. 855-874.

Zlobin, T.K. and Polets, A.Yu., 2009, Source Zones of the Catastrophic Simushir Earthquakes on November 15, 2006 (Mw= 8.3) and January 13, 2007 (Mw= 8.1) and the Deep Crust Structure beneath the Middle Kuril Segment: Russian Journal of Pacific Geology, v. 3, no. 5, p. 460-469.

APPENDIX A

Methods and results of slip-distribution inversion techniques for the 2006 and 2007 Kuril Island earthquakes

Seismic Inversions

Ji (2006 and 2007) inverted short-period P and SH and long-period Rayleigh and Love waves for both the 2006 and 2007 sources. The P and SH waveforms were bandpass filtered from 2 sec to 330 sec. For 2006, Ji (2006) used a fault plane with the GMCT moment tensor solution (strike 220º, dip 14.89º), with dimensions 400 km (along strike) by 137.5 km, divided into 220 (20 km by 12.5 km) subfaults (Table A.1). For 2007, Ji (2007) used a fault plane with the GCMT solution (southeast-dipping plane, strike 42º, dip 57.89º), but Ji shifted the USGS hypocenter's depth to 18 km to match body waves. The dimensions of his rupture zone, based upon aftershock distribution are 200 km (along strike) by 35 km, which he divides into 175 (8 km by 5 km) subfaults for inversion (Table A.2). Ji (2007) also tested variable dips for the 2007 focal mechanism; smaller dips could explain the body waves but not the long-period Love waves. Ji found maximum slip of 2006 to be 9 m located adjacent to Ushishir-Rasshua (Table A.1, Figure 4.3), from 8-19 km deep in the crust. The 2007 earthquake had two slip patches, each with a maximum of 20 m slip and 3-13 km deep in the crust; the smaller patch was adjacent to N. Simushir and the much larger one adjacent to Rasshua-Matua (Table A.2, Figure 4.3). Tsunami simulations in Chapter 4 based on Ji (2006; 2007)'s seismic inversions are referred to as *JSei06* for 2006 and *JSei07* for 2007.

Valleé (2006; 2007) inverted for slip distributions from P and SH teleseismic waves. For 2006, Valleé (2006) assumes a strike of 215º, dip of 22º and rake of 95º over a fault length of 325 km by 150 km (Table A.2). For 2007, Valleé (2007) assumes a strike of 220º, dip of 39º and rake of -106º; fault length is 250 km by 60 km (Table A.2). Valleé (2006) finds maximum slip of 10 m for 2006 occurred adjacent to Rasshua-Matua at an approximate depth of 10-30 km in the crust. The 2007 earthquake had maximum slip greater than 10 m, adjacent to the northern end of Kruzenshtern Strait from approximately 0 km to 13 km deep in the crust. I did not simulate tsunamis from Valleé (2006; 2007)'s inversions.

Yagi (2006; 2007) inverted to slip distributions from teleseismic P waves. For 2006, Yagi (2006) assumes a strike of 214º, dip of 15º and rake of 97º over a fault length of 140 km by 130 km, divided into 20 km by 15 km subfaults (Table A.1). For 2007, Yagi (2007) assumes a strike of 215º, dip of 45º and rake of -110º. Fault length is 180 km by 40 km, divided into 10 km by 10 km subfaults (Table A.2). Maximum slip for the 2006 earthquake was 8 m at two locations, both located adjacent to northern Simushir, one at shallow depths of approximately 1-5 km in the crust, and the other from 14-17 km in the crust. Maximum slip for the 2007 earthquake was 10 m, located adjacent to northern Simushir at a depth between 3 and 11 km in the crust. I did not simulate tsunamis from Yagi (2006; 2007)'s inversions.

Yamanaka (2006; 2007) also inverted slip distributions from teleseismic P waves. For 2006, Yamanaka (2006) assumes a strike of 220º, dip of 25º and rake of 96º over a fault length of 200 km by 70 km, divided into 20 km by 10 km subfaults (Table A.1). For 2007, Yamanaka (2007) assumes a strike of 220º, dip of 37º and rake of -108º. Fault length is 140 km by 40 km, divided into 20 km by 10 km subfaults (Table 2). Maximum slip for the 2006

earthquake was 13 m, located adjacent to Ushishir-Rasshua from approximately 2-6 km in the crust. Maximum slip for the 2007 earthquake was 26 m, located adjacent to Ketoi between 0 and 6 km deep in the crust. I did not simulate tsunamis from Yamanaka (2006; 2007)'s inversions.

Raeesi and Atakan (2009) obtained their slip distributions from computer codes derived from Kikuchi and Kanamori (1982 and 1991) and Kikuchi et al. (1993). For both earthquakes they used P waves, band-pass filtered with cutoff frequencies at 0.002 and 2.0 Hz. The southwestern extent of the rupture zone was chosen to coincide with the Bussol graben. The rupture area covered 280 km by 150 km with subfaults 20 km by 15 km. The strike and dip (220º and 15º) are based on the GCMT solution (Table A.1). For the 2007 earthquake, strike was fixed at 40º and dip at 46º (Table A.2). Fault dimensions were chosen based on the distribution of aftershocks. The rupture area covered 260 km by 50 km, with 20 km by 10 km subfaults. Maximum slip for 2006 occurred in three locations (Table A.1, Figure 4.4)— 6 m at 13-20 km deep in the crust adjacent to northern Simushir, 4 m approximately 9 km deep in the crust adjacent to Rasshua-Matua, and 5 m at 31-42 km in the crust adjacent to Kruzenshtern Strait. Their 2007 maximum slip is 13 m adjacent to Ketoi, 11-25 km in the crust (Table A.2, Figure 4.4). Raeesi and Atakan (2009) associate the maximum slip locations for both events with asperities that potentially will re-rupture in future earthquakes. Tsunami simulations in Chapter 4 based on Raeesi and Atakan (2009)'s seismic inversions are referred to as *RSei06* for 2006 and *RSei07* for 2007.

Ammon et al. (2008) used P, SH and Rayleigh-wave effective source-time functions to invert the 2006 earthquake to an area 320 km by 140 km, subdivided into 10 km by 10 km subfaults. Their preferred 2006 earthquake has a strike 215º, dip 15º and rake 92º (Table

A.1). They invert 2007 onto a 300 km by 60 km fault subdivided into 5 km by 5 km subfaults. The 2007 fault parameters have a strike of 43º, dip 59º and rake -108º (Table A.2). Ammon et al. (2008) chose the southwest-dipping plane because of its alignment with the trench and aftershock distribution. Maximum slip was 7 m for 2006, located adjacent to Rasshua at depths in the crust of 3-13 km. Maximum slip for 2007, occurring in two patches, was 14 m and 13 m, located adjacent to Ushishir-Rasshua and northern Simushir, respectively, both at depths approximately 0-7 km in the crust. I did not simulate tsunamis from Ammon et al. (2008)'s inversions.

Lay et al. (2009) use long-period (200-1000 s) waves, referred to as the W phase, which occur after P wave arrival until larger amplitude Rayleigh waves arrive. They also use P waves, bandpass filtered (at 0.8-2.0 Hz), and Rayleigh waves to estimate rupture velocity and fault length. For 2006, they prefer a moment tensor of a strike of 220º and dip of 15º, based the geometry of the subduction zone, but their W-phase solution and a corollary Rayleigh wave solution by J. Polet suggest uncertainties of ±15º for strike and ±6º for dip. For inversion, Lay et al. (2009) use a rupture plane with dimensions 240 km by 100 km, divided into 20 km by 10 km subfaults (Table A.1). For 2007, Lay et al. (2009)'s preferred slip distribution uses P and SH waves with variable rake, on the northwest-dipping fault (strike 220º, dip 47º), with a mechanism modified from the W-phase solution. Their rupture has dimensions 300 km by 60 km with 20 km by 10 km subfaults (Table A.2); however, the area with significant rupture is only ~220 km by 50 km. The uncertainty in slip location is approximately 10 km along strike and 5 km along dip (Alexander Hutko, pers. comm.). Lay et al. (2009)'s maximum slip for 2006 is 14 m, located adjacent to Rasshua at 3-13 km deep in the crust, and for 2007 is 15 m, also located adjacent to Rasshua from 4-10 km in the crust

(Figure 4.5). Lay et al. (2009) note that differences between their W-phase solution and the GCMT solution for 2007 are larger than for any other great earthquakes with such comparisons. They also conclude that their absolute slip may be overestimated. Tsunami simulations in Chapter 4 based on Lay et al. (2009)'s seismic inversions are referred to as *LSei06* for 2006 and *LSei07* for 2007.

Seismic and Tsunami Inversion

Baba et al. (2009) inverted P, Rayleigh and Love teleseismic waves and bottom pressure records (BPR) of the tsunami waveforms, both separately and together, to solve for the source of the 2006 earthquake. They bandpass-filtered the P waves to 4 mHz to 4Hz for the first 190 sec after initial P wave arrival. Rayleigh and Love waves were band-pass filtered at 3.0-6.0 mHz. Tsunami waveforms were from Deep Assessment and Reporting of Tsunamis (DART) buoys and seafloor cable BPR of Japan and were filtered for tides, seismic waves, and coseismic land-level change. Baba et al. (2009) used a fault plane with strike 220º and dip 10º; they derived dip from a seismic survey of the trench by Nakanishi et al. (2004). They defined the rupture area as 400 km by 140 km with 20 km by 20 km square subfaults (Table A.1). Their maximum slip is 12 m located adjacent to Ketoi-Ushishir, at 7-10 km depth in the crust (Figure 4.6). They note that when slip inversion was solved for with only P and surface waves, maximum slip was greater (12.8 m) and more "peaked"; when tsunami waveforms were included in the inversion, they had the effect of smoothing the slip pattern, and as a by product, decreasing the maximum slip. Baba et al. (2009) do not solve for the 2007 slip distribution. The tsunami simulation in Chapter 4 based on Baba et al.

(2009)'s combined seismic and tsunami inversion of the 2006 earthquake is referred to as *BSeiTs06*.

Tsunami Inversion

Fujii and Satake (2008) invert far-field tsunami waveforms to a source using data from tide gauges, DART systems, and cabled tsunami sensors. For the 2006 event, Fujii and Satake (2008) adopted the GCMT focal mechanisms with a strike of 214°, and constrained the source area using the 1-day aftershock distribution to a length either 200 or 250 km and a width of 100 km. They divided the 2006 source into three possible solutions; 8 or 10 subfaults with 15º dip for all, or 8 subfaults with 8º and 15º dip for shallower and deep subfaults, respectively, all with 50 by 50 km subfaults (Table A.1). Maximum slip for all three solutions is around 7 m (6.8-7.4 m) all adjacent to Rasshua and Matua (Figure 4.7). The 15º dip solutions have maximum slip from 5 to 31 km in the crust, and the 8º/15º solution extents from 5 to 25 km. For the 2007 event, Fujii and Satake (2008) adopted two fault planes— one northwest dipping (strike, 215°; dip, 45°; rake, -110°; length, 240 km; width, 40 km) and the other southeast dipping (strike, 42°; dip, 58°; rake, -114°; length, 240 km; width, 40 km), divided into six 40 by 40 km subfaults. Both solutions have maximum slip adjacent to Rasshua-Matua of 3.5 m slip from 7-41 km depth in the crust (Figure 4.7). The tsunami simulation in Chapter 4 based on the tsunami inversions of Fujii and Satake (2008) is referred to as *FTs06_82* for the solution of 2006 with 8º and 15º dip at a M_w 8.2 and *FTs07* for the southeast-dipping fault plane of 2007. The simulation referred to as *FTs06_84* in Chapter 4 is an increase of the *FTs06_82* earthquake solution to a M_w 8.4.

GPS inversions

Steblov et al. (2008) determine a slip distribution by inverting surface offsets during the 2006 and 2007 earthquakes of 10 GPS receivers (both continuous and survey-mode). They divide their 2006 fault plane (strike 221º) into 12 subfaults where dip increases with depth (9º, 16º, 22º); total length and width is 230 km by 150 km (Table A.1). They divide the 2007 southeast-dipping fault plane (strike 41º, dip 59º) into 4 subfaults covering 230 km along strike, with both 25 km and 50 km (preferred) widths, to cover uncertainties in 2007 fault rupture extent (Table A.2). Maximum slip for 2006 was 12 m from approximately 1 to 22 km depth in the crust and 8 m from 1 to 44 km depth in the crust for 2007, both located at the southernmost end of respective rupture zones, adjacent to northern Simushir-Ketoi (Figure 4.8). High slip is attributed to the large eastward offset seen by GPS stations on Matua, Ketoi and Urup. For the 2007 case, GPS inversions are insensitive to dip, when dip is at such a high angle; changes in dip by 10º changed slip by less than 1%. However, maximum slip on a 25 km wide fault was ~3 times higher than on the 50 km wide fault, but occurred in the same location (Steblov et al., 2008). Tsunami simulations in Chapter 4 based on Steblov et al. (2008)'s GPS inversions are referred to as *SGPS06* for 2006 and *SGPS07* for 2007.

Tikhonov et al. (2008) use the same, but fewer, GPS receiver stations as Steblov et al. (2008), including ITRP (Iturup), KUNH (Kunashir), SHKT (Shikotan), YSSK (Yuzhno-Sakhalinsk), PETS (Petropavlovsk) and PRMH (Paramushir); they do not include any station in the nearfield of the earthquake. Tikhonov et al. (2008) estimate the vertical (along dip) uplift of 2006 to be 7 m at maximum (Table A.1). The 2007 earthquake produced 5 m of

along-dip displacement (Table A.2). I did not simulate tsunamis based on Tikhonov et al. (2008).

Table A.1: Overview of earthquake parameters and different interpretations of the 2006 earthquake slip distribution for all published inversions

		Fujii and Satake (2008)	**Baba et al. (2009)**	**Steblov et al. (2008)**	**Lay et al. (2009)**	**Raeesi and Atakan (2009)**	**Ji (2006)**	**Ammon et al. (2008)**	**Tikhonov et al. (2008)**	**Vallee (2006)**	**Yamanaka (2006)**	**Yagi (2006)**
	method	tsunami inversion (tide gauges, DART and cabled tsunami sensors)	seismic (P, Rayleigh and Love waves) and tsunami (bottom pressure records)	GPS inversion (continuous and survey)	seismic (W phase, surface and P waves)	seismic (P waves)	seismic (P, SH, Raleigh, Love waves)	seismic (P, SH, Rayleigh waves)	GPS (continuous stations)	sesimic (P and SH waves)	seismic (P waves)	seismic (P waves)
model parameters	along-strike length (km)	A and C = 200 B = 250	400	230	240	280	400	320	296	325	200	140
	along-dip width (km)	100	140	150	100	150	137.5	140	58	150	70	130
	subfault length (km)	50	20	57.5	20	20	20	10	-	-	20	20
	subfault width (km)	50	20	50	10	15	12.5	10	-	-	10	15
	strike	214º	220º	221º	220º	220º	220º	215º	200º	215º	220º	214º
	dip	A and B = 15º C = 8º (shallow) and 15º (deep)	10º	9º, 16º, 22º	15º	15º	14.89º	15º	11º	22º	25º	15º
	rake	92º	calculated (90 ± 45); avg. 109º	calculated; avg. 114º	calculated; avg. 96º	calculated; avg. 100º	calculated; avg. 91º	92º ± 5º	95º	95º	96º	97º
earthquake parameters	hypocenter depth	-	20 km below sea level	30 km below sea level	12 km in crust	28.5 km below sea level	27 km in crust	11 km in crust	-	30 km in crust	28 km below sea level	27 km below sea level
	M_o (Nm)	A = 2.0 x 10^21 B= 2.5 x 10^21 C = 2.5 x 10^21	5.0 x 10^21	5.14 x 10^21	5.0 x 10^21	2.78 x 10^21	3.9 x 10^21	4.66 x 10^21	2.71 x 10^21	1.77 x 10^21	2.1 x 10^21	1.6 x 10^21
	M_w	8.1 - 8.2	8.4	8.4	8.4	8.23	8.3	8.38	8.23	8.1	8.15	8.1
slip distribution	total avg. slip/avg. slip if > 0.25 m (m)	A = 2.5/3.3 B = 2.7/4.4 C = 3.1/4.1	2.6/2.8	3.6/5.4	4.6/4.6	1.9/1.9	1.7/2.3	-	-	-	-	-
	maximum slip (m)	A = 6.8 B = 7.1 C = 7.4	11.8	12.1	14.0	5.6	8.9	~7 m	6.7	10	12.6	7.7
	location of maximum slip perpendicular to[#]	A = Rasshua and Matua B = Rasshua and Matua C = Rasshua-Matua	Ketoi - Ushishir	N Simushir - Ketoi	Ushishir - Rasshua	N Simushir; Kruzenshtern Strait; Rasshua	Ushishir-Rasshua	Rasshua	-	Rasshua - Matua	Ushishir-Rassua	N Simushir; N Simushir
	size of slip patch(es)[$] (length x width) (km)	A = 50x50 and 50x50 B = 50x50 and 50x50 C = 50 - 100 x 50 - 100	140 x 10	57.5 x 100	80 (or 60) x 50 (or 10)	60 (or 30) x 30; 45 (or 30) x 60; 20 x 15	80 x 37.5	25 x 40	-	*50 x 25*	*40 x 20*	*25 x 15 and 25 x 10*
	approximate depth in crust of maximum slip (km)	A = 18 - 31 and 5 - 18 B = 18 - 31 and 5 - 18 C = 5 - 31	6.5 - 10	0.5 - 22	3 - 13	13 - 20; 31 - 42; 9	8 - 19	3 - 13	-	*10 - 30*	*2-6*	*1 - 5 and 14 - 17*
	average slip within patch(es)[$] (m)	A = 6.8 and 4.8 B = 7.1 and 5.1 C = 6.3	10.3	11.2	11.1	4.8; 4.5; 4.1	7.5	-	-	-	-	-
	number of subfaults in slip patch(es)[$]	A = 1 and 1 B = 1 and 1 C = 3	7	2	8	5; 8; 1	12	-	-	-	-	-

= see Figure 4.1 for island names and locations

$ = "patch" defined as subfaults with at least 2/3 of maximum slip

Table A.2: Overview of earthquake parameters and different interpretations of the 2007 earthquake slip distribution for all published inversions

		Fujii and Satake (2008)	**Steblov et al. (2008)**	**Lay et al. (2009)**	**Raeesi and Atakan (2009)**	**Ji (2007)**	**Ammon et al. (2008)**	**Tikhonov et al. (2008)**	**Vallee (2007)**	**Yamanaka (2007)**	**Yagi (2007)**
	method	tsunami (tide gauges, DART, and cabled tsunami sensors)	GPS (continuous and survey)	seismic (W phase, surface and P waves)	seismic (P waves)	seismic (P, SH, Raleigh, and Love waves)	seismic (P, SH, Rayleigh waves)	GPS (continuous stations)	sesimic (P and SH waves)	seismic (P waves)	seismic (P waves)
model parameters	along-strike length (km)	240	230	300	240	200	300	180	250	140	180
	along-dip width (km)	40	50	60	40	35	60	46	60	40	40
	subfault length (km)	40	57.5	20	20	8	5	-	-	20	10
	subfault width (km)	40	50	10	10	5	5	-	-	10	10
	strike	A = 215º B = 42º	41º	220º	40º	42º	43º	222º	220º	220º	215º
	dip	A = 45º B = 58º	59º	47º	45.5º	57.89º	59º	70º	39º	37º	45º
	rake	A = -110º B = -114º	calculated; avg. -125º	calculated; avg. -106º	calculated; avg. -97º	calculated; avg. -114º	-108º'	-60º	-106º	-108º	-110º
earthquake parameters	hypocenter depth	-	30 km below sea level	4 km in crust	14 km in crust	18 km in crust	22 km in crust	-	25 km in crust	7 km below sea level	24 km below sea level
	M_o (Nm)	A = 0.96 x 10^21 B = 1.1 x 10^21	2.66 x 10^21	2.6 x 10^21	1.731 x 10^21	1.9 x 10^21	1.49 x 10^21	9.9 x 10^20	1.39 x 10^21	2.66 x 10^21	1.6 x 10^21
	M_w	7.8-8.1	8.22	8.2	8.1	8.1	8.05	7.9	8	8.2	8.1
slip distribution	total avg. slip/avg. slip if > 0.25m (m)	A = 2.5/3.3 B = 2.7/4.4	4.4/4.4	2.3/2.7	3.8/4.1	7.0/7.3	-	-	-	-	-
	maximum slip (m)	A = 3.5 B = 3.5	8.3	15.0	13.3	20.3	*12 - 14*	5.1	> 10	26.2	10
	location of maximum slip perpendicular to[#]	Rasshua-Matua	N Simushir-Ketoi	Rasshua	Ketoi	Rasshua-Matua; N Simushir	Ushishir-Rasshua; N Simushir	-	N Kruzenshtern	Ketoi	N Simushir
	size of slip patch(es)[$] (length x width) (km)	80 x 40	57.5 x 50	100 x 10	80 x 20	48 (or 16) x 15 (or 5); 8 x 15	15 x 10; 30 x 10	-	75 x 20	50 x 10	40 x 15
	depth in crust of maximum slip (km)	7 - 41	0.5 - 44	4 - 10	11 - 25	3 - 16; 3 - 16	0 - 7; 0 - 7	-	0 - 13	0 - 6	3 - 11
	average slip within patch(es)[$] (m)	3.3	8.3	12.6	11.3	16.6; 17.3	-	-	-	-	-
	number of subfaults in slip patch(es)[$]	2	1	5	7	13; 3	-	-	-	5	3

= see Figure 4.1 for island names and locations
$ = "patch" defined as subfaults with at least 2/3 of maximum slip

APPENDIX B

Simulation results

Table B.1: Closest simulated runup to field runup for all tsunami simulations generated by published slip distributions. Refer to Chapter 4 for names of simulations

Observation				Simulated runup (m)										
Field point	Longitude (ºE)	Latitude (ºN)	Runup (m)	*FTs06_84*	*FTs06_82*	*LSei06*	*JSei06*	*RSei06*	*SGPS06*	*FTs07*	*LSei07*	*JSei07*	*RSei07*	*SGPS07*
Kast225	150.5460	46.2115	7.6	1.5	0.9	1.5	1.0	1.5	4.5	0.4	1.2	1.9	1.6	1.8
Kast232	150.5485	46.2145	5.4	1.6	0.9	1.9	1.1	1.6	4.4	0.5	1.1	2.0	1.8	2.0
Pesc153	150.8920	46.5335	5.7	1.6	0.9	1.9	0.5	3.2	6.1	0.3	1.3	2.7	1.7	2.1
Pesc150	150.8920	46.5340	10.4	1.6	0.9	1.9	0.6	3.3	6.1	0.3	1.3	2.8	1.8	2.5
Pesc221	150.8960	46.5385	5.6	1.4	0.9	1.8	0.6	3.6	5.3	0.3	1.3	2.8	1.8	2.2
Pesc217	150.9060	46.5410	5.8	1.3	0.8	1.8	0.5	3.1	5.0	0.2	1.0	2.9	1.9	1.8
Pesc219	150.9010	46.5415	7.6	1.3	0.7	2.4	0.9	3.0	5.5	0.2	1.0	3.0	1.9	2.0
Spas037	151.8750	46.8330	4.3	2.9	1.8	3.7	2.3	4.3	4.3	0.7	2.5	3.8	4.0	2.8
Spas039	151.8785	46.8355	2.7	2.8	1.9	3.8	2.3	4.1	4.5	0.7	2.2	3.7	3.7	2.9
Spas082	151.8815	46.8375	7.2	2.4	1.7	3.7	2.4	4.0	4.2	0.8	1.9	4.5	4.1	3.2
Spas77b	151.8885	46.8425	5.7	2.4	1.8	3.6	2.4	3.7	4.2	0.9	2.0	4.5	4.1	3.3
Spas002	151.8905	46.8435	7.1	2.4	1.8	3.2	2.3	3.1	4.2	0.8	2.0	4.5	4.2	3.1
Spas036	151.8930	46.8465	2.2	2.8	2.0	3.0	2.2	2.8	5.1	0.9	3.2	4.4	4.0	3.1
Spas001	151.8985	46.8495	6.7	2.7	2.0	2.7	1.9	2.5	4.4	0.8	2.3	4.2	4.2	3.0
Spas079	151.9030	46.8525	6.5	2.8	1.9	2.5	1.7	2.3	4.3	0.8	2.7	4.9	3.9	2.9
Spas078	151.9060	46.8535	4.6	2.6	1.8	2.3	1.6	2.1	4.5	0.8	2.1	4.0	3.6	2.9
Opas215	152.0545	46.9400	7.2	3.5	2.4	4.0	2.4	2.3	5.7	0.9	2.7	6.3	5.1	4.1
Opas213	152.0565	46.9445	8.6	3.9	2.4	4.2	2.4	2.5	5.9	0.9	2.8	5.6	5.1	4.1
Opas212	152.0585	46.9480	6.3	4.3	2.5	4.0	2.5	2.4	6.2	1.0	3.6	6.1	5.2	4.1
Dush001	152.1580	47.0435	19.6	5.9	5.7	6.6	4.0	6.1	6.0	2.0	6.3	8.0	10.5	7.8
Dush002	152.1595	47.0465	12.2	5.7	5.9	5.8	4.0	6.4	5.8	2.1	6.0	6.8	9.3	7.6
Dush003	152.1600	47.0485	7.9	6.4	5.7	6.5	4.0	5.9	6.0	2.2	6.0	6.8	8.4	8.1
Dush005	152.1640	47.0545	11.0	6.3	5.4	6.3	4.1	5.6	6.9	2.0	6.4	9.9	10.6	8.6
Dush006	152.1660	47.0570	4.2	6.3	4.9	5.2	4.2	5.3	7.0	1.9	8.7	10.1	8.9	7.0
Dush007	152.1680	47.0595	6.3	7.5	4.5	5.9	4.7	5.8	7.2	1.9	8.0	8.6	8.0	8.1
Dush008	152.1700	47.0600	7.9	6.7	4.2	5.7	4.2	4.9	7.0	1.9	6.0	11.1	11.8	11.3
Dush009	152.1740	47.0625	6.7	7.1	4.0	5.8	4.1	5.2	7.0	2.0	5.5	14.3	13.4	10.7
Dus2_06	152.1745	47.0630	6.7	7.1	4.2	7.5	4.2	4.7	6.8	1.8	6.0	16.8	16.1	14.0
Dush012	152.1765	47.0650	6.6	6.9	3.7	8.0	4.2	5.2	7.0	1.8	10.9	18.8	20.3	13.6
Dush011	152.1785	47.0665	7.7	6.9	4.1	5.6	4.2	5.5	6.7	1.7	6.7	14.2	12.2	10.0
Dush010	152.1815	47.0685	9.3	7.0	3.8	5.1	3.9	4.3	6.3	1.7	6.1	10.6	10.1	7.2
Dush110	152.1835	47.0700	10.0	8.0	4.9	6.0	4.6	4.9	6.4	1.5	9.2	15.6	15.1	10.8
Dus1_06	152.1865	47.0705	9.8	7.9	5.0	5.3	4.4	4.8	7.5	1.7	8.8	15.6	14.9	10.7
Dush109	152.1865	47.0705	8.8	6.5	4.6	5.1	3.9	3.7	7.6	1.3	8.6	12.4	12.3	7.6
Dush108	152.1900	47.0715	11.7	4.6	3.3	5.4	3.6	2.6	5.6	1.0	5.1	9.5	8.0	5.7
Dush107	152.1920	47.0735	17.9	6.1	3.5	5.7	3.8	2.5	7.7	0.9	5.5	4.5	7.9	5.8
Dush106	152.1935	47.0760	11.5	5.9	4.3	6.6	4.6	3.8	6.7	0.9	4.3	8.4	8.7	6.0
Dush102	152.2060	47.0780	7.5	4.0	2.8	4.7	3.0	2.5	5.2	0.0	2.5	4.5	4.4	4.0
Dush103	152.2015	47.0780	10.4	5.5	3.0	5.8	3.6	2.4	7.7	0.9	5.1	6.2	6.3	4.1
Dush104	152.1980	47.0780	13.3	6.0	4.4	6.0	4.7	3.8	6.6	0.9	5.1	7.7	6.1	6.5
Dush105	152.1935	47.0780	14.9	6.7	4.0	8.0	4.7	3.2	7.8	0.9	5.2	11.3	11.2	6.5
Dush101	152.2095	47.0795	8.5	4.0	2.4	4.7	3.2	2.2	5.0	0.0	8.0	8.6	3.4	2.6
Dush100	152.2100	47.0800	12.9	4.3	2.6	5.1	3.2	1.9	4.6	0.0	8.0	8.9	4.2	3.3
Keto003	152.4905	47.2965	6.8	8.3	4.3	7.1	3.4	3.3	4.7	1.1	3.9	7.7	5.2	4.0
Keto013	152.4870	47.2975	9.2	7.8	6.0	7.7	3.7	3.9	6.6	2.0	9.3	9.5	5.9	5.3
Keto109	152.5070	47.2980	10.1	9.0	5.1	8.6	3.4	3.2	4.3	0.0	9.5	8.2	6.0	8.9
Keto111	152.5090	47.2980	10.8	9.4	5.1	9.0	3.2	2.9	3.6	0.0	9.5	9.2	8.2	7.5
Keto002	152.4855	47.2985	7.3	8.4	5.6	6.8	3.7	4.1	6.1	2.0	8.3	11.6	6.5	5.3
Keto01b	152.4840	47.2985	7.1	9.5	5.6	9.5	3.6	5.2	5.4	1.8	4.6	9.6	7.0	8.3
Keto01c	152.4850	47.2985	7.5	8.5	5.8	9.5	3.6	6.4	5.5	1.8	6.4	10.6	7.0	6.4
Keto01a	152.4830	47.2990	6.6	9.5	5.6	9.5	3.6	5.2	5.4	1.8	4.6	8.0	7.0	8.3
Keto03b	152.4825	47.2995	10.6	8.5	6.0	8.7	4.6	5.9	6.4	1.8	5.8	7.9	7.6	7.6

Observation				Simulated runup (m)										
Field point	Longitude (ºE)	Latitude (ºN)	Runup (m)	*FTs06_84*	*FTs06_82*	*LSei06*	*JSei06*	*RSei06*	*SGPS06*	*FTs07*	*LSei07*	*JSei07*	*RSei07*	*SGPS07*
Keto116	152.5145	47.2995	10.0	7.2	4.6	9.8	3.4	2.9	3.5	0.0	5.6	6.1	8.7	4.1
Keto121	152.5160	47.3005	8.6	6.7	4.1	9.8	3.4	3.0	3.7	1.2	6.3	9.4	9.0	4.0
Keto122	152.5185	47.3020	11.8	6.9	4.3	10.1	3.5	2.8	4.1	1.2	7.5	10.6	9.0	5.3
Keto124	152.5205	47.3035	11.0	7.9	4.7	10.7	3.6	2.6	4.1	1.3	6.8	7.5	8.3	5.6
Keto126	152.5225	47.3055	11.2	8.5	5.0	11.9	3.7	2.7	4.5	1.3	11.2	10.9	11.0	5.1
Keto128	152.5235	47.3060	10.1	8.5	5.1	12.4	3.7	2.6	4.3	1.3	11.3	8.5	9.3	6.7
Rypo257	152.8245	47.5260	12.8	10.1	5.4	5.1	2.6	3.8	3.0	2.6	4.9	6.4	6.4	6.1
Rypo135	152.8285	47.5325	9.0	7.9	4.5	6.4	3.0	2.7	3.7	1.8	5.1	5.9	6.6	5.1
Rypo238	152.8280	47.5325	9.4	7.5	4.5	6.4	3.0	2.0	2.8	1.8	5.1	5.9	6.6	5.5
Rypo185	152.8290	47.5330	9.9	8.5	4.5	7.0	3.2	2.7	3.8	2.1	5.1	5.9	7.3	4.9
Rypo245	152.8290	47.5330	10.8	8.5	4.6	7.0	3.2	3.2	3.8	2.1	5.1	5.9	7.3	4.9
Rypo249	152.8300	47.5335	11.2	6.8	5.6	9.2	3.4	3.3	3.7	2.3	6.3	5.2	7.7	6.5
Rypo251	152.8320	47.5355	11.8	7.5	7.2	10.1	3.7	4.0	5.1	2.8	6.4	6.6	8.3	6.6
Rypo253	152.8350	47.5365	12.2	13.7	4.8	9.1	3.4	3.7	3.7	2.3	9.4	6.7	9.2	7.4
Rypo255	152.8395	47.5370	7.4	8.8	8.1	7.7	3.4	2.8	2.7	2.9	12.6	8.4	8.5	6.6
Rypo180	152.8505	47.5485	6.5	2.3	3.4	3.3	1.7	1.6	1.8	1.6	7.3	6.3	3.6	3.5
Rass187	152.9725	47.6850	10.2	11.9	6.5	10.6	3.2	2.8	3.6	2.4	8.2	12.1	11.0	8.4
Rass177	152.9660	47.6865	7.1	5.0	5.3	5.5	4.4	3.5	5.9	3.3	5.7	4.6	5.2	5.4
Rass179	152.9675	47.6900	7.5	6.4	4.7	7.5	3.4	6.0	2.9	2.7	6.7	5.9	5.5	5.9
Rass189	152.9740	47.6910	9.4	12.5	7.2	11.3	3.9	3.9	4.7	3.2	12.6	7.8	13.5	9.4
Rass191	152.9775	47.6945	10.8	13.2	7.7	11.2	3.8	3.8	4.8	3.3	8.0	9.1	9.7	8.2
Rass181	152.9680	47.6955	6.8	7.0	9.0	8.0	4.7	6.4	3.9	3.6	6.8	6.7	6.6	5.4
Rass193	152.9880	47.6965	10.5	14.6	7.7	12.0	3.4	3.6	4.1	3.1	11.0	8.0	11.0	9.1
Rass198	152.9660	47.6985	4.7	10.0	7.4	8.9	5.0	5.0	3.7	4.5	6.2	4.6	6.2	7.7
Rass196	152.9655	47.6995	3.9	9.3	5.9	9.9	5.0	4.3	3.7	4.2	5.6	4.6	5.9	8.1
Rass183	152.9620	47.7005	4.7	6.5	6.2	6.2	4.5	4.9	3.5	2.7	9.0	4.9	4.2	6.3
Rasi507	152.9630	47.7060	9.7	4.8	5.3	6.8	3.1	2.4	3.0	2.2	6.8	7.0	7.0	6.9
Nepr195	153.0240	47.7095	10.9	11.1	8.3	8.6	3.5	4.2	3.6	3.3	9.7	14.4	11.5	8.5
NeprNor	153.0275	47.7110	11.3	12.6	7.7	9.3	4.5	4.9	3.7	3.6	12.4	14.6	15.7	9.3
Rasi144	152.9700	47.7195	8.7	5.6	4.9	5.4	3.3	3.8	3.7	2.6	4.4	6.1	5.6	4.4
Rasi142	152.9715	47.7230	9.0	7.0	3.7	4.8	2.7	3.4	3.4	2.2	4.5	4.6	5.9	4.3
Rasn205	153.0490	47.7915	10.9	12.3	6.5	13.5	4.2	3.1	3.3	2.8	8.3	16.0	11.7	7.2
Rasn201	153.0490	47.7940	11.2	9.8	4.9	11.4	3.6	3.0	3.2	2.8	9.9	12.2	9.2	7.4
Rasn209	153.0490	47.8000	12.3	10.9	4.4	7.7	2.3	3.4	2.9	2.8	8.6	9.0	10.3	7.6
Rasn203	153.0455	47.8040	19.7	12.7	8.5	9.0	2.5	3.1	3.0	2.9	11.9	12.9	13.5	5.7
Aisb153	153.2695	48.0390	7.8	12.8	5.3	6.8	2.7	3.2	4.6	2.9	16.1	10.7	11.4	7.1
Aisb152	153.2665	48.0410	7.8	12.4	7.6	6.0	3.2	3.1	5.7	3.0	16.1	10.0	9.6	6.6
Aisb142	153.2280	48.0415	13.0	9.7	6.4	6.5	2.6	3.1	5.6	3.5	19.3	17.6	15.2	7.7
Aisb222	153.2390	48.0415	6.9	7.9	6.2	9.2	3.4	2.9	6.7	2.5	20.7	16.2	15.0	5.0
Aisb224	153.2415	48.0420	5.8	8.4	7.5	8.6	3.2	3.4	6.4	2.5	16.2	10.6	10.5	4.8
Aisb228	153.2440	48.0425	7.3	8.6	6.5	8.3	2.8	3.4	3.2	2.5	13.3	10.4	10.5	4.6
Aisb151	153.2635	48.0430	7.9	8.7	8.7	8.8	3.2	3.8	6.0	3.1	10.6	10.6	9.3	5.4
Aisb126	153.2270	48.0435	21.2	12.1	6.3	9.1	3.4	4.3	5.6	3.8	20.4	9.4	13.2	7.7
Aisb133	153.2270	48.0435	20.4	12.1	6.3	9.1	3.6	4.3	5.3	3.8	21.4	9.4	13.2	7.7
Aisb148	153.2555	48.0435	4.9	7.7	4.6	6.2	2.8	2.9	3.5	3.1	13.7	11.1	10.8	5.3
Sary162	153.2745	48.0435	8.0	6.2	6.1	5.8	2.3	2.3	7.9	2.6	8.0	8.2	7.8	6.1
Aisb149	153.2565	48.0440	6.4	7.7	5.8	7.1	2.9	2.9	3.5	3.3	12.0	9.9	9.7	5.0
Aisb150	153.2590	48.0445	5.6	9.9	7.8	9.3	3.1	3.2	5.6	3.5	11.8	10.1	8.6	5.6
Aisb216	153.2485	48.0445	5.8	8.7	4.4	8.0	2.9	3.5	3.9	2.7	14.3	11.1	10.4	4.6
Sary164	153.2735	48.0445	8.5	6.6	6.1	7.6	2.5	2.6	8.1	3.0	13.4	7.4	8.2	5.7
Aisb002	153.2260	48.0450	18.3	12.1	6.3	9.1	3.6	4.6	4.3	3.8	21.4	10.0	11.9	6.3
Aisb130	153.2260	48.0455	17.3	11.6	7.4	9.5	3.6	4.6	4.4	4.5	12.2	10.0	9.6	6.2
Aisb132	153.2260	48.0455	18.5	12.1	7.4	9.5	3.7	4.6	4.4	4.5	9.5	10.0	11.9	6.3
Aisb001	153.2255	48.0460	17.3	11.6	7.4	9.3	3.6	4.6	3.5	4.5	12.2	10.0	9.4	5.6
Aisb139	153.2255	48.0460	18.4	10.5	7.4	10.1	3.8	4.6	4.4	4.7	12.2	10.0	9.7	6.9
Sary165	153.2730	48.0460	8.5	7.1	4.9	6.0	2.4	2.6	5.0	3.0	12.1	8.6	7.4	4.3
Aisb143	153.2240	48.0470	17.1	8.1	6.5	12.7	4.0	4.4	4.4	4.5	14.2	11.3	9.6	6.9
Aisb144	153.2225	48.0475	14.2	9.2	6.5	13.0	4.2	4.5	6.9	4.1	15.9	10.0	8.5	6.9
Aisb145	153.2195	48.0480	13.6	9.7	5.9	13.1	4.0	4.5	6.6	3.5	12.3	5.9	5.8	5.9
Sary166	153.2745	48.0480	9.5	6.7	4.9	3.6	2.3	2.6	3.5	2.6	12.5	6.4	8.3	4.1
Sary167	153.2745	48.0480	10.3	7.7	4.7	4.2	2.3	2.6	2.5	2.5	10.5	7.9	7.4	3.9
Sary170	153.2745	48.0500	9.8	7.7	4.4	4.3	2.3	2.6	2.5	2.5	10.6	7.9	7.1	3.3

Observation				Simulated runup (m)										
Field point	Longitude (ºE)	Latitude (ºN)	Runup (m)	*FTs06_84*	*FTs06_82*	*LSei06*	*JSei06*	*RSei06*	*SGPS06*	*FTs07*	*LSei07*	*JSei07*	*RSei07*	*SGPS07*
Sary142	153.2720	48.0520	13.8	5.4	6.8	4.4	3.0	4.0	4.3	3.6	9.4	13.6	9.5	7.3
Sary145	153.2680	48.0535	11.2	5.8	8.3	4.8	3.0	3.7	5.7	4.3	13.0	9.7	10.0	6.9
Sary147	153.2665	48.0555	16.8	6.6	6.9	6.7	3.3	3.8	6.6	5.4	18.9	12.7	12.5	6.4
Sary149	153.2660	48.0575	15.4	7.9	9.7	6.4	3.2	4.0	8.4	5.0	24.4	24.8	16.3	8.0
Sary152	153.2665	48.0590	21.7	10.2	10.7	9.1	3.6	3.6	9.9	5.0	19.4	24.0	16.2	8.1
Sary154	153.2685	48.0610	16.7	8.6	6.8	6.7	3.0	3.1	3.2	3.9	20.7	15.0	13.8	6.9
Sary157	153.2690	48.0640	12.0	9.2	6.5	6.7	3.0	3.8	4.2	3.5	12.7	12.6	7.2	6.2
Sary086	153.2690	48.0665	15.5	7.6	6.4	6.7	3.2	4.4	4.4	3.3	21.2	6.6	13.4	7.0
Sary083	153.2680	48.0695	16.9	7.6	8.2	9.7	4.7	5.3	7.3	4.9	12.5	9.6	10.8	9.1
Sary079	153.2665	48.0710	19.6	8.0	9.7	12.8	7.6	6.1	9.5	7.4	14.4	10.7	17.1	11.5
Sary073	153.2665	48.0725	17.7	10.5	9.6	14.0	7.2	6.1	7.7	7.2	11.2	8.7	11.3	10.9
Sary230	153.2825	48.0730	10.0	7.0	8.5	10.4	4.2	3.8	6.3	5.0	7.7	9.7	13.1	7.6
Sary231	153.2825	48.0730	9.4	7.3	7.3	8.6	4.5	3.9	5.7	5.9	7.1	10.3	13.1	7.3
Sary234	153.2825	48.0730	8.1	6.9	7.3	8.6	4.5	3.8	5.7	5.9	6.4	10.3	13.1	7.1
Sary069	153.2650	48.0750	12.4	9.6	8.4	7.0	4.4	5.3	6.9	4.7	21.3	8.1	11.2	8.7
Sary235	153.2820	48.0750	11.4	7.0	6.3	10.1	4.2	3.7	4.8	3.6	7.3	10.6	10.4	8.8
Sary237	153.2810	48.0765	10.5	6.9	5.5	6.4	4.2	3.5	4.7	2.9	6.0	10.6	10.4	8.8
Sary136	153.2635	48.0770	10.6	8.5	5.5	6.6	6.1	5.7	3.7	4.5	24.3	15.1	12.7	8.4
Sary133	153.2635	48.0785	12.3	8.9	7.0	7.2	5.3	5.2	5.2	2.5	10.3	16.6	7.6	9.9
Sary129	153.2650	48.0815	10.2	9.0	7.2	9.1	3.2	3.8	6.4	2.3	8.9	11.1	10.9	9.2
Sary120	153.2665	48.0840	12.6	9.2	7.9	10.0	4.6	4.7	5.8	3.9	10.1	7.0	12.1	9.6
Sary125	153.2660	48.0840	11.3	9.2	7.9	8.9	4.4	4.6	6.2	3.9	9.1	7.0	9.1	9.0
Mane005	153.2440	48.0955	18.5	6.2	3.6	4.9	2.1	2.2	3.9	2.7	14.0	14.4	10.1	4.0
Mane004	153.2430	48.0960	16.0	6.0	3.5	5.3	2.3	2.1	3.5	2.6	13.3	13.7	10.1	3.9
Mane003	153.2425	48.0965	14.3	5.9	3.5	4.6	2.3	2.1	3.4	2.6	13.5	13.3	10.1	3.9
Mane001	153.2420	48.0980	10.0	5.9	3.4	4.6	2.3	2.1	3.4	2.6	13.2	12.6	10.1	3.8
Mane002	153.2420	48.0980	13.0	5.9	3.4	4.6	2.3	2.1	3.4	2.6	13.5	12.9	10.1	3.8
Vosk001	154.0865	48.7885	5.8	5.8	3.3	2.9	1.2	3.2	3.5	0.8	2.0	2.1	2.3	2.0
LandAlt	154.6000	49.1250	3.6	6.2	3.3	1.4	0.8	1.4	3.1	0.6	1.6	1.7	1.6	1.1
SeveEas	154.4955	49.1610	5.0	9.8	5.9	2.6	1.8	1.9	5.7	1.5	2.8	4.2	3.6	2.8
SeveWes	154.4955	49.1610	6.5	9.8	5.9	2.6	1.8	1.9	5.7	1.5	2.8	4.2	3.6	2.8
MuslMSo	154.8330	49.3875	5.0	4.9	2.5	1.9	1.1	2.5	4.2	0.9	2.2	2.5	2.2	2.5
MuslMCB	154.8235	49.3900	8.5	5.0	2.6	1.9	1.1	2.4	4.5	0.9	2.2	2.5	2.4	2.5
MuslMNB	154.8235	49.3900	6.5	5.0	2.6	1.9	1.1	2.5	4.3	0.9	2.1	2.5	2.3	2.5
MuslLSo	154.8255	49.3940	6.5	5.2	3.1	1.9	1.1	2.4	5.0	0.9	2.1	2.6	2.4	2.5
MuslLCB	154.8245	49.3975	6.0	5.3	3.2	2.1	1.1	2.6	5.0	0.9	2.3	2.6	2.6	2.5
MuslLNo	154.8265	49.3990	8.0	3.6	1.9	1.7	1.0	1.2	3.1	0.9	1.4	1.3	1.5	2.4
MuslLLh	154.8285	49.4015	7.0	4.2	2.1	2.2	0.9	2.1	4.0	0.7	1.7	2.1	2.0	2.0
Blak008	154.8240	49.4020	10.0	3.7	2.1	2.1	1.3	1.8	3.7	0.9	1.6	2.4	2.2	2.1
Blak09A	154.8150	49.4065	5.0	3.7	2.0	2.1	1.0	1.5	3.8	0.6	1.3	1.7	1.6	1.6
Blak07A	154.8125	49.4145	5.0	3.6	1.9	2.1	0.9	1.5	3.5	0.6	1.3	1.7	1.6	1.6
Blak06A	154.8105	49.4250	5.0	3.7	1.9	2.2	0.9	1.5	3.0	0.6	1.2	1.6	1.4	1.6
Blak05A	154.8095	49.4355	8.0	3.7	2.0	2.4	0.8	1.1	2.7	0.6	1.3	1.4	1.4	1.5
Blak04A	154.8095	49.4405	5.0	3.8	2.0	2.4	0.8	1.1	2.8	0.6	1.3	1.5	1.5	1.6
Blak02A	154.8100	49.4610	4.0	5.9	3.0	2.8	0.8	1.5	3.4	0.7	1.4	1.5	1.5	1.8
Blak001	154.8145	49.4735	7.0	5.8	3.2	2.8	0.8	1.3	3.1	0.6	1.1	1.4	1.4	2.1

VITA

Breanyn Tiel MacInnes knew from an early age that she wanted to be a geologist. The story told by her parents is that at 3 years old she was an avid rock collector and a member of the North Carolina Gem and Mineral Club; at 4 years old she knew she wanted to be a professor like her dad. Her desire to be a geologist was reinforced when she was 15 and attended a conference on Antarctic paleoclimatology with her dad at the Byrd Polar Research Center. Her college counselor told her if she wanted to study geology, she had better attend Carleton College. Breanyn received her B.A. in Geology at Carleton in 2004, and immediately started graduate school at the University of Washington where she earned her M.S. in Geological Sciences in 2007 and her Ph.D. in Earth and Space Sciences in 2010. Breanyn has 5 published papers from her time in graduate school; three as first author. Two of the papers are in Chapters 2 and 3 of this dissertation. The other papers are:

MacInnes, B.T., Weiss, R., Bourgeois, J. and Pinegina, T.K., 2010, Slip Distribution of the 1952 Kamchatka Great Earthquake Based on Near-Field Tsunami Deposits and Historical Records: Bulletin of the Seismological Society of America, v. 100, no. 4, p. 1695–1709, doi: 10.1785/0120090376.

Bourgeois, J., and MacInnes, B.T., 2010, Tsunami boulder transport and other dramatic effects of the 15 November 2006 central Kuril Islands tsunami on the island of Matua: Zeitschrift für Geomorphologie, v. 54, suppl. 3, no. 175-195.

Levin, B.V., Kaistrenko, B.M., Rybin, A.B., Nosov, M.A., Pinegina, T.K., Razhigaeva, N.G., Sassorova, E.V., Ganzei, K.S., Ivelskaya, T.N., Kravchenovskaya, E.A., Kolesov, C.V., Evdokimov, Y.V., Bourgeois, J., MacInnes, B., and Fitzhugh, B., 2008, Manifestations of the Tsunami on November 15, 2006, on the Central Kuril Islands: Results of the Modeling of Run-Up Heights: Doklady Earth Sciences, v. 419, no. 2, p. 335–338.